Advanced Fiber Materials (2023) 5:1273–1317
https://doi.org/10.1007/s42765-023-00275-7

REVIEW

# A Novel Vision of Reinforcing Nanofibrous Masks with Metal Nanoparticles: Antiviral Mechanisms Investigation

**Farinaz Hadinejad[1] · Hamed Morad[2,3] · Mohsen Jahanshahi[1] · Ali Zarrabi[4] · Hamidreza Pazoki-Toroudi[5,6] · Ebrahim Mostafavi[7,8]**

Received: 23 November 2022 / Accepted: 13 February 2023 / Published online: 11 April 2023


## Abstract

Prevention of spreading viral respiratory disease, especially in case of a pandemic such as coronavirus disease of 2019 (COVID-19), has been proved impossible without considering obligatory face mask-wearing protocols for both healthy and contaminated populations.The widespread application of face masks for long hours and almost everywhere increases the risks of bacterial growth in the warm and humid environment inside the mask. On the other hand, in the absence of antiviral agents on the surface of the mask, the virus may have a chance to stay alive and be carried to different places or even put the wearers at risk of contamination when touching or disposing the masks. In this article, the antiviral activity and mechanism of action of some of the potent metal and metal oxide nanoparticles in the role of promising virucidal agents have been reviewed, and incorporation of them in an electrospun nanofibrous structure has been considered an applicable method for the fabrication of innovative respiratory protecting materials with upgraded safety levels.

**Keywords** Nanoshield · Facemask · Antiviral · Metal nanoparticles · Electrospinning · Immunity booster

## Introduction

Human coronaviruses have been considered nonlethal pathogens, which usually cause mild upper respiratory diseases and around 15% of prevalent colds [1]. However, in the past two decades, severe pneumonia and human death have been caused by two animal-transmitted coronaviruses, severe acute respiratory syndrome coronavirus (SARS-CoV) and Middle East respiratory syndrome coronavirus (MERS-CoV) [2]. And lately, in 2019, the prevalence of a novel viral disease, COVID-19, which originated from the same family and officially named after a well-known antecedent, SARS-CoV-2, based on World Health Organization (WHO), as killed over 6.04 million people and infected over 455 million people all around the world which undoubtedly has been the most catastrophic issue of human health in the twenty-first century so far.

Finally, on 12 March 2020, the WHO announced COVID-19 as the fifth recorded pandemic, after Spanish flu (H1N1) in 1918 [3], Asian flu (H2N2) in 1957 [4], Hong Kong flu (H3N2) in 1968 [5], and Swine flu Pandemic (H1N1) in 2009 [6], which respectively led to around 50 million, 1.5 million, 1 million, and 300,000 deaths.

✉ Hamed Morad
morad.h@iums.ac.ir; h.morad55@yahoo.com

✉ Ebrahim Mostafavi
ebi.mostafavi@gmail.com; ebimsv@stanford.edu

1 Nanotechnology Research Institute, Faculty of Chemical Engineering, Babol Noushirvani University of Technology, Babol 4714873113, Iran

2 Department of Pharmaceutics and Pharmaceutical Nanotechnology, School of Pharmacy, Iran University of Medical Sciences, Tehran 1475886973, Iran

3 Ramsar Campus, Mazandaran University of Medical Sciences, Ramsar 4691710001, Iran

4 Department of Biomedical Engineering, Faculty of Engineering and Natural Sciences, Istinye University, Istanbul 34396, Turkey

5 Physiology Research Center, Faculty of Medicine, Iran University of Medical Sciences, Tehran 1449614535, Iran

6 Department of Physiology, Faculty of Medicine, Iran University of Medical Sciences, Tehran 1449614535, Iran

7 Stanford Cardiovascular Institute, Stanford University School of Medicine, Stanford, CA 94305, USA

8 Department of Medicine, Stanford University School of Medicine, Stanford, CA 94305, USA

Although the severity and mortality of COVID-19 are less than most of other epidemic coronaviruses (i.e., SARS-CoV and MERS-CoV), it is much more transmissive and can be easily spread via the virus-containing droplets originating from sneezing, coughing, exhalation, or by contacting contaminated materials [7]. The aerosol pathway cannot be neglected as the most critical and dominant way of the virus to spread [8]. Even though a majority of the population in developed and developing countries have received vaccines, high mutation rates in the genome of COVID-19 [9] have been leading to emergence of new variants (i.e., Omicron [10]) that can cause a whole different type of symptoms, sometimes more severe and long-lasting complications, beyond the immunizing power of the vaccines which were introduced so far. Besides, there are still some unvaccinated populations due to specific beliefs or vaccine hesitancy. Therefore, wearing face masks as the first line of defense is still part of the WHO protocol and the best-recommended strategy for managing the outbreak due to the reduction of the risk of infection and preventing transmission of droplets, small carriers of respiratory viruses, either from the surroundings to the healthy wearer or from the infected wearer to the surroundings [8].

These masks mostly contain a nonwoven layer with a specific pore size to impede the passage of the pathogens, and durability of manufacturing material [11], fitness, flexibility, and comfort are the most important concepts in the design process, which subsequently impact the perception of users and their tendency for using masks [12]. Ideal air filtration materials should also be able to effectively capture the aerosol particles and allow airstream to pass through them simultaneously [13]. Substituting nanofibers for conventional filter media could be a proper approach to fulfilling the abovementioned criteria [14].

The first effort to employ electrospun nanofibers with the aim of air filtration begins in the early 1980s [15]. The outstanding properties of the nanofibers, including small fiber diameter and pore size, high porosity, interconnected pore structure [16], high ratio of surface area to volume, promising mechanical strength, and controllable morphology, are beneficial for improving filtration performance and capturing particles [17]. Besides, less resistance of the nanofibrous media to airflow leads to minimization of leakage and enhances the chance of capturing the particles without needing a perfect seal, which can reduce the exposure levels of wearers considering the case of using ordinary masks [14].

Electrospinning is the most promising technology producing high-efficiency nanofibrous air filters from a vast range of polymers that have been widely used in many fields, including disposable respirators, indoor air purifiers, cleanroom air purification systems, and automotive cabin air filters, among other devices [18]. The application of the filtration media consisting of fine fibers in the structure of the catalyst of photoelectrochemical oxidation-assisted indoor air purifiers facilitates the capturing stage of the pollutant, especially for microscopic particulate matter due to increasing of the surface area [19]. Compared to melt-blown fibers, electrospun nanofibers are about one to two orders thinner weigh less (0.02–0.5 $g.m^{-2}$ compared to 5–200 $g.m^{-2}$ for melt-blown filters), possess higher surface area, and smaller diameter pores [14, 20]. Theoretical models depicted that in the case of employing smooth, lightweight, and less-than-micron-sized fibers with circular cross-sections, capturing aerosol particles can be enhanced [21]. However, focusing on the safety of the human body and environment, the electrospun filter membranes should be green, nontoxic, and environmentally friendly [14].

Figure 1 depicts a number of polymers that have been exploited to produce electrospun nanofibrous filters with superior performance to date, including polyacrylonitrile (PAN) [22, 23], polycaprolactone (PCL) [24], polyethylene terephthalate (PET) [25], polyvinyl alcohol (PVA) [26], Nylon 66 [27], Nylon 6 [28], polyamide [29], polyurethane (PU) [30], polysulfone (PSU) [31], Poly (ethylene oxide) (PEO) [32], cellulose acetate [33], chitosan [34], and lignin [35].

Unwantedly, the moist warm condition inside a face mask could turn it into an appropriate breeding ground for various micro-organisms and expose the wearers to an extra hazard [36]. So, the mask could act as a two-edged sword, which intends to be a protective shield, but unfortunately, it could also increase the delivery of viruses to three main body entries. Therefore, there is an unmet need to upgrade this shield by utilizing antiviral agents to intensify the guarding preparations. Among different functionalization agents, metal nanoparticles (NPs) can act as effective antiviral agents, which can cause disturbing viral replication or inhibit the receptor binding sites and block the entry of viruses into the cells [37].

There is also a favorable cellular interaction between metal NPs and biomolecules within and on the surface of the cells [38]. Moreover, they can be engineered to have specified binding properties, which enables them to target defined cells that enhance the therapeutic efficiency of the metal NPs [39].

Metal NPs like copper, gold, silver, iron, zinc, etc., and their oxides have demonstrated antiviral activity against a wide range of virus infections. However, a limited number of these NPs being processed for FDA approval since the administration of these NPs inside the host cells may cause toxicity and pose the risk of metal accumulation in the lungs [40, 41], and other organs [42, 43]. Therefore, it would be beneficial to use them as an exterior antiviral agent to prevent respiratory diseases, especially COVID-19.

This review aims to introduce metal and metal oxide NPs and their mechanism of action against different viruses.

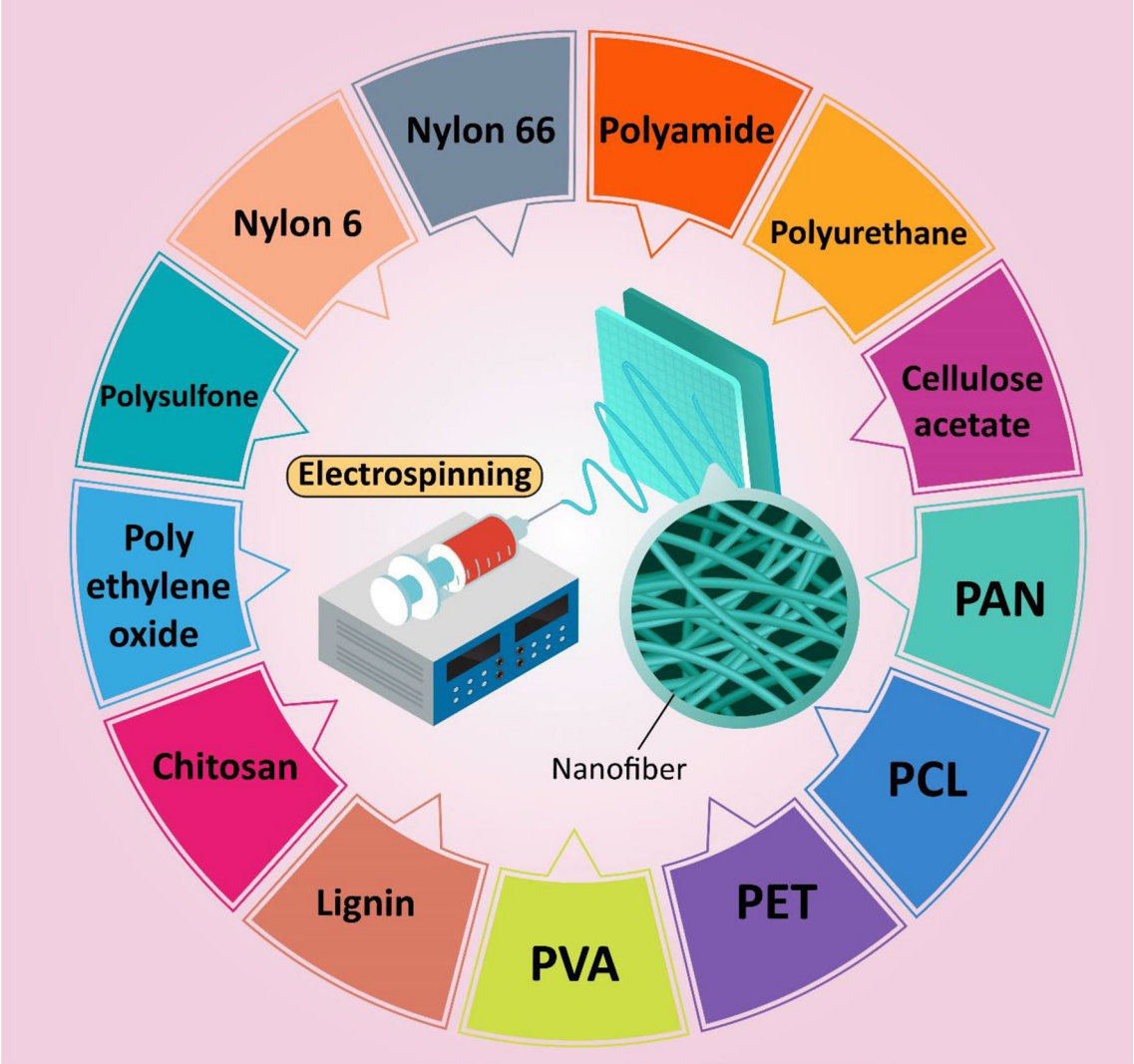


**Fig. 1** Different polymers utilized to produce electrospun nanofibrous filters

Besides, the effectiveness of various metal/metal oxide NPs is compared to find the most effective NPs against COVID-19. The air filtration activity of electrospun nanofibers made of different biocompatible polymers is also explored. And finally, the most practical face mask based on the metal/metal oxide NPs decorated electrospun nanofibers as an effective protector in the predicted everlasting COVID-19 pandemic will be suggested.

## Mechanistic Basis of Antiviral Actions of Metal NPs

It is believed that small-sized NPs demonstrate a brilliant antiviral activity in contrast with large NPs which have no antiviral properties [44]. This phenomenon has been reported to be related to the effect of local-field enhancement by NPs [45]. Due to this effect, the viral surface local field gradient can be intensified, which facilitates the adsorption of NPs on the viral surface as the most important factor in the antiviral effectivity of the NPs [46]. The virus binding to the receptors of the cell surface is the first stage in the viral infection process, followed by endocytic internalization of the virus particle [47]. The cellular attachment proteins and conformations of the viral envelope are the main factors that affect cell binding [48, 49] and membrane fusion [50] accordingly. Any conformational changing in these molecules can inhibit the virus binding [49–51]. Therefore, the main pharmacological mechanism of the small NPs against viruses is interfering with the viral attachment and entrance to the host cells. Moreover, it has been observed that smaller NPs with diameters below 6 nm have lower toxicity due to their easy clearance by renal execration, which takes away the accumulation-related problems [52, 53]. Concerning their antiviral properties, metal NPs can trigger pathways and cascades or modify the existing ones, whether inside

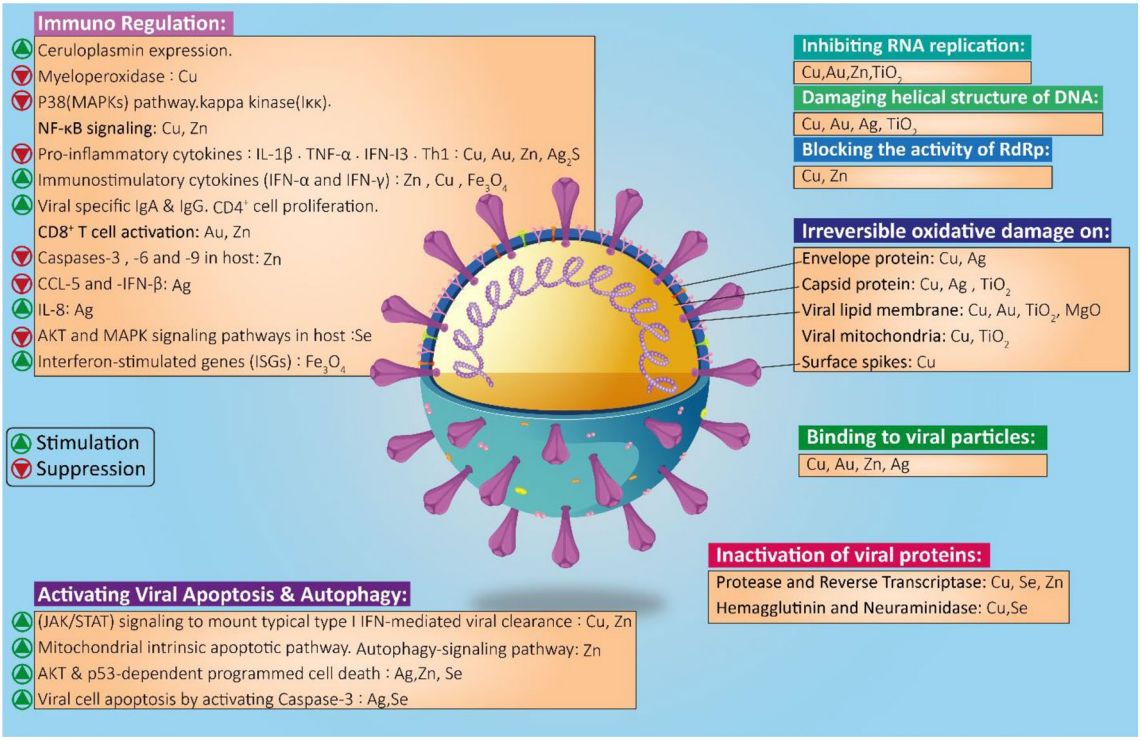


**Fig. 2** Schematic overview of the mechanism of antiviral actions of metal NPs on a model virus (SARS-CoV-2)

the viral cell or the host. In general, we can categorize these pathways under the following main labels: oxidative stress, direct interference in viral morphology and replication cycle, and regulatory effect on inflammatory and other immunological responses of the host (Fig. 2).

The activity of a ribonucleic acid (RNA)-dependent RNA polymerase (RdRp) is vital for the replication of the viral genome of SARS-CoV-2, which includes a positive-sense RNA [9]. In comparison to other metal ions, cupric ions ($Cu^{2+}$) demonstrated the greatest inhibition against the activity of RNA polymerase for more than 60% and blocked the activity of RdRP [54]. Another virucidal activity of copper is due to triggering the reactive oxygen species (ROS) pathway which leads to irreversible oxidative damage of capsid protein and surface spikes, viral membrane, envelopes, viral genomic material, nucleic acids, and viral mitochondria that are all caused by the generation of hydrogen peroxide-derived radicals in the Fenton reactions induced by copper [55, 56]. The reaction between $Cu^{+}$ and hydrogen peroxide ($H_2O_2$) leads to the formation of copper-hydroperoxo complexes formed that can cause Deoxyribonucleic acid (DNA) damage [57]. Copper is also capable of damaging the nucleic acids by forming cross-links within and between strands of DNA that may contribute to helical structure disorders and DNA denaturation [58]. Another viral inactivation mechanism of $Cu^{+}$ is through the lipid peroxidation by the following reactions: $Cu^{+} + LOOH \longrightarrow Cu^{2+} + LO\cdot + OH^{-}$ and $Cu^{2+} + LOOH \longrightarrow LOO\cdot + H^{+}$ [59]. As the influenza virus envelope is mainly composed of lipids, $Cu^{+}$ can inactivate this group of viruses by oxidizing the lipids [56]. The free radicals that are generated through the redox signaling pathway can also degrade viral proteins such as hemagglutinin (HA), neuraminidase (NA), and protease [56]. Copper can also act as a booster of the immune response during inflammation and infectious events due to its stimulatory effect on ceruloplasmin expression and accordingly, inhibition of myeloperoxidase (MPO) [60]. The regulatory effect of copper in response to a viral-induced inflammation is stimulation of the antioxidant defensive system in which the pathways including p38 mitogen-activated protein kinases (MAPKs) and Nuclear factor kappa B (NF-κB), activated by virus-induced ROS and accountable for the proinflammatory response, are suppressed and as a result, the generation of adhesion molecules, cytokines and, chemokines related to inflammation will be decreased and thereby the host cells will be protected against oxidative injury [61]. Copper maintains the anti-viral defense of host cells by activation of autophagy and apoptosis as well [62]. The autophagy process for eliminating the infection initiated with conveying viral particles for lysosomal break-down and proceeds by employing a receptor with inherent pattern recognition ability named Toll-like receptor (TLR)-7, and activation of Janus kinase/signal transducer and activator of transcription proteins (JAK/STAT) signaling to organize a typical viral clearance mediated by type I interferon (IFN) [63].

Gold nanoparticles (AuNPs) interact with double-stranded viral DNA and inhibit viral DNA and RNA replication and inactivate virus particles before penetrating host cells, or by binding to viral particles, AuNPs are capable of impeding the connection between the virus and host cells' receptors and as a result, inhibit the viral cycle onset. Adsorption of AuNPs on the surface of host cells can successfully block the viral penetration due to alteration of membrane permeability potential [64]. The affinity of AuNPs to bind with thiol and amine groups cause interactions leading to ROS generation and their releasing strongly correlated with the increase in membrane permeability and can cause oxidative stress, lipid peroxidation in the cytoplasmic membrane, and ultimately pathogens' death pathways [65]. AuNPs are capable of enhancing mucosal cellular immunity in BALB/c mice against H3N2 infection by promotion of the level of Immunoglobulin A (IgA) and Immunoglobulin G (IgG) that are viral specific, inducing IFN-γ- secretion which is antigen specific, proliferation of CD4 + cell and stimulating CD8 + T cell [66].

Zinc oxide nanoparticles (ZnONPs) and $Zn^{2+}$ possess rather similar antiviral mechanism to other potent metal NPs including: impeding the entrance of the virus inside the host cell, suppressing of folding and processing of polypeptides, inactivation of protease and reverse transcriptase of the virus, blocking the replication process in full length genome expressing cells, disrupting RdRP activity in any or all stages of its function including template binding, initiation or elongation either through direct binding or by acting as the rival of metallic ions required by RdRp [67], inducing mitochondrial inherent apoptotic pathway triggered by ROS, as well as the signaling pathways leading to autophagy or programmed cell death (dependent on p53) [68], exerting anti-inflammation responses via inhibiting the activity of kappa kinase (Iκκ) and NF-κB signaling, leading to further downregulation of proinflammatory cytokines production [69], activating the synthesis of immunostimulatory cytokines (IFN-α and IFN-γ) through (JAK/STAT) signaling initiated in the immune cells which were infected by the virus, with the aim of expressing a vast number of antiviral genes, while inhibiting the binding of IFN-l3, a proinflammatory cytokine, to its receptor Interferon lambda receptor 1 (IFNLR1) [70] and, activating antiapoptotic cascades by inhibition of caspases-3, -6 and -9 to protect host cells [71].

The first inhibitory mechanism of silver nanoparticles (AgNPs) that happens outside the viral cell is to bind the outer coat of the virus and interrupt the viral binding to the cell receptors. AgNPs and Ag+ ions can interact with viral cell structure and biomolecules and cause denaturation of the functional proteins by altering the three-dimensional (3D) structure of the proteins using interference with disulfide bonds and blockage of the active binding sites. The silver nanomaterials such as AgNPs, silver colloids, and silver nanowires are reported to show an inhibitory effect on the initiation of transmissible gastroenteritis virus (TGEV) infection by the mechanism of attaching to the spike (S) glycoproteins that are placed on the surface of the viral particle and altering them to diminish their ability of recognition and binding to the host receptors [72]. Additionally, Ag+ ions can decrease DNA stability by electrostatic repulsion caused by similar polar charges and hybridizing helical structure of the DNA via breaking the base pairs' hydrogen bonds in anti-parallel strands by intercalating between the purine and pyrimidine base pairs, changing its relaxed form to condensed that lastly restrain the replication process and gene transcription. Electrostatic repulsion is another way of disintegrating the structure of DNA by AgNPs because AgNPs and DNA possess the same polar charge [73].

As a result of AgNPs mediated ROS production, glutathione (GSH) may be reduced to glutathione disulfide (GSSG), which contributes to activation of oxidative signaling pathways, oxidative stress, and apoptosis [74]. On the other hand, modulation of superoxide dismutase, nicotinamide adenine dinucleotide phosphate (NADPH)-dependent flavoenzyme, catalase, and glutathione peroxidase function, as antioxidant ROS metabolizing enzymes, is another result of AgNPs induced generation of ROS [75, 76]. Silver sulfide ($Ag_2S$) nanoclusters are reported to inhibit RNA synthesis and viral budding and suppress coronavirus proliferation, which has been argued to be the result of interferon-stimulated genes (ISG) proteins' function and cytokines that promote inflammation [77]. In influenza virus-infected lung tissue, AgNPs can block the autophagic response in epithelial cells by downregulating the release of Chemokine (C–C motif) ligand 5 (CCL-5) and -IFN-β as two immunologically important cytokines, by inhibition of retinoic acid-inducible gene I (RIG-I) while activating the antibacterial responses in the host. AgNPs are also capable of disorganization of the mitochondrial structure and prevent Interferon Regulatory Factor 7 (IRF-7), an inhibitory factor for viral transcription, from fluxing into the nucleus [78]. The previous report on the antiviral potency of AgNPs functionalized with polyethyleneimine (PEI) and antiviral small interfering RNA (siRNA) against Enterovirus 71 (EV71) showed that this Ag-containing compound can successfully block the virus from infecting host cells with the mechanism of preventing DNA fragmentation, chromatin condensation, inhibition of viral-induced ROS accumulation, and triggering protein kinase B (AKT) and p53 pathways, and facilitating viral cell apoptosis by activating an important mediator called caspase-3 that acts by decomposition of diverse cellular substrates, such as Poly (ADP-ribose) polymerase (PARP). This Ag-containing antiviral compound also demonstrated inhibiting effect on EV71-induced apoptosis of Vero cells [79].

Outside of the viral cell, titanium dioxide nanoparticles ($TiO_2$NPs) may interact with the proteins of the viral capsid

such as the residues of alanine, glycine, and proline, and after that, they may trigger death pathways by destabilization of the lysosomal membrane and peroxidation of viral lipids, cause disruption of mitochondrial function, inhibit the viral reproduction by attaching to the genome of the virus in conservative zones and finally, provoking signaling cascades related to oxidative stress, inflammation, cycle arrest and, apoptosis in the viral cell [80, 81].

Previous studies on human bronchial epithelial cells demonstrated that Cerium dioxide nanoparticles ($CeO_2$NPs) are capable of increasing ROS generation, follow by a potent promotion of Nuclear Heme Oxygenase-1(HO-1) by activating p38-nuclear factor erythroid 2-related factor 2 (p38-Nrf-2) signaling [82].

Magnesium oxide nanoparticles (MgONPs) are reported to have potential utility for cancer management by creating ROS and lipid peroxidation in the liposomal membrane of the viral cells, which demonstrates the main deactivating mechanism of MgONPs against the viruses [83].

Selenium nanoparticles (SeNPs) are reported as promising antiviral agents that are usually used in the surface-modified form by drugs against drug-resistant viruses such as H1N1 influenza. Surface modified SeNPs by arbidol, for instance, acted as a potent antiviral with the mechanism of HA and NA inhibitory, blocking the generation of ROS (from 460 to 150%), impeding DNA fragmentation, chromatin condensation, and restraining the function of caspase-3 (from 435 to 210%), p53 pathway, mediated by ROS, and viral-induced AKT and MAPK signaling in Madin-Darby canine kidney (MDCK) cells [84]. In the case of using β-thujaplicin functionalized SeNPs, compared to β-thujaplicin alone, for treatment of H1N1 infected MDCK cells, 45% more cells survived. The mechanism of antiviral action was blocking chromatin condensation and DNA fragmentation, preventing MDCK cells from generating ROS, and mechanistically, triggering apoptosis with inhibition of AKT and p53 signaling [85].

Gallium (Ga) has similar characteristics to iron, but $Ga^{3+}$ cannot be reduced as $Fe^{3+}$ does, hence, in case of binding to Fe-specified sites in the enzyme structure, it will be defective. Besides, most of the proteins that need Fe to function properly cannot differentiate $Ga^{3+}$ from $Fe^{3+}$; therefore, the presence of Ga potentially disrupts all the pathways in bacterial or viral cells that are dependent on Fe, leading to inhibition of their growth and ultimately, eliminating them [86].

A report on studying the impact of Iron (II, III) oxide nanoparticles ($Fe_3O_4$NPs) on the immune system of four mammalian cells revealed that dimercaptosuccinic acid (DMSA)-coated $Fe_3O_4$ magnetic NPs activate comprehensive immune responses of two immunocytes like virus (Abelson murine leukemia virus-induced tumor (RAW264.7) and acute monocytic leukemia patient-derived human monocytic cell line (THP-1)), inducing the production of many kinds of cytokines and expressing ISGs, which are closely related to antivirus [87].

## Application of Metal NPs as Antiviral Agents

### Gold Nanoparticles (AuNPs)

Among metal-based NPs, AuNPs are being extensively explored due to their inertness and lower cytotoxicity [88, 89]. The historical records demonstrated that medicinal preparations based on gold had been employed since 2500 BC in China [90]. The primary applications of gold compounds as drugs include their useful application in rheumatoid arthritis cases in the forms of myocrisin (sodium aurothiomalate), solganol (aurothioglucose), and auranofin [91].

In the modern world, Blough et al. have done the earliest trial (in 1989) of using gold for treatment of the most concerning viral infection at the time, human immunodeficiency virus (HIV), and reported that aliphatic compounds which contain gold are capable of inhibition of reverse transcriptase [92].

Among the different oxidation states of gold, the majority of formulations that have exhibited potent inhibition against HIV consist of gold (I) (+1 oxidation state). More thermodynamic stability of gold (I) in comparison with gold (III) results in minimizing the toxic effect of gold (I), noting that reduction of gold (III) to gold (I) is feasible in most of the complexes [93].

The AuNPs are evaluated for application in formulating vaccines to be used in combination with recombinant S protein, with the aim of immunization, functioning as both antigen carrier and adjuvant causing an increase in the T cells (T lymphocyte and thymocyte) proliferation and activation of B cells (B lymphocyte) due to organizing antigens on the surface of the particles, with releasing immunoregulatory mediators such as cytokines and chemokines [2]. The coronavirus, for instance, binds to cellular receptors by S protein, which acts as a mediator in membrane fusion in the process of interring to the host cells, and because of that is an important choice to be targeted by the vaccines for neutralizing infection caused by a coronavirus which can be successfully done by employing AuNPs [94].

Peña-González et al. placed peripheral sulfonate on the structure of carbosilane dendrons to stabilize AuNPs with a mean diameter of 2.4 nm and studied the anti-HIV effect of AuNPs and dendrons. The infection was quantified by performing a luciferase-based assay on HeLa cell-derived TZM. bl cells containing b-galactosidase and luciferase genes. The toxicity evaluations were carried out by 48 h exposure of peripheral blood mononuclear cells (PBMCs) at 100 mg. $L^{-1}$ as a nontoxic concentration. The results indicated that

dendronized AuNPs possessed higher inhibitory effects on HIV-1 compared to dendrons [95].

Gianvincenzo et al. coated 2 nm AuNPs with 50% density of sulfate-ended ligands and assessed the inhibitory properties of NPs on HIV-1 infected human lymphocyte cell line (MT-2 cells) with a recombinant virus that carried reporter genes named Renilla. The results of viral replication assessments after 48 h showed that by using nanomolar (2.6 μM and 1.3 μM) concentrations, NPs could bind to a glycoprotein (gp120) of the viral envelope and highly inhibited the infection of HIV in MT-2 cells [96].

Sekimukai et al. evaluated the capability of AuNPs with a diameter of 40 nm to act as an adjuvant to induce strong IgG responses to S protein in the case of SARS-CoV (Frankfurt 1 strain) infection. They confirmed the immunogenicity of this nanoformulation by performing studies on subcutaneously immunized 6-week-old female mice with doses under 1 μg (1 μg, 0.5 μg, 0.1 μg, or 0.05 μg) of AuNP-adjuvanted S protein and further histological tests based on the numbers of eosinophils counted in the mice's lungs. The results demonstrated that the nanoformulation could induce an antigen-specific IgG response in the mouse model. But it was unsuccessful in inducing protective responses in the immune system, and after viral infection, caused limitations for eosinophilic infiltrations [2].

The acceptable anti-herpes simplex virus (HSV)-1 efficacy of AuNPs capped with mercaptoethanesulfonate (Au-MES NPs) with a diameter of 2 nm considering their intrinsic nontoxicity, prove them to be interesting choices for topical application against the threat of microbes and numerous viruses. Bowman et al. published primal reports on employing a small molecule (mercaptobenzoic acid) coated with AuNPs as an efficient HIV-1 infection inhibitor with to investigate PBMCs [97]. A while after that, Baram-Pinto et al. illustrated the ability of 4 nm-sized Au-MES NPs to imitate the function of heparan sulfate (HS) as a receptor placed on the surface of the cells. Based on their plaque-reduction assay on infected African green monkey kidney (Vero) cells, Au-MES NPs could interfere with the process of viral binding and block the entrance of the virus to the host cells and spread this way from cell to cell which leads them to suggest this nanoformulation for using in prophylaxis and therapy of HSV-1 infection [98]. In another study, Cagno et al., used the same Au-MES NPs formulation and reported that these NPs possess virustatic function. They made efforts on changing the virustatic properties of these Au-based NPs to virucidal activity. For this purpose, the linkers were manipulated to achieve multivalent attachment, which could cause irreversible local distortion. Most viral attachment ligands (VALs) bear closely repeating generated units in the binding sites; hence, they are suitable for multivalent binding. As all the heparan sulfate proteoglycans-mimicking NPs (HSPG-mimicking NPs), such as Au-MES NPs, provide short linkers to viral ligands, and considering that the sulfonate linkers have a relative rigidity, therefore the attachment would be provided to a few numbers of repeating VALs units which lead to a reversible and weak bind. Therefore, in this study the AuNPs were coated with undecanesulfonic acid (MUS)-containing ligands whose long and flexible linkers led to a strong multivalent attachment and brought an irreversible virucidal efficacy. Their activity against HSV, human papillomavirus (HPV), respiratory syncytial virus (RSV), dengue, and lentivirus was proved by in vitro study. Moreover, their ex vivo and in vivo functions were observed in HSV-2-infected human cervicovaginal histocultures and RSV infected mice respectively [99].

Carja et al. employed self-assembly to organize the AuNPs surface (with a diameter of 3.5 nm) by layered double hydroxide nanoparticles (AuNPs/LDHs) with low cytotoxicity for antiviral applications. The results of viral load quantification in hepatoma-derived HepG2.2.215 cells revealed the presence of sequestered hepatitis B virus (HBV) particles within the treated cells in the exposure of AuNPs/LDHs, which indicates that AuNPs/LDHs hold significant potential to act as novel therapeutics for the treatment of HBV. There were also synergetic effects between the plasmonic gold and the particular LDHs environment [100].

Lysenko et al. fabricated two formulations with AuNPs, employing silicon dioxide ($SiO_2$) as a shell for one of them and as a carrier for the other, which both had low toxicity and showed antiviral action against adenovirus in cellular evaluations on MDBK (Madin-Darby bovine kidney line) and Hep-2 (larynx epidermoid carcinoma) cells. Two tested groups of NPs demonstrated inhibitory behavior against adenovirus, but the levels of inhibition varied in two groups of NPs, and the second one in which 5–20 nm AuNPs placed on the surface of 50–200 nm-sized $SiO_2$NPs, inhibited 90%–100% of the virus from reproduction in the concentration of $10^{-3}$ to 10 mg. $L^{-1}$ [64].

Vijayakumar et al. studied AuNPs stabilized with polyethylene glycol (PEG) for testing the in vitro toxicity and anti-HIV-1 effect and reported that AuNPs with $IC_{50}$ of $(1.12 \pm 0.05) \times 10^{-3}$ mg.$L^{-1}$, had inhibitory activity against the proliferation of endothelial cells induced by Vascular Permeability Factor(VPF)/ Vascular Endothelial Growth Factor (VEGF165), which proved that they possess a great potential for therapeutic applications in cases of neoplastic disorders, chronic inflammations, rheumatoid arthritis and, pathological neovascularization [101].

Papp et al. functionalized AuNPs with sialic acid (SA)-terminate glycerol dendron to study their inhibitory effect against Influenza A X31 virus. AuNPs were synthesized and tested in two sizes of 2 and 14 nm for determination of the antiviral properties in exposure to MDCK cells. Unlike AuNPs with a diameter of 2 nm, 14 nm AuNPs were

effective in nanomolarities and there is a significant dependency between their effectiveness against the virus and nanoparticle diameter and distributing of molecules in the space. A similar trend was observed for sialylated AuNPs, proving their inhibitory effect against viral infection [102].

Tazaki et al. reported that the employment of rod-shaped AuNPs conjugation enhanced the adjuvanticity of polycytidylic acid (poly (I: C) s) with a low molecular weight that is an adjuvant for HA vaccination against influenza via the intranasal route. Au nanorods increased the antiviral activity without causing inflammatory cytokine production in dendritic cells and application of them in a low dose (1 fmol) led to a reduction of viral replication in a nasal wash [103].

A summary of the abovementioned antiviral mechanisms of various Au-containing nanoformulations, such as AuNPs, Au nanorods, Au-MES NPs, and AuNP-adjuvanted S protein is depicted in Fig. 3.

## Zinc Oxide Nanoparticles (ZnONPs)

The cellular evaluations followed by an in vivo study by Mishra et al. introduced that ZnO micro–nano-particles when capped with numerous nanosized spikes, act as imitators of cell-induced filopodia, which targets the initial step of HSV-1 pathogenesis. Interestingly they have shown strong prophylactic activity against HSV-1 in infected Chinese hamster ovary (CHO-K1) cells and zebrafish embryos as an animal model by putting the virions in a trap by making them disabled from entering into human corneal fibroblasts. The viral blocking was significantly observed in a concentration of 100 mg. $L^{-1}$ of the ZnO-containing formulation. The inhibitory effect of the formulation against HSV-1 was highly enhanced as a result of the UV-light illumination treatment of the particles [104].

Ghaffari et al. demonstrated an interesting virucidal effect of ZnONPs and PEGylated ZnONPs sized from 20 to 50 nm against the H1N1 influenza virus with inhibition rates of 52.2 and 94.6%, respectively. This investigation confirmed that surface PEGylation of NPs leads to enhancement of antiviral activity against this virus and also reduces the cell cytotoxicity in MDCK-cDNA of human 2,6-sialtransferase (SIAT1) cells. The results of in vitro experiments showed that the inhibitory effect of ZnONPs against the influenza virus is restricted to the stage after viral entry into the host cells [105].

The above results had been also proven by Tavakoli et al. that reported the inhibitory effect of 92% for PEG-coated ZnONP sized 20–50 nm against HSV-1. Based on the results of cellular studies on infected Vero cells they also claimed that in the case of using these NPs 1 h after exposure to the virus, the highest anti-HSV-1 activity would be achievable [106].

In another study, ZnONPs were employed as a scaffold for anchoring active moieties: hydroxyl group

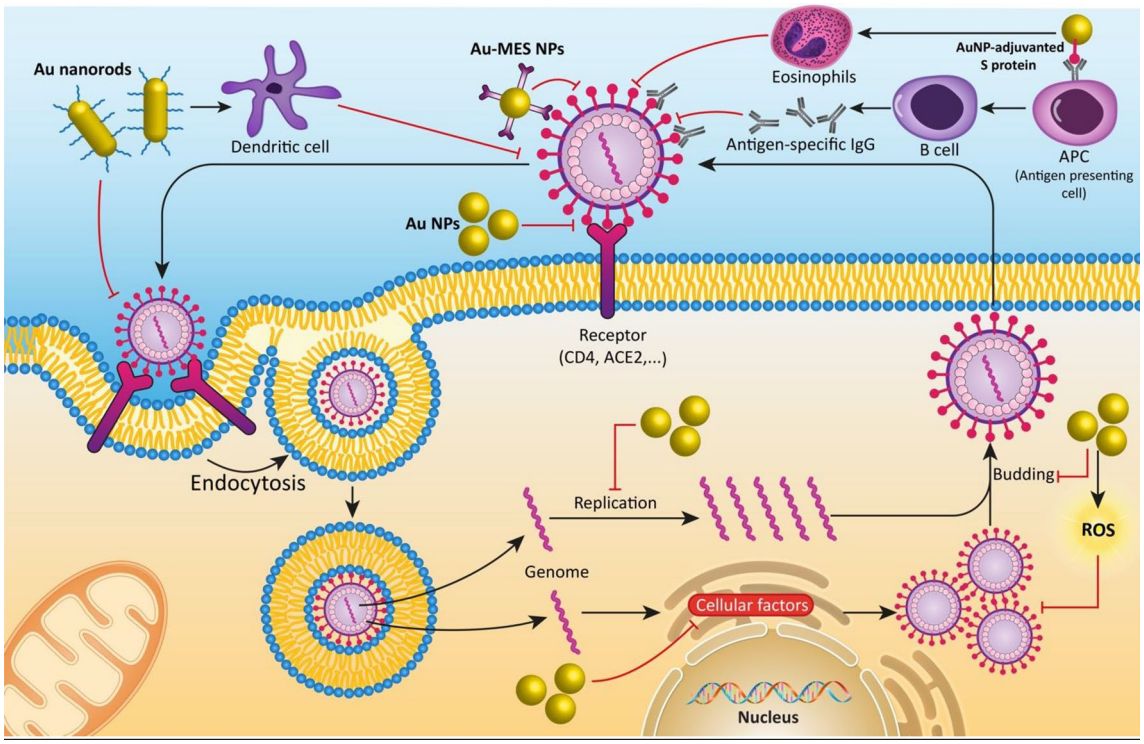


**Fig. 3** Illustrative mechanism of the antiviral activity of various Au nanoformulations

(H- ZnONPs), oleic acid (OA-ZnONPs), and chitosan (C-ZnONPs) for anti-HSV-1 applications. Results showed that surface-functionalized ZnONPs can successfully interfere with the entry of the virus into cells via targeting cellular receptors or neutralizing the virus. With this regard, for H- ZnONPs and OA-ZnONPs pretreated Vero cells, reduction of the viral infectivity in the order of 12.9% and 7.7% was observed, while C- ZnONPs were ineffective. On the other hand, within a 24 h incubation, H- ZnONPs and C- ZnONPs exhibited greater time-dependent inhibition and completely inactivated HSV-1, while OA- ZnONPs showed the lowest reduction (15%) in the viral titer [107].

Antoine et al. provided evidence about prophylactic and therapeutic applications of flame transport synthesized zinc oxide tetrapod (ZnOTs) micro-nanostructures. Their studies on vaginal epithelial and HeLa cells declared that ZnOTs significantly block the entry and spreading of HSV-2 virions and neutralize them. They also showed that illuminating ZnOTs with UV light can enhance attaching and hence, the inhibition efficacy of ZnOTs [108].

## Silver Nanoparticles (AgNPs)

AgNPs are the most popular particles possessing significant antiviral and antibacterial properties [109]. As was mentioned in the reported results of Gaikwad et al., the AgNPs with smaller sizes (4–13 nm) possess a more inhibitory effect [110]. They showed that in the case of employing AgNPs synthesized by fungi, a significant decline in the HSV-1/2 and human parainfluenza virus type 3 (HPIV-3) mediated infection levels can be obtained. However, AgNPs with larger diameters (about 50 nm), caused more cytotoxicity than the smaller ones (about 10 nm) [111]. Different capping agents may also be used for AgNPs, like citrate, polyvinylpyrrolidone (PVP), PEG, etc., which increase the biocompatibility of NPs and preserve the ability of infectivity reduction. On the other hand, the addition of those capping/coating agents may reduce the effectivity of AgNPs toward some types of viruses, for example, employing polysaccharide coating material, has an adverse effect on the antiviral property of AgNPs against Tacaribe virus (TCRV) and act as a protector for viral cell toward AgNPs induced toxicity [112].

Besides the effectivity of AgNPs in the early stages of viral infection, their anti-HIV activity in pre-infected Vero cells was reported to be potent. That's probably because AgNPs inhibit the activity of HIV-1 after entering the host cell by disrupting viral protein functions or by direct attaching to the RNA or DNA structure and reducing the rate of reverse transcription or pro-viral transcription [113]. Furthermore, the direct attachment of AgNPs on the surface of the vaccinia virus (VACV) fusion complex is another potential mechanism of its antiviral effect [114]. Figure 4 illustrates the potential mechanism of action in the use of AgNPs as an antiviral agent.

Lara et al. reported that PVP capped AgNPs with a diameter of 30–50 nm inhibited the replication of HIV in MT-2 cells and evaluation of the viral titer in the infected cervical

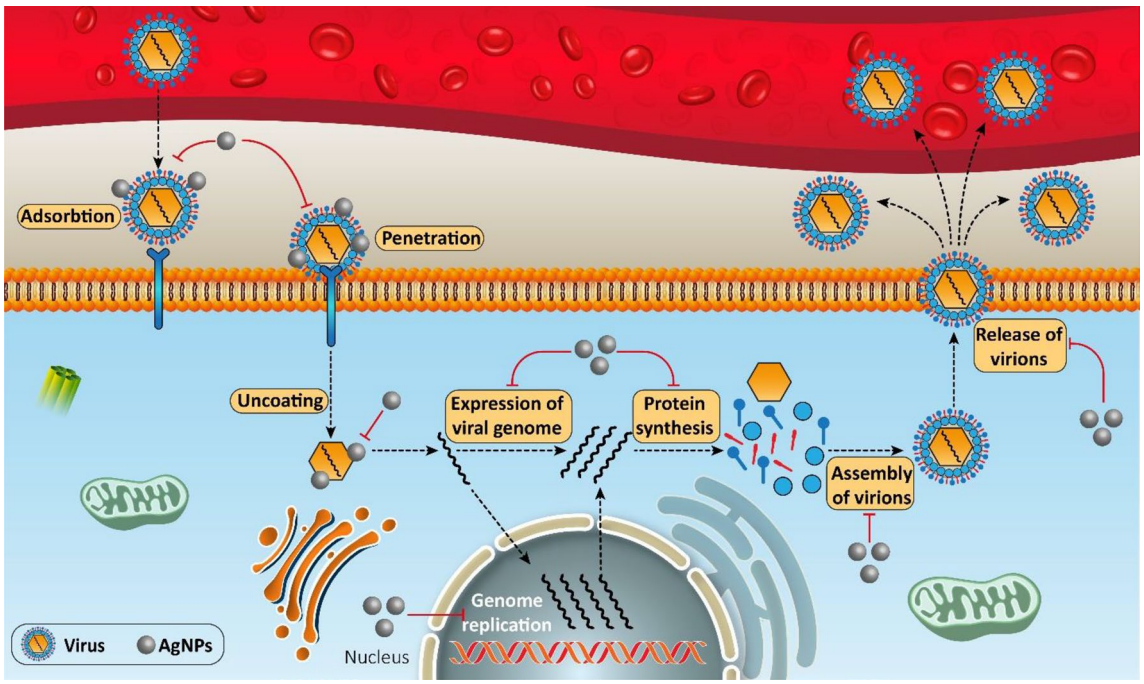


**Fig. 4** Potential mechanism of antiviral action in the use of AgNPs

tissue after 48 h demonstrated that NPs in the concentration of 150 mg. $L^{-1}$ offered long-lasting protection against HIV without causing any cytotoxicity in the explants. It was claimed that the interaction of AgNPs with HIV glycoproteins placed on the surface of the virus, drastically limits the fusion ability and binding of HIV into the host cells [115].

Castro-Mayorga et al. studied the effectivity of AgNPs for inactivating feline calicivirus (FCV) and murine norovirus (MNV) as the main causes of viral gastroenteritis. It was conducted by employing PHBV3 (poly (3-hydroxybutyrate-co-3-hydroxyvalerate)) films coated with electrospun PHBV18/AgNPs fiber mats to produce active biopolymers with antiviral effects, especially suitable for food preservation and medical contact surfaces. AgNPs showed dose-dependent effectiveness in decreasing FCV and MNV infectivity on CRFK cells (ATCC CCL-94) and RAW 264.7 cells, respectively, and after 24 h exposure to PHBV18/AgNP coated PHBV3 films, no infectious FCV recovered from the samples and MNV titers declined by 0.86 logs. The highest antiviral activity was achieved by employing $7 \pm 3$ nm-sized AgNPs in the concentration of 21 mg. $L^{-1}$ [116].

Xiang et al. investigated the interaction of AgNPs with the H1N1 virus to introduce a creative clinical strategy during the early dissemination stage of influenza virus infection. Both the immunofluorescence and NA inhibition assay showed an enhancement in shielding activity of 10 nm AgNPs against influenza virus for MDCK cells with no risk of cytotoxicity [117].

Mehrbod et al. determined the anti-H1N1 effectivity of AgNPs and also assessed the cytotoxicity of NPs considering a variety of temperatures employing Hemagglutination assay, reverse transcriptase-polymerase chain reaction (RT-PCR), and DIF (Direct Immunofluorescent) methods, and found that AgNPs can destruct the virus membrane glycoprotein knobs and the cells, but they were completely non-toxic to MDCK cells of the host at a concentration up to 1 mg. $L^{-1}$. Besides, they claimed that treatments with AgNPs at a concentration of 0.5 mg. $L^{-1}$ were a successful way for reduction of the viral infectivity and partially limited the interaction of glycoprotein knobs and antibodies [118].

In another survey on the impact of size on the viral inhibition of AgNPs, Sun et al. employed AgNPs conjugated with three different capping agents: PVP, a recombinant F protein from RSV (RF 412), and Bovine Serum Albumin (BSA) to study the inhibition of RSV infection in HEp-2 cells. They reported that the PVP-coated AgNPs possess the ability of binding to the RSV surface based on a regular spatial arrangement, interact with G proteins, and distribute on the RSV envelope, and claimed that the small size (4 to 8 nm) and uniformity of PVP-coated AgNPs in comparison with other forms, may cause the effectiveness of the binding. As a result, unlike the PVP-coated AgNPs with 44% inhibition, NPs which were coated by BSA or RF 412 failed to demonstrate any significant anti-RSV properties [119].

Lu et al. analyzed the ability of AgNPs to inhibit HBV replication in HepAD38 cells using different dimensions: 10, 50, and 800 nm. AgNPs with a diameter of 800 nm were determined as highly toxic to consider antiviral while particles with a diameter of 10 nm and 50 nm demonstrated potent anti-HBV activities (80% in 10 nm and 92% in 50 nm) and minimum toxicity. They also compared the inhibitory effect of 10 nm AgNPs with 10 nm AuNPs and reported the significantly higher anti-HBV activity of AgNPs compared to AuNPs [111].

Lara et al. was another research group that confirmed the anti-HIV effectivity of AgNPs at the beginning of viral replication, their ability to disrupt the entrance of the virus, and their virucidal activity. They considered a panel of viral isolates and tested 30–50 nm-sized AgNPs against them reaching the result that IC50 of AgNPs (the concentration at which infectivity was inhibited by 50%) were placed in the domain between 440 and 910 mg. $L^{-1}$. They employed a human cervical tissue culture model to elucidate the anti-HIV-1 activity of AgNPs only 1 min after the topical treatment and this culture conserved its viral protection for 48 h, showing a long-lasting shielding effect of AgNPs. They claimed that AgNPs are a potent antiviral in the infections of both cell-free (clinical isolates, T and M tropic strains, laboratory strains, and resistant strains) and cell-associated viruses and still is a threat to HIV-1 after its entrance to the host cell [120].

Gaikwad et al. demonstrated the size-dependent interaction of AgNPs with HSV-1 and 2 and HPIV-3. In this study, the effect of some physicochemical characteristics of NPs on their inhibitory activity was evaluated. They synthesized AgNPs using different fungi and claimed that the system of nanoparticle production has a direct impact on its antiviral activity. AgNPs produced by *C. indicum* and *F. oxysporum* demonstrated the most potent inhibition, especially against HSV-1 and HPIV-3. Regarding the diameter impact on virucidal ability, they reported that *F. oxysporum* and *Curvularia* species-mediated AgNPs, with the diameter of 4–13 nm and 5–23 nm, respectively, demonstrated the most potent inhibition (80%–90%) against HSV-1 and HPIV-3 and had lower cytotoxicity to Vero cells. In contrast, 7–20 nm AgNPs synthesized by *Alternaria* and *Phoma* species, had less antiviral activity; so, smaller sized AgNPs were capable of inhibiting the viral replication. They also studied the zeta potential influence on antiviral effectivity. AgNPs synthesized by *F. oxysporum* and *Curvularia* species that were more stable (zeta potential = $-32.9$ mV and $-22.1$ mV) were reported to be more effective antivirals. Although AgNPs produced by *Alternaria* and *Phoma* possess higher zeta potential, they are weaker antiviral agents because of their larger size [110].

Elechiguerra and colleagues' study on the mechanism of interaction between AgNPs and HIV-1, revealed the size-dependent interaction and exclusive attachment of 1–10 nm-sized AgNPs to HIV-1 and introduced the exposed sulfur-containing parts of the glycoprotein knobs of HIV-1 as attractive interaction sites with AgNPs, which inhibit the virus from attaching to the MT-2 cells by preferential attachment to the gp120 glycoprotein knobs. Elechiguerra et al. also observed different trends in HIV-1 inhibition that was because of using different capping agents in the preparation process. BSA- and PVP-coated NPs, were reported to show less inhibitory effect since the surface of the nanoparticle was directly bonded to the capping agents [121].

Mori et al. prepared Ag NP/chitosan formulations possessing an average diameter of 3.5, 6.5, and 12.9 nm, with anti-H1N1 activity in MDCK infected cells. Based on the test results of all the samples, anti-H1N1 activity enhanced in a dose-dependent manner with increasing AgNps concentration. They also observed a size-dependent form that AgNPs with smaller diameters were more potent antivirals [122].

Sreekanth et al. employed 5 to 15 nm-sized AgNPs synthesized by the aqueous extract of Panax ginseng roots to investigate their virucidal effects on MDCK cells against the influenza-A virus. The results showed that AgNps were slightly antiviral with an inhibition rate of 5.31%, 4.18%, and 5.97% when used in certain amounts (0.005, 0.01, and 0.15 M). In a concentration-dependent manner, by increasing the amount of AgNPs (0.02 and 0.25 M) the inhibition of H1N1 reached 7.10% and 15.12%. The toxicity assessment of all tested samples demonstrated no threat to uninfected MDCK cells [123].

Huy et al. investigated the cytotoxicity and antiviral activity of pure AgNPs towards poliovirus. AgNPs were synthesized by electrochemical method and had a quasi-spherical shape, sized around 7.1 nm, which is lesser than poliovirus particle size (25–30 nm) facilitating the mobility and free interaction of AgNPs to viral particles, impeding them to bind to host cells. After 48 h, poliovirus infected human rhabdomyosarcoma (RD) cells treated with 3.13 ppm of AgNPs demonstrated up to 98% viability and AgNPs successfully defeated all poliovirus particles. Furthermore, it was reported that the electrochemical method produced less toxic AgNPs compared to the chemical method. Interestingly, even by using 200 ppm of AgNPs, the figures for cell viability remained high: 90% at 24 h, 87% at 48 h, and 83% at 72 h [124].

The research plan of Baram-Pinto et al. was to design mercaptoethane sulfonate-capped AgNPs (Ag-MES) based on the well-known mechanism of the binding and entrance of HSV-1 into the host cells and the interaction of HS placed on the surface of the host cell with glycoproteins of HSV envelope. AgNPs, which had no toxic effects on the host cells, aim at the virus and act as a rival to bind with cellular HS, causing disruption of the viral passage and preventing the subsequent infection. The results of the plaque reduction test in Vero cells showed that HSV-1 was disabled in the presence of Ag- MES and that's because of the multivalent nature of MES and its organized presence on the surface, which imitates HS of the host membrane and makes NPs interact with HSV-1 and prevent the infection. They also suggested using AgNP that contains numerous functional groups could be a potential way to inhibit more than one virus at a time [125].

Adenovirus type 3 (Ad3) was another target for testing the antiviral effect of AgNPs. Chen et al. revealed that AgNPs with a diameter of about 11.4 nm exhibited remarkable inhibition against Ad3 in vitro. Besides, in HeLa cells infected with AgNPs treated with Ad3 any cytopathic effect (CPE) was not visible. TEM images showed the morphologic changes in Ad3 suggesting that AgNPs altered fiber and capsid proteins and disabled them to trigger endocytosis and the rest of the infection process steps [126].

Rogers et al. ran in vitro tests to evaluate the inhibitory influence of 10–80 nm AgNPs with (Ag-PS) or without polysaccharide coating to combat monkeypox virus (MPV) infection. Among the samples, Ag-PS-25 (polysaccharide-coated, 25 nm) and Ag-NP-55 (non-coated, 55 nm) showed a significant dose-dependent influence on the mean number of plaque-forming units (PFU) and decreased them without any cytotoxicity to host cells. The 10 nm AgNPs restrained MPV infection, and the polysaccharide-coated AgNPs, 10 (AgPS-10), 25 (Ag-PS-25), and 80 (Ag-PS-80) nm nanoparticles, and Ag-PS-10 successfully reduced MPV-induced plaque formation when using in 12.5 to 100 mg. $L^{-1}$. But finally, they announced 10 nm Ag-PS at all tested concentrations as the most potent anti-MPV agent causing a statistically significant decline in MPV plaque formation [127].

Speshock et al. focused on evaluating the inhibitory effects of AgNPs against TCRV from the arenavirus family. This virus could be transmitted person-to-person by aerosols. This transmission mechanism is similar to COVID-19. Surprisingly in vitro test results demonstrated a significant decline in the TCRV RNA replication and promising infection control after treatment with AgNPs, as long as it is used within the first 2 to 4 h (early phases) of virus replication. Toxicity tests showed that uncoated 10 nm AgNPs were toxic to Vero cells in concentrations higher than 50 mg. $L^{-1}$ but significantly successful in declining viral production at 25 mg. $L^{-1}$, while polysaccharide-coated AgNPs at 100 mg. $L^{-1}$ were toxic to Vero cells, which is not a concern because 50 mg. $L^{-1}$ is a perfect dose for total inhibition of TCRV replication. Therefore, the polysaccharide coating acted in favor and against the anti-TCRV efficacy of AgNPs while protecting the host from the risk of AgNPs cytotoxicity, possibly impeding the interaction of Ag and virus particles [112].

Xiang et al. investigated another virus from the influenza virus family. They studied the inhibitory effect of AgNPs on H3N2 infection and claimed that the anti-apoptosis influence of AgNPs on host cells in case of H3N2 infection was significant. TEM photos of the H3N2 influenza viruses demonstrated viral morphologic destruction of the virus structure in a time-dependent manner from 30 min to 2 h. The minimum amount of AgNPs (12.5 mg. $L^{-1}$) caused a significant decline in HA activity compared to H3N2 control. Furthermore, the application AgNPs via the nasal route proved to be an effective treatment to enhance the post-infection survival rate in mice by restraining viral growth and pathologic lesions in the lungs [128].

#### Toxicity of AgNPs

Navarro et al. reported the negligible toxicity of AgNPs, being 7665 times less toxic than Ag ions [129]. Silver ions can endanger the cell membrane integrity by impairing the structure of the cell membrane. Furthermore, Ag ions tend to interact with thiol groups in the enzyme structure [130] and disturb the normal functioning of surface respiratory chain enzymes that are present in viral mitochondria [41]. Munger et al. evaluated the effect of AgNPs in the amount of 10 and 32 ppm in healthy humans and ran serum and urine tests to detect Ag contents. They concluded that oral administration of AgNPs in the abovementioned dosage had no adverse consequences such as morphological alterations in the heart, lungs, and abdominal organs clinical changes in human metabolic and hematologic characteristics or disorganizing pulmonary ROS, or pro-inflammatory cytokine generation in case of entering via inhalation [131]. However, the production of excess nitric oxide is an unwanted result of AgNPs mediated cytotoxicity in unsafe dosages.

### Titanium Dioxide Nanoparticles ($TiO_2$NPs)

Akhtar et al. investigated the antiviral efficiency of $TiO_2$ nano-colloids with 8 nm-sized spherical particles, which were found to be highly stable based on the measured zeta potential value (40 mv). They demonstrated inhibitory properties against the Newcastle virus (NDV). Antiviral evaluations on embryonated chicken eggs revealed antiviral activity at a minimum dose of 6.25 mg. $L^{-1}$. Authors suggested that the mechanism of anti-NDV action described as disrupting the viral envelop and spikes by causing protein and glycoprotein damage which leads to blockage of their attachment to the host cells that disables them from initiating infection [132].

Mazurkova et al. demonstrated the anti-influenza (H3N2) property of $TiO_2$NPs. $TiO_2$NPs with a diameter of about 4–10 nm were obtained by $TiCl_4$ hydrolysis. MDCK cell culture was used for the viability test of the virus against the attained NPs. The obtained results demonstrated that $TiO_2$NPs expressed inactivation action on influenza virus in a concentration of 2000 and 7000 mg. $L^{-1}$ only after 30 min incubation. Interestingly, this antiviral effect is not connected to the photocatalytic effects of these NPs. The authors also claimed that the disintegration of the virion due to the destruction of the lipoprotein membrane of the virus envelope by $TiO_2$NPs is the main mechanism of inactivation. They also proposed that inactivating action of $TiO_2$NPs toward the influenza virus is mainly based on the direct contact between NPs and viral particles. $TiO_2$NPs adhered to the external surface of the virus envelope only after 15 min of incubation making spinules glued together on the outer surface of the virus, leading to breaking the structure of the envelope. After 30 min, by increasing the level of annihilation, the virus envelope was fragmented and due to the penetration of contrasting substances into the virus vesicle, viral particles aggregated. The results revealed that $TiO_2$NPs were toxic for MDCK cell culture in the concentration above 7000 mg. $L^{-1}$ [133].

### Cerium Dioxide Nanoparticles ($CeO_2$NPs)

Lokshyn et al. studied the inhibitory effects of 2–3 nm diameter $CeO_2$NPs against influenza virus A/FM/1/47 (H1N1) and HSV-2 at different concentrations of $CeO_2$ preparation, which was varied from 1:20 to 1:1280 dilutions. They employed a colloidal chemical method to synthesize $CeO_2$NPs and the solution of $CeO_2$NPs by hydrolysis of cerium salts.

In the case of HSV-2, the virus was transferred into the culture of rabbit kidney cells (RK13) and the minimal inhibitory concentration of NPs was established as 1:80, which had high virus inhibition (inhibitory activity (logID50 = 2). Similar experiments for the case of H1N1, which were performed using the dog kidney cell culture (MDCK), demonstrated that in 1:20 to 1:80 concentration, the best inhibitory activity (logID50 = 4.0) was observed. The authors mentioned that the inhibitory properties of NPs depend on the shape, size, and concentration. However, the constitutive materials of NPs do not influence antiviral activity. They also claimed that local-field interaction of NPs and viruses result in a sharp decline in the infection levels. This inhibitory mechanism of $CeO_2$NPs can be obtained without requiring any surface modification by biomolecular covers. They also described the antiviral effect of AuNPs based on the above-mentioned process and explained the physical aspects of the mechanism of viral inhibition [134].

### Magnesium Oxide Nanoparticles (MgONPs)

Motoike et al. reported the antiviral properties of MgO in the granular form mostly in the size range of about 100 to

300 nm. It was produced from heating a natural mineral named Dolomite. Antiviral tests were performed using embryonated specific-pathogen-free (SPF) hen's egg and the heated Dolomite powder with a concentration of 0.025 mass% in water. MgO and magnesium hydroxide ($Mg(OH)_2$) powders with a purity of more than 98% were separately tested for antiviral activity. The partially hydrated MgO in comparison with fully hydrated Mg $(OH)_2$ against Influenza virus (H5N3) considerably demonstrated a higher antiviral effect [135].

Koper et al. studied the antiviral properties of halogenated nanocrystalline MgO (chlorinated MgO) powder with a crystallite size of 4 nm. It was reported that, in the concentration of 1000 mg. $L^{-1}$, chlorinated MgO completely inhibited MS2 bacteriophage, a surrogate of human enterovirus, in only 5 min exposure to contaminated water [136].

Rafiei et al. investigated the effects of under 50 nm-sized MgONPs on the Foot-and-mouth disease virus (FMDV), a member of Picornaviridae, which causes an extremely transmissible disease in cloven-hoofed animals. The maximum non-cytotoxic concentration for MgONPs is up to 250 mg. $L^{-1}$. The results of the plaque reduction assay on Razi Bovine kidney (RBK) cell line revealed that MgONPs interacted with FMDV particles that the concentrations above 50 mg. $L^{-1}$ could significantly inactivate more than 90% of the viruses at the early stages of infection, but not after penetration. They also claimed that cell-free viruses were probably more sensitive to the MgONPs [137].

## Selenium Nanoparticles (SeNPs)

Li et al. employed SeNPs with a diameter of 200 nm as both an antiviral agent and a carrier for oseltamivir (OTV) to conquer the constraint of drug-resistant viruses. OTV-loaded SeNPs, containing 0.125 mM of Se, exhibited enhanced ability to prevent H1N1 infection in MDCK cells. OTV-loaded SeNPs use these mechanisms for inactivation of the viruses: inhibiting the action of HA and NA, blockage of chromatin condensation and DNA fragmentation, suppressing ROS generation, and inducing p53 phosphorylation and Akt [138].

Lin et al. designed a co-delivery system employing surface-decorated SeNPs with zanamivir (ZNV) to inhibit H1N1 infection. Morphological analysis showed that ZNV-loaded SeNPs had a smaller average size (82 nm in comparison with 142 nm for SeNPs) and higher stability (zeta potential = − 24.5 mV for SeNPs enhanced to − 34.8 mV), which made them more proper antiviral agents. ZNV-loaded SeNPs interrupt viral binding and endocytosis by direct interaction with H1N1 viral capsid proteins. They investigated viral proliferation by evaluating cytopathic influence and determination of the amount of viral nucleic acids by RT-PCR. Treatment of host cells with ZNV-loaded SeNPs resulted in the regulation of caspase-3 and PARP protein as critical factors in the apoptosis process. Obtained results showed that ZNV modified SeNPs successfully inhibited H1N1 proliferation and a superior level of viability was observed in MDCK cells. Besides, the cellular assessments confirmed that ZNV-loaded SeNPs were more potent in decreasing H1N1 levels in MDCK cells than ZNV alone [139].

Ramya et al. synthesized spherical shape SeNPs with the size range of 100–250 nm employing *Streptomyces minutiscleroticus*. In the extracellular process of synthesis by the mentioned bacterium, it was seen that the incubation time directly affects the size of the NPs. Their antiviral activity was assessed against the dengue virus (DENV) type-1. Standard plaque assay was used for this evaluation and based on the obtained results, increasing in SeNPs dosage enhanced the antiviral activity. The optimum concentration of SeNPs was 700 ppm, which demonstrated the sharpest reduction in viral growth [140]. Liu et al. prepared SeNPs with the particle size of 200 nm employing a chemical method using $Na_2SeO_3$ solution and vitamin C as reagents and through a cellular study proved that the presence of SeNPs with the concentration of 0.25 mM inhibited the H1N1-induced apoptosis and increased the survival rate of infected MDCK cells up to 82.5% [141].

SeNPs have the potential of being a part of protective and treatment strategies on the battlefield of viral infections. However, further laboratory and clinical studies are required for moving forward in this direction [142].

## Gallium Nanoparticles (GaNPs)

Choi et al. investigated the antiviral activity of GaNPs for controlling the simultaneous HIV and *Mycobacterium tuberculosis* infection by preloading monocyte-derived macrophage (MDM) with GaNPs. It was reported to have less toxicity and even enhance the activity and efficacy of existing therapies against HIV infection. They used monocytes of healthy volunteers and synthesized GaNPs from gallium (III) meso-tetraphenylporphyrin and Poloxamer 407 (P407) pluronic polymer with the method of high-pressure homogenization resulting in rod-like shape NPs with drug loading of up to 48%, which led to sustained release of drug in 15 days. MDMs that were treated with GaNPs showed reduced interleukin (IL)-6 and IL-8 production by modifying the macrophage signaling pathways and/or due to overcoming *Mycobacterium tuberculosis* and HIV infection. GaNPs significantly inhibited the replication of both HIV and *Mycobacterium tuberculosis* with no toxicity against the MDMs in concentrations below 0.5 mM [143].

Narayanasamy et al. presented another report on the validation of macrophage targeted long-acting Ga nanoformulation against HIV-mycobacterium co-infection. The human monocytes were derived from HIV-1 and hepatitis

B seronegative volunteers employing leukapheresis. The synthesized GaNPs were rod shape and had an average size of 305 nm and can enter and stay in macrophages. GaNPs contained 48% of Ga tetraphenyl porphyrin whose sustained release ability for 15 days assured the possibility of their prolonged action. Gallium did not show cytotoxicity in the macrophage at concentrations up to 2 mM for up to 37 days [86]. There are several important enzymes in the structure of *Mycobacterium tuberculosis* that presence of Fe is a very crucial factor for their survival. They include catalases and superoxide dismutase, ribonucleotide reductase, and Fe-containing cytochromes. Replacing Ga instead of Fe in their structure is the key to inhibition for the multi-targeted GaNPs. It provided inhibition in the growth of mycobacterium and HIV following single drug loading for up to 15 days [144].

### Iron(II, III) Oxide Nanoparticles ($Fe_3O_4$ NPs)

Kumar et al. tested the inhibitory influence of glycine-coated $Fe_3O_4$ NPs with a diameter of 10–15 nm to defeat pandemic influenza PR8-H1N1. They employed monkey African green kidney (MA104) cells for plaque inhibition test and RT-PCR for determination of antiviral activity based on the observed changes in RNA transcripts of H1N1 in a 24 h timeline. The results demonstrated a decline in viral RNA (for eight-fold) after aspiration of H1N1 inoculums and incubation of infected media by addition of 2000 pg/$L^{-1}$ of $Fe_3O_4$ NPs for 72 h. The presence of only 7 pg of $Fe_3O_4$ NPs made a ≈100-fold reduction in viral transcript 24 h after infection with PR8-H1N1 (at 1.0 multiplicity of infection). This high inhibitory ability could be related to the size-dependent interaction between the virus and NPs. The molecular antiviral mechanism of $Fe_3O_4$NPs might be the Iron oxide's interaction with –SH groups of viral proteins and disrupting them [145].

Furthermore, it is worth pointing out that Fe is a key factor in the interactions of virus and host. There is a reciprocal interaction between iron and viruses like HIV, which needs chelatable Fe, as a vital component in the DNA phase of HIV replication to reach optimal efficiency [146].

### Copper Nanoparticles (CuNPs)

Copper ions have been vastly investigated as viral inhibitory agents due to their capability of suppressing a wide spectrum of enveloped and non-enveloped viruses. Cuprous ions ($Cu^+$) act as a catalyst in a Fenton-like reaction, followed by ROS formation which can be the main cause of viral toxicity of copper ions [147]. For example, ROS demonstrated vigorous antiviral influence on the influenza virus by disrupting the structure of functional proteins, such as HA and NA [56]. It takes only about 6 h for copper to inactivate $10^4$ influenza A virus particles [148]. $Cu^{2+}$, released from $CuSO_4{\cdot}5H_2O$, cannot generate hydroxyl radical (•OH), so certain nanoformulations are needed for obtaining antiviral properties [56]. In this case, CuINPs are considered efficient virus inhibitors because of their ability to continuously release $Cu^+$ ions. Due to their tendency for interacting with the cellular plasma membrane, nucleic acids, and proteins, copper ions have been considered toxic compounds to humans and most other living organisms [149].

Gledhill et al. suggested that copper can inhibit Coccolithovirus by disrupting the lytic cycle with a transcriptional block. Thus, contributes to interfering with the synthesis of DNA that ultimately inactivates the virus [150].

Therefore, copper in its metallic forms, especially in the form of NPs, can be employed as an antiviral agent, releasing copper ions in a controlled way into the infected cell cultures that ultimately inactivate viruses by the above-mentioned mechanisms [151].

#### Copper(I)Iodide Nanoparticles (CuINPs)

Fujimori et al. planned research on the possibility of employing CuINPs with an average diameter of 160 nm as antiviral agents to inhibit the H1N1 virus infection. The plaque titration assay on MDCK cells upon incubation with CuINPs showed a decrease in the viral population in a dose-dependent way and the concentration of IC50 after exposure to the virus for 60 min was about $17 \times 10^6$ mg. $L^{-1}$. $Cu^+$ produces both·OH and $O^{2-}$, resulting in the disruption of the H1N1 proteins such as HA and NA. Modification of viral proteins by myeloperoxidase resulted in antiviral activity [152], which, was confirmed in this study by sodium dodecyl-sulfate polyacrylamide gel electrophoresis (SDS-PAGE) analysis. Moreover, the authors proposed CuI, a white color compound that is more stable to air and water in comparison with other cuprous halides. It is a suitable agent for viral invasion protection without altering the appearance and color of the products such as masks, filters, and protective clothing [56].

Shionoiri et al. tested the inhibitory effect of 100–400 nm-sized CuINPs on FCV, which is non-enveloped and a well-known reason for infectious gastroenteritis. The authors declared that the presence of CuINPs without using any reducing agents led to the prolonged release of $Cu^+$ ions in aqueous solutions, which increased gradually with time. The high surface and low diameter (160 nm) of these NPs contributed to the effective $Cu^+$ release. This monovalent copper ion might involve in ROS generation, including ·OH that leads to the oxidation of amino acids in the structure of proteins in the FCV capsid. The obtained results showed that after 60 min exposure of the infected cells to 1000 mg. $L^{-1}$ of CuINPs, which can release 3.6 μM $Cu^+$ ions, the

infectivity of FCV to Crandell-Rees feline kidney (CRFK) cells reduced for seven orders of magnitude [149].

Sucipto et al. examined the inhibitory influence of copper (II) chloride dihydrate ($CuCl_2.2H_2O$) on the replication of DENV-2 in African green monkey kidney cell culture. DENV-2 is a mosquito-borne arbovirus that acute systemic diseases are the main consequence of its invasion of the human body. The maximum inhibitory concentration (IC50) of $CuCl_2.2H_2O$ against DENV-2 was 0.13 mg. $L^{-1}$. Inhibition of viral replication enzymes like RNA polymerases and formation of the complex with RNA introduced as the probable antiviral mechanism of $CuCl_2.2H_2O$ [153].

### Copper (II) Oxide Nanoparticles (CuONPs)

Borkow et al. employed copper (II) oxide-impregnated polypropylene (PP) fiber as a mean of viral filtration in contaminated liquids. They designed round-shaped two-layer filters. The upper layer with a diameter of 5 cm and thickness of 2 cm, consists of 500 mg nonwoven mesh made of 5%(wt/wt) CuO, loaded into fibers of PP. The bottom layer had a thickness of 0.2 cm consisting of 100 mg of nonwoven fibers made of activated carbon to entrap released copper particulates and ions from the first layer during the process of filtration.

The filter was tested by passaging solutions that were contaminated by 12 different enveloped and non-enveloped viruses. The results showed a significant decline in the viral titers, ranging from 0.47 $\log_{10}$ to 4.6 $\log_{10}$, varying from one viral strain to another (Table 1).

As exhibited in Table 1, the reduction of viral titer was insignificant for Rhinovirus 2 (HGP), Punta Toro virus (Adames), Pichinde virus (AN 4763), and Vaccinia virus (WR), which demonstrate that there was no correlation between susceptibility of the virus to CuO and items such as family, being enveloped or not, or containing RNA or DNA genome because the mechanism of antiviral action is damaging the key viral component, such as inactivating HIV-1 protease as an essential protein for viral replication, during the process of filtration. The filtration tests also showed a reduction in the flow rate could lead to a further reduction in the viral infection level. In the case of HIV-1, flow rate decline (2.5-fold), contributed to achieving a 1.7-fold rise in neutralization. Preliminary data indicated that the CuO-containing filters did not destroy the red blood cells and factor of coagulation in plasma [154].

A while after that, Borkow led another survey based on the former study to design a practical filtration system against HIV-1 transmittance via breastfeeding and infected blood donations. For achieving this purpose, culture media of HIV-1 spiked cells such as PBMCs, cMAGI, U937, MT2, and H9 + cell lines were placed in contact with CuO in the form of powder or CuO-loaded fibers or passed through filters made of the mentioned fibers. The levels of viral infection were determined in all of the mentioned treatments. The authors designed two-layered filters, including CuO powder in the upper layer and activated carbon for the second one that can absorb released CuO particles from the upper layer in the filtration process. However, the reduction of the flow rate was an unwanted outcome. To overcome this problem, they loaded the CuO particles on the PP fibers. The final filter was safe for the tested cells and successfully decreased the infection level by 99.9% in all samples: twelve wild-types, drug-resistant clinical or laboratory, T-cell-tropic and macrophage-tropic, clade A, B, or C, HIV-1 isolates [155].

Inspired by this filtering system, Borkow et al. designed a facemask including three non-woven layers of CuO incorporated PP fibers as a respiratory protector against human influenza A virus (H1N1) and avian influenza virus (H9N2). The facemask was capable of filtrating more than 99.85%

**Table 1** Detailed information about tested viral titers and reduction by CuO-containing filters [149]

| Virus (viral strain) | Enveloped (N)/nonenveloped (NE) | Genome | Cells used in assay | $\log_{10}$ reduction (mean ± SD) | *P*-value |
|---|---|---|---|---|---|
| Rhinovirus 2 (HGP) | NE | RNA | HeLa Ohio-1 | 2 ± 1.7 | 0.2 |
| Yellow fever virus (17D) | E | RNA | Vero-76 | 1.1 ± 0.5 | < 0.05 |
| Influenza A virus (Panama/2007/99 H3N2) | E | RNA | MDCK | 1.77 ± 0.87 | < 0.001 |
| Measles virus (Chicago) | E | RNA | CV-1 | ≥ 3.67 | < 0.001 |
| Respiratory syncytial Virus (A2) | E | RNA | MA-104 | 1.5 ± 0.5 | < 0.01 |
| Parainfluenza virus 3 (14,702) | E | RNA | MA-104 | 1.11 ± 0.5 | < 0.05 |
| Punta Toro virus (Adames) | E | RNA | LLC-MK2 | 1.73 ± 1.55 | 0.09 |
| Pichinde virus (AN 4763) | E | RNA | BSC-1 | 1.7 ± 1.47 | 0.08 |
| HIV-1 (IIIB) | E | RNA | MT2 | 4.6 ± 0.6 | 0.001 |
| Adenovirus type 1 (Ad-HIVluc) | NE | DNA | cMAGI | 2.2 ± 0.36 | 0.001 |
| Cytomegalovirus (AD169) | E | DNA | Fibroblasts | 4.3 ± 0.26 | < 0.001 |
| Vaccinia virus (WR) | E | DNA | Vero-76 | 0.47 ± 0.45 | 0.095 |

of aerosolized viruses under breathing conditions (28.3 $L.min^{-1}$) and demonstrated biocidal effects on the remaining viral particles in the mask without altering the physical barrier properties. Thirty minutes after passing the aerosolized viruses through the mask, no viral titer of H1N1 and H9N2 were recovered from the CuO-loaded face masks, while about ordinary masks, $4.67 \pm 1.35$ $\log_{10}$ 50% tissue culture infective doses ($TCID_{50}$) and $5.03 \pm 0.54$ $\log_{10}TCID_{50}$ infectious titers were recovered for H1N1 and H9N2, respectively.

Under simulated breathing conditions, copper elution to the air from the CuO-loaded masks in 5 h was $0.467 \pm 0.47$ pg, which was $> 10^5$ folds below the reference range of respiratory copper permissible exposure limit. And in the worst possible condition, if the facemask is soaked in saliva, the amount of copper elution would be 7.24 mg. $h^{-1}$, significantly lower than the reference level of oral exposure for a 50 kg weighted person (20.8 $mg.h^{-1}$). Besides, the incorporation of 2.2% CuO in the outer layers of the masks didn't sensitize or irritate the animal skin model [156].

Hang et al. explored the antiviral influence of $45.4 \pm 6.8$ nm-sized CuONPs on the Hepatitis C Virus (HCV) using Huh7 cells (Huh7 CD81 −) in the cellular culture. The results demonstrated that at non-toxic concentrations ($\leq 16$ mg. $L^{-1}$) CuONPs had inactivating ability against HCV and can block the virus in the stages of binding and entry but did not show any significant inhibitory effect on infectious viral particles in HCV cell culture and also were not able to reduce the level of HCV genome in the subgenomic replicon cells [157].

Yugandhar et al. synthesized 2–69 nm-sized CuONPs using *Syzygium alternifolium* fruit extract and employed them as a viral inhibitory agent against Newcastle Disease Virus (NDV). The efficacy of CuONPs examined by the hemagglutination (HA) test and embryonic development and viability of 0-day laid eggs treated with NDV were continuously observed for 96 h. The results of in ovo-antiviral activity tests demonstrated that CuONPs had significant antiviral activity against NDV in the concentrations of 100 mg. $L^{-1}$ [158].

Tavakoli et al. examined the antiviral effects of CuONPs on HSV-1 infection. The presence of HSV-1 infected African green monkey kidney cells exposed to the non-toxic dosage (100 mg. $L^{-1}$) of 40 nm-sized CuONPs resulted in a 2.8 log10 TCID50 decline in viral concentration (83.3%) compared with viral control ($P < 0.0001$). The enhancement of CuONPs concentration to 140 mg. $L^{-1}$, led to the reduction of the cell viability to 63.07%. The authors suggested that disorganizing capsid integrity and disruption of the HSV-1 genome due to the presence of CuONPs could be the possible antiviral mechanism of action [159].

**Toxicity of CuONPs** Exceeding the intake of CuNPs, through the means like ingestion or inhalation may have toxic effects in different parts of the human body, like the respiratory tract, gastrointestinal tract, and other tissues [160], which is more serious in the case of using NPs than microparticles, because the penetration of NPs is easier through the skin or by means of inhalation and ingestion [161] which contributes to pathological damage to liver, kidney, spleen and even central nervous system [43], especially in higher concentrations and smaller nano-sizes. Based on an in vivo toxicity assessment on mice, the median lethal dose ($LD_{50}$) for oral gavage exposure of CuNPs with the size of 23.5 nm, microparticles sized 17 μm and, $Cu^{2+}$ ions with the approximate size of 0.072 nm emitted from ($CuCl_2{\cdot}2H_2O$) reported to be 413, > 5,000 and 110 mg/kg body weight, respectively. Considering Hodge and Sterner Scale, the toxicity of copper in both forms of nanoparticle or ion was in class 3 (moderately toxic), and for micro-copper was in class 5 (practically non-toxic) [160].

The toxicity of CuONPs in lung tissues, which occurs by the inhalation route is one of the most significant concerns in human safety. Even in the case of intravenous injection, it was observed that CuO was mostly localized in the lung and spleen [42].

There have been some in vitro and in vivo surveys so far, to investigate the mechanisms of CuONPs' adverse effects, especially on the human lung cells. Before beginning toxicity surveys, physicochemical properties of NPs such as morphology, size, crystal structure, surface chemistry, and purity, should be properly characterized.

In vitro studies have indicated that CuONPs, mostly in the size of 20–50 nm, are capable to induce cytotoxicity through autophagy [162], genotoxicity [163, 164], DNA damage, and alteration in the expression of specific genes [165–170], ROS-mediated apoptosis [165–167] and oxidative stress [55, 164, 171, 172] in respiratory system cells.

Sun et al. reported that the toxicity of CuONPs to human lung epithelial A549 cells is more than other popular metal oxide NPs and carbon NPs and nanotubes [162].

Although the association between the release of Cu ions from the structure of CuNPs has been reported before [169, 171], some other investigations demonstrated that the dissolved portion of Cu ions is insufficient for triggering the cytotoxicity reactions and suggested that in case of using CuO, the toxicity is mostly caused by the exposure of cells to CuO rather than released Cu ions from the NPs' structure [166]. In some cases, the contribution of dissolved Cu ions was less than 50% of the total observed cytotoxicity [167, 170].

In vivo studies on male wistar albino rats demonstrated that after CuO NP exposure, the number of antioxidant enzymes including superoxide dismutase and catalase was lower in lung tissue homogenate and histopathological tests showed the formation of fibrosis and granuloma in rat lungs [40].

Cho et al. observed acute and chronic inflammatory responses in female wistar rats, 24 h and 4 weeks after Intratracheal instillation of under 50 nm CuONPs [173].

Intratracheal instillation of 0.5 mg/rat of 33 nm CuONPs, induced neoplastic lesions in F344 male rats [174]. The same rats demonstrated a severe inflammatory response after treatment with a dose of 2 mg/rat of the 33 nm CuONPs for 28 days [175]. Further investigations are required to study the in vivo responses in lung tissue after inhalation of CuONPs.

#### Other Copper Containing Formulations

In one of the trials with the aim of suppressing HSV-1, Sagripanti et al. used a combination of Cu (II) and ascorbate. The results showed that treating HSV-infected African green monkey kidney cells with Cu (II) and ascorbate reduced HSV-1 plaque formation to less than 0.006% of the initial viral population while maintaining 30% viability for the host cells. The authors suggested that the mechanism of inactivation of HSV using copper is similar to copper-mediated DNA damage. Despite the observed antiviral effects, considering the reported 70% cellular cytotoxicity, the antiviral effect of this formulation against HSV is not acceptable and requires modifications [176].

Miyamoto et al. examined the anti-influenza effect of thujaplicin–copper chelates. Thujaplicin is a chemical extract from the wood-heart of the cedar tree and the combination of its isomers with other metal chelates like iron and magnesium was tested separately against the different types of influenza virus such as H1N1, H2N2, and H3N2. The results indicated that thujaplicin–copper chelates with the minimum effective concentration of 5 mM, had an inhibitory effect on influenza-induced apoptosis in MDCK cells. This property was independent of the subtype or types of the influenza virus and could occur 2 to 4 h after infection. Other metal chelates did not show any inhibitory effect against the mentioned types of the virus [177].

Borkow et al. suggested the application of copper, as an effective metallic agent with antiviral properties against a vast majority of viruses, in the structure of antiviral gloves and filters using Latex and fibers impregnated with copper for prevention of transmission and deactivation of HIV-1. They also determined the skin-sensitizing properties of these products by irritation tests on guinea pig and rabbit skin [178].

Imai et al. incorporated 0.5 $g.m^{-2}$ $Cu^{2+}$ ions in a cotton textile (CuZeo-textile) to determine the capability of this compound to inhibit influenza virus H5 subtypes. They employed RT-PCR to detect the virus genes and embryonated chicken eggs for histopathological and immunohistochemical examinations on vascular endothelial cells of the heart, liver, lung, brain, spleen, and kidney. The results demonstrated the effective inactivation of extremely pathogenic H5N1 and minor pathogenic H5N3 subtypes in MDCK cells exposed to CuZeo-textile even in case of a brief incubation time. All the CuZeo-textile treated embryos inoculated with Ck/Yamaguchi/7/04 AF virus survived during the observation period and no noteworthy histological lesions were detected in embryos (whether dead or alive) and no antigens were observed in surviving embryos treated on the CuZeo-textile. It is well known that the presence of certain compounds like feces or mucosal secretions enhances the resistance of the virus to the physicochemical agents. Surprisingly, even with fetal bovine serum (FBS) and feces in the media, CuZeo-textile demonstrated a fast and intensified inhibitory impact on H5N1. Such properties will be helpful in actual applications and guarantee the applicability of CuZeo-textile in comprehensive healthcare items including protective masks, clothes, and gloves [179].

Bleichert et al. examined the intrinsic ability of the copper surface to inactivate viruses by testing MPV and VACV. They employed African green monkey kidney cells for all viral experiments. The results showed that in the presence of copper the VACV as well as extremely pathogenic MPXV were killed in less than 3 min(termed as contact-killing). On the contrary, stainless-steel surface contributed to a small decrease in viable viruses even after 30 min exposure [180].

Previous studies reported that copper surfaces are capable of inactivating a variety of human viruses e.g., influenza A and Norovirus [148, 181].

The contact-killing of viruses employing nanocopper surfaces is more efficient than conventional copper. Therefore, Sundberg et al. used the cold spray method to design a surface by depositing nanocopper powder on aluminum substrates. High cold spray velocity (600–1000 $m.s^{-1}$) impact on the copper powder leads to the formation of a low porosity coating (< 1%). The viral test results on MDCK cells demonstrated that nanocopper reduced 99.3% of the influenza A virus titer. The authors also suggested that the roughness of the copper surface can contribute to enhancing the contact-killing ability of nanocopper against influenza A [182].

Gordon et al., with the aim of finding a more effective inactivating method against amantadine-resistant S31N M2 mutation of influenza A, examined the possibility of blockage of the M2 channels of this virus by copper complexes. The results demonstrated that copper in the form of $Cu^{2+}$ made tight binding and adhered to M2 channels. So, the copper complexes, while reducing the cytotoxicity of $Cu^{2+}$ by about tenfold, could significantly decrease the infection of MDCK cells that were infected with three IAV strains, two of which were amantadine-insensitive and the other one was amantadine-sensitive [183].

To conclude this session, it would be helpful to consider an investigation by Sunada et al. They have done a

comparative study about the antiviral properties of the solid-state copper-containing compounds such as cuprous and cupric chloride, oxide, and sulfide particles. The obtained results showed that cuprous compounds such as Copper(I) oxide ($Cu_2O$) with the diameter of 0.5–5 μm, 4–95 μm sized $Cu_2S$, CuCl and CuI (size was not mentioned) have demonstrated a much higher reduction in the titers of bacteriophage Qß ($\log_{10}(N/N0) = -5.8, -4.6, -6.6$, and $-6.0$, respectively) in comparison with cupric compounds. Therefore, solid-state cuprous compounds had an extremely potent inhibitory influence, whereas cupric compounds exhibited mild inhibition. The mentioned results introduced the oxidation states as the major factor leading to a large difference in the antiviral activity of copper compounds regardless if they are oxides, sulfides, or halides. The authors also suggested that the deactivation of viruses by solid-state compounds is predominantly triggered by the direct contact of the virus and the surface of copper-containing compounds, which leads to denaturation or degradation of biomolecules like viral proteins, leading to their suppression. They employed enzyme activity measurement for alkaline phosphatase as a model enzyme to examine the denaturation of proteins. The results showed that the adsorption and denaturation abilities of $Cu_2O$ were extremely more than CuO. So, $Cu_2O$ adsorbed and denatured more proteins than CuO, which contributed to the higher antiviral activity of $Cu_2O$, which approved the above-mentioned results. They also reported that ROS and leached copper ions from $Cu_2O$ and other cuprous compounds didn't contribute to their antiviral activity, which is in contradiction with the findings of the above-mentioned essays [184]. Table 2 shows a comprehensive list of antiviral properties for most extensively used metal and metal oxide NPs.

## Polymers with Intrinsic Antiviral Property

### Natural Polymers

#### Alginate

Some of the natural polymers have strong intrinsic inhibitory activity against viruses, such as alginate, which based on the report by Yoh Sano is capable of inhibiting tobacco mosaic virus (TMV) infection in this plant and the strength of inhibitory effect relates to the stiffness of polymer chain of alginate. Sano also reported that the addition of alginate led to forming large aggregates of TMV. The antiviral activity of this natural polymer is probably because of blocking the decapsulation process in the proteins of the membrane surface and compromising the structure of TMV cells [187].

#### Chitosan

Chitosan (deacetylated chitin) is another natural polymer with unique biological activities such as the ability to prevent viral infection in plants and animal cells and even inhibition of phage infection in infected microbial cultures. This polymer has also been widely used as a promising carrier in drug delivery [188, 189]. Amending the natural chemical characteristics of the chitosan molecule and modification of its physicochemical properties including the positive charge, the mean polymerization degree, and the degree of N-deacetylation have a strong impact on its antiviral activity.

Chitosan stimulates the functional performance of the auxiliary cells such as macrophages and granulocytes, which involve in immune responses by releasing related mediators like IL-1 that led to triggering the T-helpers' proliferation. The abovementioned process as well as the ability of chitosan and chitin to induce the synthesis of interferon, which is known for the prevention of virus replication by the deterioration of the translation ability of the genomic RNAs or early viral mRNAs [190], are crucial in inhibition of virus-mediated infection of the cells (Fig. 5).

The interaction of chitosan with the surface of cells is partly similar to the observed process during the interaction of chitosan and plant plasma membrane, which leads to increasing the permeability of cell membrane and non-specific binding of polycationic chitosan molecules ultimately causing destruction of the cell membrane. Although chitosan and its derivatives are capable of viral inhibition in the various biological systems, the mechanism of retroviral suppression in animal cells by anionic chitosan is different from the mode of action of polycationic chitosan molecules for inhibition of viral infection in plants and phages [191].

Chitosan can accelerate the induction stage of immune responses, for example, in mice, the generation of certain antibodies (IgA and IgG) stimulated by chitosan along with purified HA and NA, directly increase the local and systemic immune responses (Fig. 5) to influenza virus type A (Texas H1N1) and B (Panama) [192]. Besides, sulfated derivatives of chitosan have the specific ability of replication inhibition of retroviruses, such as N-carboxymethyl chitosan-N, O-sulfate that act as an inhibitor in the process of virus-specific proteins synthesis by blocking the interactions of glycoprotein receptors in viral coat and impedes the replication of HIV-1 by the competitive suppression of HIV-1 reverse transcriptase in a culture of T-cells and Rausher murine leukemia virus in mouse fibroblasts culture. Interestingly, no cytotoxicity caused by this chitosan derivative was not observed in these cell cultures [193].

**Table 2** Summary of the literature review on antiviral properties of metal and metal oxide NPs

| Antiviral agent | Average size (nm) | Characteristics of NPs | Virus | Type of the study | References |
|---|---|---|---|---|---|
| AuNPs | 2.4 | Stabilized in carbosilane dendrons | HIV-1 | Cellular | [95] |
| AuNPs | 2 | Coated with sulfate-ended ligands | HIV-1 | Cellular | [96] |
| AuNPs | 40 | Coated with Bis(p-sulfonatophenyl) phenylphosphine dihydrate dipotassium salt (BSPP) | SARS-CoV | In vivo | [2] |
| AuNPs | 2 | Capped with mercaptoethanesulfonate | HIV-1 | Cellular | [97] |
| AuNPs | 4 | Capped with mercaptoethanesulfonate | HSV-1 | Cellular | [98] |
| AuNPs | 15 | Capped with mercaptoethanesulfonate | HSV, HPV, RSV, dengue and lenti virus | In vitro | [98] |
| AuNPs | 3.5 | Assembled on the layered double hydroxide nanoparticles' surface | HBV | Cellular | [100] |
| AuNPs | 5–20 | Coated with $SiO_2$ shell and placed on the 50–200 nm sized $SiO_2$ NPs as a carrier | Adenovirus | Cellular | [64] |
| AuNPs | 17 | Stabilized with polyethylene glycol | HIV-1 | Cellular | [185] |
| AuNPs | 2 and 14 | Functionalized with sialic acid (SA)-terminate glycerol dendron | Influenza A | Cellular | [102] |
| ZnO inter connected micro-nano structures | Thickness of 100–500 and length of 1000–5000 | Capped with multiple nanoscopic spikes | HSV-1 | Cellular and in vivo | [104] |
| ZnONPs | 20–50 | Naked and/or coated with polyethylene glycol | Influenza H1N1 | In vitro | [105] |
| ZnONPs | 20–50 | Coated with polyethylene glycol | HSV-1 | Cellular | [106] |
| ZnONPs | 5 and 7 | NPs were used as scaffolds for Hydroxyl group, oleic acid and, chitosan | HSV-1 | In vitro | [107] |
| ZnO tetrapod micro-nano structures | Thickness of 200–1000 of and length of 5000–30,000 | Structured with Polyvinyl Butyrol | HSV-2 | Cellular | [108] |
| AgNPs | 30–50 | Capped with poly (N-vinyl-2-pyrrolidone) | HIV-1 | Cellular | [115] |
| AgNPs | $7 \pm 3$ | Incorporated in PHBV18 electrospun fibers | FCV and MNV | Cellular | [116] |
| AgNPs | 10 | – | Influenza H1N1 | Cellular | [117] |
| AgNPs | – | – | Influenza H1N1 | In vitro | [118] |
| AgNPs | 4–8 | Conjugated with: PVP, BSA and, a recombinant F protein | RSV | In vitro | [186] |
| AgNPs | 10, 50, and 800 nm | – | HBV | Cellular | [111] |
| AgNPs | 30–50 | – | HIV-1 | In vitro | [120] |
| AgNPs | 4–13<br>5–23<br>7–20 | Synthesized by different groups of fungi | HSV-1 and HPIV-3 | In vitro | [110] |
| AgNPs | 3.5, 6.5 and, 12.9 | Prepared in the form of composite with chitosan | Influenza H1N1 | Cellular | [122] |

**Table 2** (continued)

| Antiviral agent | Average size (nm) | Characteristics of NPs | Virus | Type of the study | References |
|---|---|---|---|---|---|
| AgNPs | 1–10 | Coated with BSA and/or PVP | HIV-1 | Cellular | [121] |
| AgNPs | 5–15 | Synthesized by using Panax ginseng roots extract | Influenza A | Cellular | [123] |
| AgNPs | 7.1 | Electrochemically synthesized in the presence of trisodium citrate | Poliovirus type 1 | Cellular | [124] |
| AgNPs | 4 ± 1 | Capped with mercaptoethane sulfonate | HSV-1 | Cellular | [125] |
| AgNPs | 11.4 | – | Adenovirus type 3 | In vitro | [126] |
| AgNPs | 10,25, 55,80 | Naked and/or coated with polysaccharide coating | MPV | In vitro | [127] |
| AgNPs | 10 | Naked and/or coated with polysaccharide coating | Tacaribe virus | In vitro | [112] |
| AgNPs | 9.5 | – | Influenza H3N2 | In vitro and in vivo | [128] |
| $TiO_2$NPs | 8 | – | NDV | In vitro | [132] |
| $TiO_2$NPs | 4–10 | Synthesized by hydrolysis of $TiCl_4$ | Influenza H3N2 | Cellular | [133] |
| $CeO_2$NPs | 2–3 | – | Influenza H1N1 and HSV-2 | Cellular | [134] |
| MgONPs | 100–300 | Synthesized by thermal decomposition of Dolomite powder | Influenza H5N3 | In vitro | [135] |
| MgONPs | 4 | With nanocrystalline structure in the complexed form of chlorinated MgO | Human enterovirus | In vitro | [136] |
| MgONPs | 40 | – | FMDV | Cellular | [137] |
| SeNPs | 200 | NPs carry oseltamivir | Influenza H1N1 | In vitro | [138] |
| SeNPs | 82 | surface-decorated with zanamivir | Influenza H1N1 | In vitro | [139] |
| SeNPs | 100–250 | Synthesized by *Streptomyces minutiscleroticus* | DENV-1- | In vitro | [140] |
| GaNPs | – | Synthesized by high-pressure homogenization technique from gallium (III) meso-tetraphenylporphyrin and P407 pluronic polymer | HIV and *Mycobacterium tuberculosis* coinfection | In vitro | [143] |
| GaNPs | 305 | Synthesized by high-pressure homogenization technique from gallium (III) meso-tetraphenylporphyrin and P407 pluronic polymer | HIV and *Mycobacterium tuberculosis* coinfection | In vitro | [144] |
| $Fe_3O_4$NPs | 10–15 | Coated with glycine | Influenza H1N1 | In vitro | [145] |
| CuINPs | 160 | – | Influenza H1N1 | In vitro | [56] |
| CuINPs | 100–400 | – | FCV | In vitro | [149] |
| Copper (II) chloride Dihydrate | – | – | DENV-2 | Cellular | [153] |
| CuO particles | – | Loaded in the structure polypropylene fibers | HIV-1, RSV, Adenovirus type-1, Influenza H3N2, Cytomegalovirus, Parainfluenza virus 3 | Cellular | [154] |

**Table 2** (continued)

| Antiviral agent | Average size (nm) | Characteristics of NPs | Virus | Type of the study | References |
|---|---|---|---|---|---|
| CuO particles | – | Loaded in the structure polypropylene fibers | HIV-1 | Cellular | [155] |
| CuO particles | – | Loaded in the structure polypropylene fibers | Influenza H1N1 and H9N2 | In vitro | [156] |
| CuONPs | 45.4 ± 6.8 | – | HCV | Cellular | [157] |
| CuONPs | 2–69 | Synthesized by using Syzygium alternifolium fruit extract | NDV | In vivo | [158] |
| CuONPs | 40 | – | HSV-1 | Cellular | [159] |
| Cu (II) | – | In combination with ascorbate | HSV-1 | Cellular | [176] |
| Copper | – | Chelated with thujaplicin | Influenza H1N1, H2N2, and H3N2 | Cellular | [177] |
| Copper | – | Loaded in cotton fibers, latex, or polyester | HIV-1 | In vitro | [178] |
| Cu (II) | – | Loaded in zeolite and incorporated into cotton textiles | Influenza H5N1 and H5N3 | Cellular | [179] |
| Copper coupons | – | – | MPXV and VACV | Cellular | [180] |
| Nano copper surface | 25,000 | – | Influenza A | In vitro | [182] |
| Copper complexes | – | Cu(cyclooctylamineimino diacetate) and $Cucl_2$ | Influenza A | Cellular | [183] |
| Cuprous compounds | 500–5,000<br>4,000–95,000 | $Cu_2O$, $Cu_2S$, CuCl and, CuI | Bacteriophage Qß | In vitro | [184] |

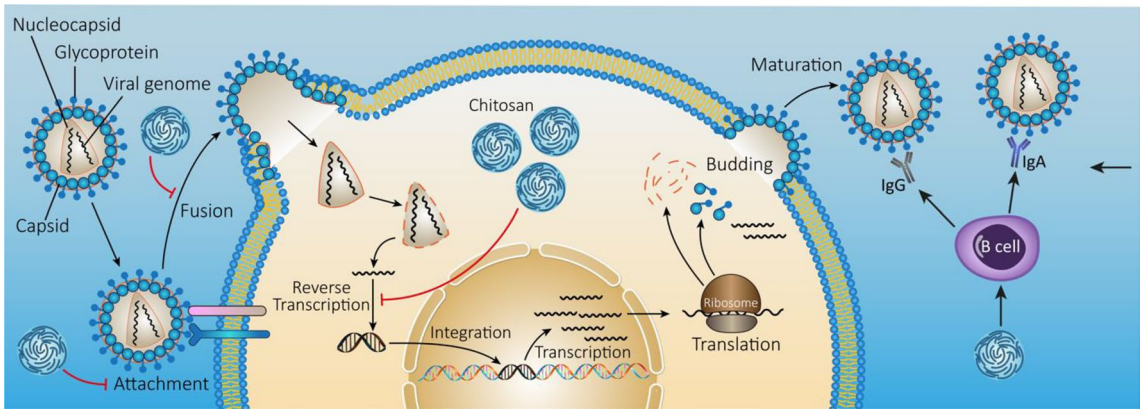


**Fig. 5** Interference of chitosan with different phases of the viral cycle inside and outside of the host cells

## Marine-Based Polymers

Recently, a vast majority of bioactive extracts that belong to marine-based polymers have been known to possess antiviral activity, especially against HIV-1. Brown algae are one of the potential sources of these anti-HIV-1 agents, for example, contain a high concentration of phlorotannins, which are bioactive polymers from phloroglucinol (1,3,5-trihydroxybenzene) units and reported to demonstrate anti-HIV activity along with 8,8'-bieckol and 8,4'''-dieckol by suppressing protease and reverse transcriptase of HIV-1 [194].

Marine algae, as the main source of sulfated polysaccharides (SPs), are known as the potent replication inhibitor to enveloped viruses such as rhabdovirus, arenavirus, flavivirus, herpesvirus families, togavirus, and orthopoxvirus [195]. SPs might also inhibit the viral attachment to the target cell surface molecules. In vitro evaluations of the protective effects of sulfated glucuronogalactan, another

member of SPs, which was extracted from red algae Schizymenia dubyi, against the virus-induced cytopathogenicity demonstrated that in the amount of 5 mg. $L^{-1}$, the mentioned polysaccharide is capable to fully suppress the syncytial formation of HIV-1 in MT4 cells without causing cytotoxicity. This is suggested to be attributed to the inhibition of the HIV-host cell binding in the early step of the infection [196]. Lectins or carbohydrate-binding proteins are other groups of bioactive compounds, which are found in different species such as algae, fungi, plants, etc., and are able to impede HIV-host cell attachment and prevent viral infection [197]. Bioactive peptides originated from the hydrolysis of marine proteins, introduced as the anti-HIV agents in the previous articles, and can be enzymatically extracted from different species of Oyster and Marine sponges. Callipeltin A is one of these novel antiviral agents derived from *Callipelta* sponge, a cyclic depsidecapeptide that based on the findings of in vivo experiments on CEM4 lymphocytic cell lines, is able to inhibit the cytopathic effects induced by HIV-1 at an ED50 value of 0.01 mg. $L^{-1}$ [198].

### Nucleic Acid Polymers

Another member of the class of natural antiviral polymers is nucleic acid polymers (NAPs), which have a vast inhibitory effect due to the amphipathic properties of phosphorothioated oligonucleotides. In vivo experiments on HBV infected ducks [199] as well as in research on patients [200] confirmed the hypothesis of disruption of viral surface antigens by NAPs released from infected hepatocytes through a non-immunostimulatory mechanism inside the infected cells (Fig. 6), which encouraged them to employ NAP therapy in chronic HBV infection that decreased the amount of those antigens in serum.

### Derivatives of Dextran

Neyts et al. investigated the antiviral activity of several water-soluble derivatives of dextran (poly (α, 1–6) glucose), which contained various amounts of carboxymethyl, benzylamide, and sulfonate groups against the enveloped and non-enveloped viruses. They inoculated confluent cultures of Vero, HeLa, or human embryonic skin-muscle ($E_6$SM) cells with the viruses and also used human embryonic lung (HEL) fibroblasts, MDCK cells, and MT4 cells specifically for the evaluation of human cytomegalovirus (HCMV), influenza A and B, and HIV, respectively. The results of the antiviral assessments demonstrated that most of the above-mentioned polymers had a potent and selective inhibitory influence on various types of enveloped viruses, such as HCMV, HSV-1, HSV-2, RSV, HIV-1, and HIV-2 but not against non-enveloped ones. To be more specific, RSV, HIV, and HCMV were generally more fragile than HSV in treatments based on derivatized polymers. Interestingly, the presence of excessive amounts of benzylamide and benzylamide sulfonate groups in the polymer mixture empowers the treatment to defeat HSV. The inhibitory mechanism of the polymeric compounds against retroviruses such as HIV and herpes viruses like HCMV is ascribed to the inhibition of the beginning phase of the replicative cycle, which is virus-cell binding. In detail, these compounds suppress HIV-$CD4^+$ cell binding, shield off the V3 loop of HIV-1 gp120, and impede gp120 from attaching to the CD4 receptor [201].

Based on the previous studies [202], Heparan sulfate (HS), which is present on the cell surface is known as the initial interaction site between herpesviruses (e.g., HCMV and HSV) and the host. Therefore, heparin and other carboxylated and sulfated polymers can disrupt this interaction by attaching to positively charged sites of the viral envelope, crucial for binding to the anionic HS proteoglycan component of the cell surface.

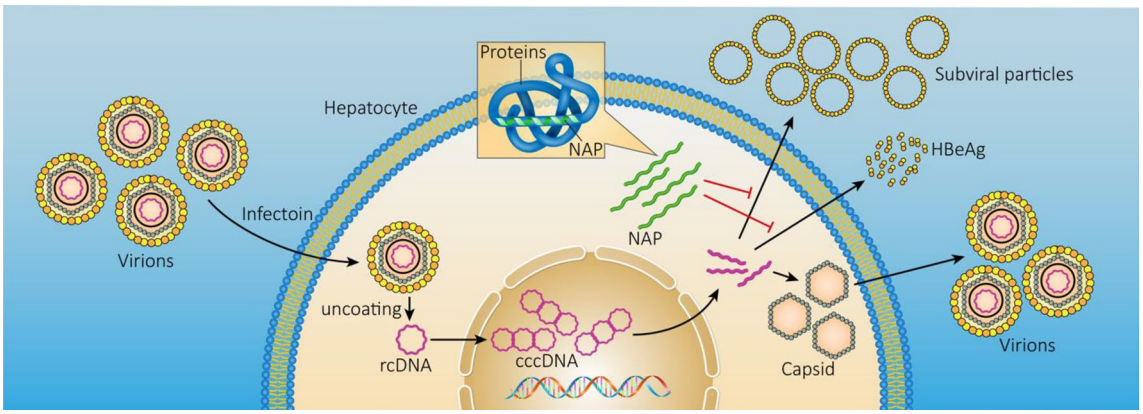


**Fig. 6** Therapeutic effect of NAP against HBV infection: impeding the secretion of viral antigen HBsAg and rapid clearance of HBsAg, increasing anti-HBsAg antibodies titers, transcriptionally inactivating closed circular DNA (cccDNA) and reducing copy number

### Cellulose and its Derivatives

Yamamoto et al. investigated the anti-HIV effect of cellulose and branched cellulose with the side chains of D-glucopyranose or D-galactopyranose sulfated with piperidine N-sulfonic acid or $S0_3$-dimethylformamide complex. The results of in vivo experiments on infected MT-4 cells demonstrated that during the six days of incubation, cell cultures containing sulfated polysaccharides derived from cellulose in the concentrations higher than 10 mg. $L^{-1}$, were viable but, in the absence of these biopolymers, all MT-4 cells were dead on the sixth day. The mechanism of antiviral action of these biopolymers is suggested to be due to their inhibitory effects in the process of viral binding with MT-4 cells [203].

Previous literature mentioned that cellulose acetate phthalate (CAP) possesses in vitro inhibitory ability against HCMV, HSV-1, HSV-2, and HIV [204]. Gyotoku et al. formulated CAP with colloidal silicon dioxide and topically applied it through the vaginal route of Swiss-Webster female mice to evaluate the anti-HSV-2 properties of the CAP in vivo. The results revealed that CAP exhibited an anti-HSV-2 effect in genital infection of mouse models when formulated in an appropriate way. CAP significantly reduces the chance of HIV-2 incidence and death due to severe infection even at a 1:20 dilution, but in animals with the developed disease, CAP was not capable to decrease the severity of the lesions, which suggests that CAP acted prophylactically [205].

In another study, the antiviral potential of CAP against HIV-1 with more focus on recognition of binding sites employing enzyme-linked immunoassays and flow cytometry was investigated. In vitro antiviral tests demonstrated that the potent attachment of CAP to HIV-1 hindered the accessibility of the virus to antibodies against the gp120 V3 loop that is involved in coreceptor binding. Other than the mentioned binding site, CAP binds to the envelope glycoprotein gp120 resulting in suppression of the HIV-1 infection. The industrial availability, non-toxicity and safety, and inactivating HIV-1 rather than causing reversible inhibition, made CAP an appropriate compound for intra-vaginal application to prevent HIV-1 transmission [206].

### Proanthocyanidin Polymers

In an invention, by Tempesta et al., a plant-based polymer isolated from Croton or Calophyllum species was introduced as a potent antiviral agent with an inhibitory effect against various types of RSV and herpes viruses, which is appropriate for prophylaxis in systemic and localized (such as topical) applications by a variety of administration routes, like oral, topical, parenteral, or by inhalation. Proanthocyanidin polymers contain 2 to 30 flavonoid units such as catechins, flavanols, anthocyanidins, etc. They are water-soluble and can easily be formulated with very low toxicity and no teratogenicity. Two groups of experiments, cellular and in vivo, were performed to determine the antiviral effect of the proanthocyanidin polymer A, which was extracted from *Calophyllum inophyllum*. The results of the cellular tests on human HeLa, HEp2, mouse L929, monkey Vero, and canine MDCK cells demonstrated that proanthocyanidin polymer A, with low cytotoxicity values, caused the same viral growth suppression as ribavirin against RSV A and B (subtype variants: A2-Tracey, A-Long, B-46791, B-47063), parainfluenza virus (PIV) 1 and 3, and influenza A and B (subtype variants: A-Taiwan (HIN1); A Leningrad (H3N2); B-USSR; B-Tama) in vitro.

In vivo test results exerted that in the case of treating Hispid Cotton Rats inoculated with RSV-A2, orally administrated proanthocyanidin polymer A in the amount of 10 mg/kg body weight had a more effective anti-RSV influence than ribavirin and significantly lowered RSV titers. Groups of three RSV-infected African green monkeys were treated intravenously with proanthocyanidin polymer A at 1.0 mg. $kg^{-1}$, and the treatment had a significant beneficial effect on reducing the infection in monkeys.

Proanthocyanidin polymer A moderately inhibited the influenza A/NWS/33 (H1N1) infection in male and female BALB/c mice after 8 days of treatment with 10 mg.$kg^{-1}$. $day^{-1}$ of the polymer. Twelve African green monkeys this time were infected by PIV-3 to prove that a daily dose of 3.3 and 10 mg.$kg^{-1}$ of the polymer is capable of reducing the virus titers in the throats of infected monkeys and alleviating other symptoms of infection. A statistically significant decline in the average value of lesion score of HSV-2(E194 strain) compared to the placebo control was observed as a result of the daily injection of 30 mg.$kg^{-1}$ of proanthocyanidin polymer A to intravaginally infected Swiss Webster female mice. The abovementioned treatment increased the survival percentage in model animals (40%) compared to the placebo treatment (15%) with no apparent toxicity [207].

## Synthetic Polymers

### Quat-12-PU

Park et al. [205] developed an antiviral coating based on N, N-dodecyl, methyl-polyurethane (Quat-12-PU). They used a 20 wt.% solution of Quat-12-PU in tetrahydrofuran (THF) for electrospinning process employing a voltage of 18 kV and 25 × 25 mm sized polyethylene slides in the distance of 15 cm as a base material and collector of resulting continuous and uniform nanofibers. In another sample preparation, they simply sprayed the solution of Quat-12-PU in THF (5000 mg. $L^{-1}$) on the polyethylene slide.

Antiviral evaluation by the plaque assay test performed on the Quat-12-PU-coated slides exhibited strong antiviral properties of this polymer against the enveloped influenza virus (Wuhan strain, A/Wuhan/359/95). However, the surfaces coated with Quat-12-PU, could not suppress poliovirus (Chat strain). The probable mechanism of the virucidal effect of the hydrophobic Quat-12-PU coatings, based on the previous reports for N, N-dodecyl, methyl-PEI coatings, is the disruption of the lipid envelope of the virus which normally protects the structure of RNA [208]. Besides, nanofiber-coated surfaces were found to have an antibacterial effect against *S. aureus* and *E. coli* and a bacterial log reduction of 7.5 for both cells [209].

#### (PPE)-Based Polyelectrolytes

Wang et al. performed a survey to evaluate the probable antiviral activity of conjugated polymeric materials using cationic conjugated polyelectrolytes (CPE) based on poly (phenylene ethynylene) (PPE) and oligo-phenylene ethynylenes (OPE) against T4 and MS2 bacteriophages and monitored the results in UV/visible lighting and without that. In the dark situation, and by suppression of the viral infection pathways and deterioration of the virus structure, most of the compounds from both polymeric groups had high inhibitory activity against MS2 phage with induction of higher than 6-log inactivation, whose inhibitory effect against T4 phage was quite moderate. The presence of UV or visible light enhances the influence of CPEs and OPEs on the virus by providing the condition for corrosive ROS generation that cause chemical disruption to the structure of the virus and capsid protein.

At the highest level of antiviral activity, PPE conjugated with DABCO (1,4-diazabicyclo [2.2.2] octane) with the formula of $N_2(C_2H_4)_3$, induced higher than 6 orders of magnitude of viral suppression against T4 and MS2 bacteriophages in both dark and light irradiation situation. This unique ability is likely due to the high positive charge density on the side of the PPE-DABCO polymer chain that facilitates the interaction of the polymer with the negatively charged viruses, and because of being spacious and highly hydrophobic, prevents the aggregation and enhances the availability of polymer to associate with viral cells [210].

## Carbon Dots as Antiviral Agents

Carbon dots are a novel class of nanomaterials with a particle size of less than 10 nm that exhibit fluorescent properties [211]. Their characteristics of low production cost, surface hydrophilic functionality, high stability and biocompatibility along with low toxicity make them a very convenient candidate for biomedical applications such as controlled drug and gene delivery, bioimaging, biosensing, diagnosis of viral infections, and most recently, viral therapy [212]. The main mechanism of their viral inhibition is considered to be the alteration of viral attachment and penetration stage, for example, Dong et.al, observed that in the case of human norovirus invasion, the presence of carbon dots prevents norovirus virus-like-particles from binding to histo-blood group antigens receptors on human cells, but the viral capsid integrity remains intact [213]. The observation of other inhibitory mechanisms of Carbon dots such as impeding viral replication after entering the host cells and hindering the budding stage by inhibition of ROS generation, in porcine epidemic diarrhea virus, as a model coronavirus [214], inhibition of viral replication by causing adverse impacts on κB signaling pathway [215], exhibited promising prospects of their application against coronavirus and inspired employing carbon dots in the COVID-19 combat, which is yet to be proven in vivo.

## Granting Antiviral Properties to Polymeric Compounds

There are many reports about the employment of biocompatible polymers along with metal ions and plant extracts to design antiviral active food packaging such as green tea extract-loaded chitosan as an edible coating [216] and Cinnamaldehyde-loaded polyhydroxybutyrate (PHB) [217] both against MNV, polylactic acid (PLA) containing Ag ions against FCV [218], and AgNP- loaded PHBV against MNV [116].

Ueda et al. designed a coating material for the antiviral application that was made of a transparent film containing a complex of cuprous oxide ($Cu_2O$) and titanium dioxide ($TiO_2$) particles. In the production process, a liquid dispersion was made including $TiO_2$ and 0.1 to 20 wt.% of $Cu_2O$ particles with an average primary diameter of 2 to 80 nm and a phosphate ester-based anionic surfactant. They also employed a binder resin containing chlorinated polyolefin for coating film composition. For increasing the transparency of the film, the resultant metal complex particles need to be 50 to 150 nm on average, in the sizes smaller than 50 nm, the crystalline structure of primary particles would be broken, and in the secondary structures, happening of excessive dispersion process leads to reduction of the photocatalytic activity and antibacterial performance, this reduction also occurs for the samples with secondary particles sizes more than 150 nm, that's because of the very small surface area of the particles. Determination of antiviral activity was performed by an alternate method named indoor lighting environment-Test method employing bacteriophage Q-beta under fluorescent irradiation of 1000 Lx for 1 h. The results demonstrated that the copper complex $TiO_2$

dispersion could maintain high dispersion even in the high concentrations, which facilitated increasing the transparency of the produced coating composition. Moreover, the coating agent designed in this project exerted potent antibacterial and antiviral performances [219].

Loading chemical virucidal drugs into various polymers (carriers) is another way of fabricating antiviral polymeric compounds. The negligible toxicity, sustained delivery, long-term efficacy, and durability and maintenance in the female reproductive tract, made electrospun nanofibers a promising technology to impede sexually transmitted viral infections such as HSV-2. Towards this, Aniagyei et al. fabricated the electrospun nanofibers based on poly(lactic-co glycolic acid) (PLGA) (50:50) and poly(DL-lactide-co-ε-caprolactone) (PLCL) (80:20) containing Acyclovir (ACV) as a model drug to investigate the anti-HSV-2 effect of this formulation via an in vitro experimental model. The electrospun nanofibers were produced using the polymeric solution containing 20% w/w ACV (to polymer) with flow rates of 0.5–3.0 $mL.h^{-1}$ in a voltage range of 15–27 kV and were collected at a distance of 25 cm from the needle tip. The antiviral activity of the electrospun mat was then tested by performing plaque assay on Vero E6 cells, and the findings revealed that not only the ACV-loaded electrospun nanofibers provide great encapsulation efficiency and sustained delivery of ACV in 30 days to protect the cells against HSV-2 infection, but also the blank PLGA and PLCL electrospun nanofibers acted as an efficient physical barrier to infection [220].

Palza Cordero et al. suggested that the antiviral property of the materials caused by the release of the metallic ions could be also achieved by using a resin, particularly PP, which can shape a plastic material with the capability of the controlled release of ions during the long periods. Metallic copper particles in the preferable diameter range of 10 to 80 nm were appropriately embedded in the resin and formed the secondary structures and the particles did not protrude from the surface of the material. The resultant polymeric material could be a promising candidate for manufacturing threads for production of fabrics, nets, extruded, laminated, or injected plastic products, which are applicable in making coating surfaces, containers, cleaning tools, intra-hospital use materials, and air filters with biocidal properties [221].

Carraher et al. collected information about the antiviral properties of a group of metal-containing compounds, organotin polymers, which are mainly known as the anticancer agents, but a vast range of these tin-containing polymers exhibited antiviral activities as well [222]. One of these polymeric compounds is made of hydroxyl-capped PEG and dibutyltin dichloride ($Bu_2SnCl_2$). PEG by itself is ready to access both the nucleus and the cytoplasm of the infected cells because of its water solubility. As a result, PEG is capable of inhibiting both the VACV, an RNA virus, which replicates in the cytoplasm, and HSV-1 as a DNA virus that its replication is restricted to the nucleus of the host cell [223]. On the other hand, the tin-containing dibutyltin dichloride in the concentration of 150 mg. $L^{-1}$ can inhibit the activity of vaccinia and HSV-1, in about 20% of the exposed cells. Compounding dibutyltin dichloride with PEG (400 amu), led to enhancement of viral protection against vaccinia to 30% in a tenfold lower concentration (15 mg. $L^{-1}$) in comparison with the dibutyltin dichloride alone. Besides, polymerization of dibutyltin dichloride with 2,5-dimethyl-3-hexyn-2,5-diol, resulted in 50% inhibitory activity against HSV-1 at the concentration of 150 mg. $L^{-1}$ [224]. These examples showed that the nature of the attached moiety to the organotin plays a key role in the antiviral activity of the produced compound that this effect is virus-specific, even if the viruses possess the same genome types.

The highest protection ability against the HSV-1 between the bioactive polymers studied in this report belonged to a member of hydroquinone polymers, 2,3-dicyanohydroquinone, which was functional at a concentration of 300 mg. $L^{-1}$ and could suppress HSV-1 infection in 80% of the polymer treated cells [224].

The method of action of hydroquinone polymers has been related to the interaction of pi-related secondary bonding of the aromatic ring structure with the entities such as pyrimidine and purine rings on the DNA that in combination with the presence of active sites on tin, facilitate the activity of these polymers within the cells. These polymeric bioactive materials have also the ability to interact with the cells from the outside, which is also another way of impeding the virus' attack to the cells [223].

## Antiviral Fibers and Textiles

### The Method of Incorporating Metal NPs into the Structure of Electrospun Nanofibers

There are two main methods for synthesis of metal NPs impregnated fibers, in the first one metal NPs were synthesized separately through different methods by reducing metallic ions from metal salt and employing chemicals, heat, or cavitation to accelerate the process. There are also chances to employ bioactive compounds of herbal extracts as capping and reducing agents [225]. For incorporation of the synthesized NPs into the nanofiber structure, they should be dispersed into the polymeric solution and carefully homogenized to be prepared for the electrospinning process. Choosing an appropriate solvent is a crucial factor for achieving a homogeneous dispersion in the electrospinning solution. The second common method includes

an in-situ synthesis of metallic NPs in the electrospinning solution in which the solvent provides the necessities of the reduction process and the polymer chain acts as a stabilizing agent. After achieving a homogenized NP-containing solution, it is loaded into a syringe and will be placed in an electrospinning device in which a high voltage creates an electrically charged jet of polymer solution at the tip of the needle that in case of overcoming the surface tension of the polymer solution will cause the jet stretching out as a narrow polymeric strip which loses its solvent during the way of traveling toward the collector by vaporization and finally forms nanometer-scale metallic NPs-containing fibers [226].

## Antiviral Nondimensional Materials

Takayama et al. introduced bioactive compound-loaded nanofibers as functional materials for the production of a surgical mask with antibacterial and antiviral properties. The polymeric material for fabrication of electrospun nanofibers could be selected from a group comprising: Zein, fibroin, collagen, chitosan, chitin, PVA, polyvinyl chloride, PLA, PU, nylon and methoxy methylated nylon, polyester, polystyrene, PAN, polyamide and, PET. The bioactive compound that are the main functional substances in the mask structure may consist of at least one of these natural compounds: persimmon tannin polyphenols, grape seed polyphenols, catechin polyphenols, coffee polyphenols, lemon peel polyphenols, soybean polyphenols, ellagic acid phenyl carboxylic acid and, coumalin. These compounds possess antioxidative, antibacterial, antiviral, and deodorizing effects that are ideal characteristics for a surgical mask. The preferable diameter of electrospun fibers is in the range of 1 to 2,000 nm with a weight per unit area of 0.005 $g.m^{-2}$ to 10 $g.m^{-2}$ and air-permeability of 1 $cc.cm^{-2}.sec^{-1}$ to 1,000 $cc.cm^{-2}.sec^{-1}$. In the process of producing each test sample, an electrospinning solution containing a mixture of the selected base polymer and the concentration of 20 wt.% bioactive compound prepared, and after the characterization of physical properties (Table 3), all samples were employed for further evaluations.

Besides, two other samples were synthesized in the form of three layer-reinforced nanofibers, one of them comprised catechin polyphenol loaded methoxy methylated nylon nonwoven fabric with an average diameter of 150 nm as the base layer and catechin polyphenol-containing PU with the average size of 500 nm was employed as the reinforcing nanofiber and the weight per unit area for this sample was 0.1 $g.m^{-2}$. In the second sample PVA with an average diameter of 250 nm was the substitute for methoxy methylated nylon. The results of evaluations exhibited that all fabricated samples had strong antimicrobial activity and showed potent filtration efficiency and high trapping performance of more than 99% for both fine particles bigger than 3 µm and 0.1 µm. Furthermore, the air permeability for all of the synthesized face masks was 100 $cc.cm^{-2}.s^{-1}$ or higher, which enhances the mask wearability along with antioxidative, antimicrobial, antiviral, and deodorizing effects provides favorable properties for an ideal surgical mask [227].

Gabbay invented an antiviral textile containing ionic copper particles that can be used for the production of condom

**Table 3** Summary of test results carried out by Takayama et al. for production of nanofibers using various polymers and bioactive compounds

| Polymer | Bioactive compound | Average fiber diameter (nm) | weight per unit area of fiber ($g.m^{-2}$) |
|---|---|---|---|
| Polylactic acid | Catechin polyphenol | 500 | 0.5 |
| | Persimmon tannin polyphenol | 2,000 | 0.5 |
| | Phenyl carboxylic acid | 1,000 | 0.5 |
| | Ellagic acid | 1,500 | 0.5 |
| | Coumalin | 1,500 | 0.5 |
| | Coffee polyphenols (chlorogenic acid) | 500 | 0.5 |
| Polyvinyl alcohol | Catechin polyphenol | 250–500 | 0.01 |
| Polyvinyl chloride | Catechin polyphenol | 150 | 0.1 |
| Polyethylene Terephthalate | Catechin polyphenol | 500 | 0.7 |
| Polyurethane | Catechin polyphenol | 500 | 0.5 |
| Methoxy methylated nylon | Catechin polyphenol | 500 | 0.3 |
| | Tea leaves extract | 450 | 0.2 |
| Polyglutamic acid | Catechin polyphenol | 1,000 | 0.2 |
| Zein | Catechin polyphenol | 500 | 0.15 |
| Fibroin | Catechin polyphenol | 500 | 0.5 |
| Nylon 6.6 | Catechin polyphenol | 150 | 0.1 |

sheaths, surgical gloves, and tubing. The author suggested that different types of natural (i.e., silk, cotton, wool, and linen) and synthetic fibers such as cellulose and cellulose acetate fibers, regenerated protein fibers, PU fibers, acrylic fibers, vinyl fibers, and polyolefin fibers, excluding polyester and nylon fibers, can be used for formation of the textile. After choosing the proper textile material and soaking it in a solution that contains one or more metal cationic species with two or more positive oxidation states, the activated textile will be produced. Then a reduction process needs to happen in contact with the textile leading to the production of a metalized textile.

The chosen textile material in this invention is polyamide, which contains water-insoluble ionic copper particles in powder form that supplies by adding 25 g of a mixture of CuO and $Cu_2O$ Powder yielding a 1% mixture. An in vitro antiviral test was performed to evaluate the effectivity of CuO-$Cu_2O$ impregnated fibers to inhibit the HIV-1 infection in MT-2 cells. The results exerted that 1% CuO and CuO Fibers showed 26% inhibition, while the suppression for the positive control (CuO and $Cu_2O$ powder) was 70%. Then, they impregnated a latex glove with 1% or more $Cu^{2+}$ ions and after 20 min of exposure, more than 95% of the subsequent virus infectivity of lymphocytes that is known as the main target of HIV-1, was neutralized [228].

Years later Gabbay suggested a practical method of incorporating copper (II) oxide (CuO) particles with the size of 0.5 to 2 µm into the rayon fibers that are manufactured from regenerated cellulosic fiber with the aim of producing antiviral fibers. The antiviral activity of the fibers is the result of releasing $Cu^{2+}$ ions in the exposure to water or water vapor. The method is comprising these steps: first, the addition of CuO particles to the rayon viscose in the amount of 0.25 and 10% of the initial cellulose dry weight, then the rayon fiber produce using an acid bath containing sulfuric acid by extruding the viscose through a spinneret into the bath, and a group of particles will place on the surface of the fibers and protruding from there. The produced fibers will exhibit antiviral properties [229].

## Nanofibrous Air Filters and Face Masks

The aerosol pathway is a critical way of spreading viruses, especially for highly transmittable respiratory infections such as H1N1 [8], which is capable of changing the cluster size of the virus according to temperature, atmospheric pH, and hygroscopicity that can directly influence the movement of virus particles in the nasopharyngeal passages [230]. Furthermore, H1N1 can shape clusters with the size of 400 nm and then they grow larger in the saliva to form aerosols the size of 0.7 mm to 6 µm, which can easily spread in the environment by the change in airflow trajectory during sneezing and coughing [231]. The design process of the respiratory masks performs based on the concepts of material durability, flexibility, fit, and comfortability that theoretical models exhibited that constructing them with smooth, long, smaller than a micron, and circular cross-section fibers lead to increasing the aerosol capture efficiency [232].

Conlon claimed that integration of nanofibers in the middle layer of the mask structure even in the form of one or more discrete layers or strips of melt-blown fibers or spun bound small diameter fibers, can be formed by extruding molten thermoplastic materials and turning them into filaments, reduce the deflection of exhaled air and pressure drop, while enhancing the filtration of airborne particles, such as pathogens (Fig. 7). The author supported the above-mentioned claim by performing comparative pressure drop

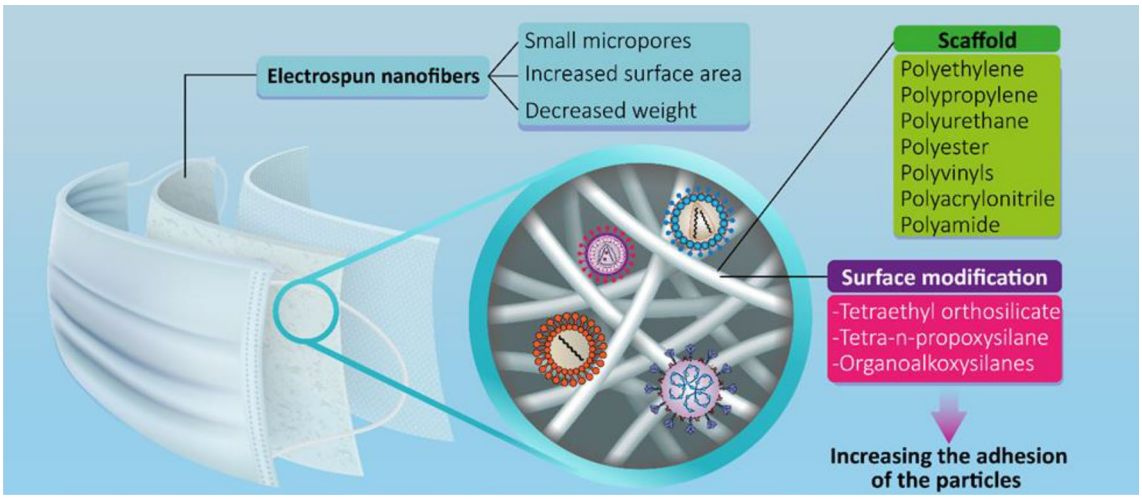


**Fig. 7** Development of surface-modified multilayered masks using polymeric electrospun nanofibrous scaffolds as a protective barrier against spreading viral infections

measurements on multilayered facemasks containing nonwoven fibers in the inner and outer layer, which can be made of polyethylene or PP and a nanofibrous mat with a fiber diameter of about 150 times smaller than non-woven fibers that is placed in the middle layer for filtration and may contain polytetrafluoroethylene (PTFE). The results demonstrated that the pressure drop in non-containing discrete nanofiber layers is 18 times higher, directly related to the amount of deflected air in the facemask, resulting in less airflow through the facemask. The bidirectional flow of air in nanofibrous masks was enhanced, and they also had greater filtration efficiency than other masks [233].

Electrospun nanofibers are smaller than melt-blown fibers for about 1 to 2 orders of magnitude [234] and the process of electrospinning leads to the generation of smaller micropores, increased surface area, and decreasing the weight of electrospun mat in comparison with melt-blown mat, 0.02–0.5 $g.m^{-2}$ versus 5–200 $g.m^{-2}$, respectively [235].

The ideal characteristics of electrospun air filtration materials including small fiber diameter and pore size, guarantee the effective particle capturing and facile passing of airstream through the filter and can be optimized by regulation of electrospinning parameters such as voltage, the distance between the needle tip and the collector, time, concentration of the polymeric solution, etc. [236].

Based on the above-mentioned criteria, Reyes et al. designed a membrane of nongrafted electrospun Nylon-6 fibers with a size of 100 to 150 nm that can be employed to capture virus-containing exhaled breath aerosols to act as a lightweight diagnostic device. The results of the aerosol capture evaluation of a uniformly thick electrospun Nylon-6 fiber membrane with the size of 15 cm × 93 cm in a simulated breathing apparatus demonstrated that they exhibited higher breath capture overall, 39 to 50% higher than commercial woven and nonwoven controls, and 60 to 95% of 0.2 mm to 6 μm sized aerosol droplets were successfully captured by the membrane due to the morphological properties of the electrospun membranes such as high surface area, smaller interfiber pores, and reduced fiber diameter, which despite their less weight (20 times less than the commercial controls) they did not rupture or degraded during the tests [237].

The electrospun nanofibrous mat exhibits great potential to be employed as High-Efficiency Particulate Air (HEPA) and Ultra Low Penetration Air (ULPA) grade filter media, by comparing the filtering efficiency of a nanofibrous mat and melt-blown nonwoven filter media. The very first trials for the formation of air filters were simple fibrous assembly using cotton, wool, and later, polyester, PP, fiberglass, and other proper materials for removing biological agents. Removing almost 99.9998% of *Bacillus subtilis* moving spores in the airstreams with low velocity employing slag wool with a thickness of 3 inches (7.62 cm) in the survey of Terjesen and Cherry [238], was one of the first trials in this field of air filtration. Decker et al. used a spun-glass fiber mat with a fiber diameter of less than 1.25 μm as a filter with a thickness of 0.5 inches (1.27 cm) along with an electrostatic precipitator for removing 95.7–100% of airborne viruses for removing *E. coli* [239].

In another survey, *Staphylococcus aureus* cells in the aerosolized form were retained using a single thickness glass fiber mat as the filter media, capable of holding back 98.5–98.7% of nebulized aerosols [240]. Incorporation of the cell lytic enzymes into the nanocomposites is another way of preventing pathogenic bacteria, such as surface incorporation of endolysin for inhibition of the *listeria* bacteriophage [241].

Gogotsi et al. [242] suggested a composite matrix as highly flexible material for application in producing membranes to make filtration devices. The composite was comprised of a porous scaffold to support the electrospun nanofibers, which photocatalytic metal oxide particles, were electrosprayed on them and uniformly deposited in the fibrous structure without agglomeration. The candidates for photocatalytic metal oxide particles were $TiO_2$, Zirconium dioxide ($ZrO_2$), ZnO, and Tungsten trioxide ($WO_3$) in the average diameter of about 5 to 50 nm or more preferably, 10 to 30 nm and the amounts of 0.5–20% or more favorably 3–10% of the total suspension weight. The porous scaffold might be synthesized from a single or mixture of polymers including polyethylene, PP, PU, polyester, polyvinyls (i.e. polyvinyl chloride or polyvinyl alcohol), PAN, polyamide, etc., and with the aim of increasing the adhesion of the particles, the scaffold could pass a surface modification step prior to electrospraying, comprising treatment with a proper binder material that may include one or more silica precursors (i.e. tetraethyl orthosilicate (TEOS), tetra-n-propoxysilane, organo alkoxysilanes, etc.) (Fig. 7).

The preferable pH range is 2 to 5 and the binder material may contain inorganic or organic acids such as phosphoric acid, nitric acid hydrochloric acid and, sulfuric acid or acetic acid, dichloroacetic acid, trifluoroacetic acid, and benzene sulfonic acid. The fibers were suggested to be nanosized with a diameter of 500 nm to about 1 μm, and the proper concentration for electrospinning solution is 4 to 20 wt. % of the polymer solution total weight that should be selected to possess the capability of adhering to the porous scaffold, and may comprise polyamides, poly (vinyl acetate), poly(acrylonitrile), poly (Vinylidene fluoride), PEO, PVP, PCL, chitosan, cellulose, cellulose acetate, fibrinogen, collagen, silk, and styrene/isoprene copolymer or polymer blends that are soluble in a common solvent, for example, polylactide-blend-PVP, PEO-blend-poly(methyl methacrylate), polystyrene-blend-polyester, poly (vinylidene fluoride)-blend-poly (methyl methacrylate), etc.

As a practical example, they first washed a PP filter substrate with a mixture of deionized water and polar solvent and employed that as the porous scaffold. Then polyamide nanofibers were deposited on a silica-coated scaffold by electrospinning the solution of polyamide 11 in formic acid/dichloromethane. Then, a suspension of $TiO_2$ NPs (with a diameter of 10–15 nm) in deionized water and ethanol (50:50 w/w) was electrosprayed onto the polyamide nanofibers.

They compared the above method with the process of dip-coating of NPs, found that the particle distribution in the dip-coating process was not uniform and led to agglomeration of $TiO_2$ NPs that because of decreasing the effective surface area, reduced the antimicrobial and antiviral activity in comparison with the same number of smaller particles. Therefore, electrospraying is considered the more appropriate method for the uniform distribution of metal particles, which can preserve the antiviral activity of metallic NPs [242].

Leung suggested a double layer filtration medium comprising a microfibrous coarse layer that is positioned proximal to the airflow direction and attached to a fine layer of nanofibers that can be produced of electrospun or melt-blown polymers and placed distal to the airflow direction. The nanofibrous layer with a fiber diameter of 150 nm to 200 nm enhances the chance of capturing and molecular diffusion through fibers due to the high surface area to volume ratio, which is in the range of $1.3 \times 10^7$/meter to $4 \times 10^8$/meter. The electrospun nanofibers also carry an electrical charge generated through the electrospinning process that awards them the ability to intercept particles with an opposite electrical charge in the air stream. The microfibrous coarse filter layer with an average fiber diameter of 1 to 30 μm and a thickness of about 0.1 to 20 mm, possesses a high solid holding capacity and larger voids for trapping larger particles, while the nanofibrous layer with smaller voids is appropriate for capturing finer particles. The preferred weight ratio of the nanofibers to microfibers is 10%:90% and the nanofibrous layer can be directly electrospun onto the coarse surface of the non-woven microfibers that could also be placed in a liquid medium and the liquid subsequently be removed under the vacuum and ultimately the two layers form a rigid structure by mechanical compressing by using a trace amount of adhesive substance. The final filtration medium may also include a hydrophobic layer of non-polar polymers such as PTFE, nylon, glass composites, acrylic, and polyethersulfone (PES) to allow free gas exchange and prevent the entrance of virus bearing water droplets. For empowering the filter to antibacterial characteristics, the metallic NPs of MgO, $TiO_2$ with potent ability to produce oxidation reactions under the ultraviolet light, silver (Ag) compounds such as silver nitrate, and organic compounds such as poly (*N*-benzyl4-vinyl pyridinium chloride) with the strong affinity to virus bacteriophage T4, could be added to the fibrous structure through the electrospinning process or grafting anti-microbial polymers onto the filter surface through atom transfer radical polymerization from an initiating surface, leading to non-leaching covalent attachment of the anti-microbial agents, or even by using initiated condensed vapor deposition (iCVD) technology, which is used for coating anti-microbial substrate on non-woven fibers surface without the risk of blocking the inter-fiber pores [243].

Li et al. developed a face mask using PSU electrospun nanofibers for filtration of PM2.5 (particulate matter with a diameter of 2.5 microns or less) in the polluted air. The PSU solution with the concentration of 18wt.% was prepared using Dimethylacetamide (DMAc)/acetone (9:1) as the solvent and the process of electrospinning was performed in different time durations. The SEM results indicated that in the time duration of 15 min, the nanofibers showed random orientation and high porosity with a diameter of about 500–800 μm and an interfiber distance of 1–3 μm. The nanofibrous masks exhibited an acceptable rejection efficiency of more than 90%, showing a high PM2.5 rejection capability in comparison with disposable non-woven masks (32.9%). The percentage of PM2.5 rejection enhanced with increasing the time of the electrospinning process resulting in a thicker mat of nanofibers and in the time of 60 min, the rejection capability reaches 99.4%. It is believed that there is a contradictory relationship between air permeability and particle rejection, and with increasing the air permeability, PM2.5 rejection decreases and vice versa. Between the tested samples, the nanofibrous mask produced via 15 min electrospinning, exhibited the highest air permeability and PM2.5 rejection contrast, as well as possessing a great PM2.5 rejection value of 90% and suitable pressure drop and air permeability [244].

Qin et al. reached a dramatic decrease in the pressure drop of the membrane produced by electrospinning of 10 wt.% and 5 wt.% solutions of PAN that were made of thin microsphere loaded nanofibrous scaffold, which their presence in the structure contributed to larger pore size leading to enhancement of the filtration efficiency and capturing of PM2.5 and more importantly reduction of the pressure drop by decreasing the clogging of the membrane [245].

It has proved that the filtration efficiency of electrospun PVA microporous membrane is mathematically proportional to the pore size [236]. Although membranes with smaller pore sizes demonstrate higher filtration efficiency, their tiny pore size generally contributes to easier clogging in the filtration process [246].

Choi et al. designed an air filter comprising polyester and aluminum with the ability to capture and inactivate airborne microorganisms simultaneously. The potent electrostatic

interactions of fibers in the filter structure with charged bacteria led to filtration of about 99.99% of *Escherichia coli* and *Staphylococcus epidermidis* bacteria with about 10 times lesser pressure drop per thickness in comparison with commercial efficient air filters and this capability was maintained after cyclic washing of the filter, which indicated the reusability of polyester and aluminum filter. The process of adding Al to the fiber structure was performed by dip-coating of a polyester nonwoven filter with a fiber size of 30 μm and porosity of 78.3% into an Al precursor ink, $AlH_3O(C_4H_9)_2$ and the comparative antibacterial test results demonstrated that growing Al nanograins on the fiber structure, improved the inactivation efficiency of the filter from 89.3 to 94.8% for *E. coli* and from 79.7 to 96.9% for *S. epidermidis* that considered to be a result of enhancing surface roughness and hydrophobicity after the addition of Al to the filter structure [247].

In another report, a washable nanofibrous membrane composed of PAN/AgNPs nanofibers was designed as an antibacterial mask with the aim of two-way prevention of bacterial passage from person to surroundings and vice versa. The preparation of PAN/AgNPs membrane was performed by dipping the PAN nanofibrous mat in a solution that contained 1000 mg. $L^{-1}$ silver nitrate and the effect of different dipping cycles on different physicochemical characteristics of the membrane was investigated. The results of TEM demonstrated that the mean size of pure PAN nanofibers was 263 nm and after loading AgNPs, reached 290, 250, and 302 nm for one, two, and three dipping cycles, respectively. The size distributions of AgNPs also ranged from 18 nm to the maximum diameter of 39 nm in the third dipping cycle. The mechanical properties of PAN nanofibers were also improved after loading AgNPs and the tensile strength of the fibers increased even after 120 h washing with deionized water. Based on the release profile of the AgNPs loaded fibrous mat, when the negligible amount of AgNPs (2,247 ppm /gr nanofiber) was loaded into the nanofibers, the nanofibrous mat showed a two-stage release pattern, and the controlled release of Ag from PAN structure during 120 h confirmed that this method is appropriate for preparing washable antibacterial membranes. The antibacterial test results exhibited the effective antibacterial activity of the PAN/AgNPs membrane against Pseudomonas and Staphylococcus bacteria and had more inhibitory effects against Pseudomonas than against Staphylococcus. Although the presence of a high concentration of AgNPs caused by using two and three dipping cycles for loading of AgNPs led to the highest cytotoxicity, the sample with one cycle loaded AgNPs demonstrated the minimum rate of toxicity, as well as the optimal antibacterial properties, while keeping high biocompatibility [248].

Hashmi et al. produced and characterized a membrane made of CuO-loaded PAN electrospun nanofibers for antibacterial face mask application. The authors mentioned that the aim of producing about 60% of nanofibers is biomedical employment and loaded spherical shape CuO NPs with the size of $37 \pm 9$ nm as a stable and cost-effective antibacterial candidate in four different concentrations on pure PAN nanofibers with the average size of 141 nm and produced PAN nanofibers containing an optimum amount of 1.00% CuO with the size of 197 nm. The incorporation of CuO NPs significantly improved the tensile strength of nanofibers and imparted crystallinity and higher hydrophilicity to the membrane. Surface area is another factor that was found to be proportional to the CuO concentration in the membrane and based on the Brunauer–Emmett–Teller (BET) test results, the PAN nanofibrous mat containing the optimum amount of 1.00% CuO had a higher surface area of $20.63 \pm 0.087$ $m^2$. $g^{-1}$ than the neat PAN nanofibrous mat $8.09 \pm 0.012$ $m^2$. $g^{-1}$. The results of the breathability test by the upright cup method exhibited that the water uptake and breathability of the membrane are enhanced with the addition of CuO NPs. Furthermore, the presence of CuO in the intrinsically compact structure of neat PAN nanofibrous mat led to a reduction of its high resistance to the airflow by increasing the porosity of the mat and the value of air resistivity (R) declined from 24.05 for neat PAN, to 10.08 for 1.00% CuO containing mat, exhibiting better air permeability of the CuO loaded filter membrane. The results of analyzing the drug release behavior showed that the structure of CuO loaded PAN nanofibers was retained after socking in water for 72 h, that the nanofibers successfully released Cu without the occurrence of fiber dissolution in the aqueous medium, that the quantity of Cu was directly proportional to the CuO concentration in the PAN fibers. Based on the results of the MTT analysis, after passing the incubation period of 120 h more than 50% of the total cells survived. The CuO-loaded PAN nanofibers demonstrated a great antimicrobial effect on both gram-positive and negative bacteria (*E. coli* and *B. subtilis*) and the inhibition zone expanded with increasing the amount of CuO, representing the potent intrinsic antibacterial characteristic of CuO [249].

Seo et al. designed a facemask comprising three types of the fibrous membrane, one of them was a built-in adsorptive membrane made by stacking an adsorptive layer produced by accumulating ion-exchange nanofibers forming a mat with a pore size of about 3 μm or less on a supporting layer of woven or nonwoven fabrics, thicker and possessing larger pore size, forming a membrane with the capability of adsorbing ionic and ultrafine substances from the environment and high purification performance. The nanofibers could be either anion or cation exchange and the web shape adsorptive layer preferred to be coated with oil to activate the adsorption process in functional groups on the nanofiber surface. The second fibrous membrane that

can be laminated on the first one, was made of electrospun dopamine-loaded nanofibers with the aim of gathering and maintaining the moisture of the breath to a certain degree in the nanofibrous web. The dopamine-loaded nanofibers were also functionalized by attaching active groups to dopamine under UV or plasma irradiation, or by acid or base treatment, to function as a negative charge ($SO_3H^-$) or positive charge ($NH_4^+$) functional group to adsorb heavy metals, bacteria, and viruses of the passing air. The last fibrous membrane could be formed by electrospinning of a polymeric solution that contains silver nanomaterial (from $AgNO_3$, $Ag_2SO_4$, and AgCl) that may be stitched to the supporting layer and the potent antibacterial property of silver enables the facemask to kill the bacteria that may be contained in the airflow. Based on the abovementioned characteristics, this mask can be utilized for medical, industrial, or daily applications with stable breathing and convenient use [250].

Zhang et al. designed a smart face mask that was capable of monitoring human breath in case of emotional changes or during the exercise employing a humidity sensor made of silver nanoparticle-containing alginate fiber that was fabricated by a three-step procedure comprising electrospinning of sodium alginate, ion exchanging of the sodium and silver ions, and ultimately reduction of AgNPs in situ. The mean diameter of alginate nanofibers was 240 nm that the AgNPs were uniformly dispersed throughout the nanofiber that the resultant sensor exhibited appropriate humidity sensitivity in the relative humidity (RH) range of 20% to 80% and was capable of accurately capturing the rate and depth of the respiration [251].

Yang et al. introduced a face mask with thermal management ability consisting of a commercially available nanoporous polyethylene (nanoPE) sheath with 50−1000 nm pores and high infrared (IR) transparency of 92.1% and the nylon-6 nanofibers with a diameter of < 100 nm and transmittance up to 85% on the top of it with potent particulate matter (PM) adhesion and PM2.5 capture efficiency of 99.6% while exhibiting low pressure drop. Since the moist warm environment inside the face masks exposes the wearers to an extra hazard, the evaluation of thermal properties such as conduction or insulation could be a significant factor in the process of design that is conventionally determined by the thickness of the fibers. Manipulation of the thermal properties by changing the fiber thickness which is strongly correlated to the removal capability and air permeability is challenging considering the fact that other thickness-dependent performances could be also affected. Therefore, modification of this filter material using nanoPE, added an excellent radiative cooling effect to the fibrous layer while maintaining the unique characteristics of great PM capture capability and low pressure drop. The authors also found that coating nanoPE substrate with silver has a warming effect that the resultant face mask can keep the user face comfortable, cool in summer, and warm in winter while protecting them from polluted air or infections in case of indoor use in hospitals [252].


**Fig. 8** Methods of fortifying nanofibrous mats for filtration applications

## Fortifying Nanofibrous Mats for Filtration Applications

While the possibilities of making improvements in the filtration efficiency of the present mainstream fibrous air filtration materials like melt-blown fibers, cellulose fibers, and glass fibers are limited because they comprise microfibers [253], the electrospun nanofibers, are known as a privileged platform for the production of air filtration materials possessing advantages such as packing structure with tunable nano-dimensional fiber diameter [254], highly porous structure and flexibility [255], remarkable electrostatic effect and, the feasibility of producing them from a wide range of raw materials [256]. But for employing nanofibers on the industrial scale some of the structural flaws should amend to fulfill the expectations of a great filtration material (Fig. 8).

### The Multilayer Structure

The strategy of employing a multilayer structure is based on the fact that increasing the weight of the electrospun filter membrane leads to improvement of the filtration efficiency [257]. But the practical method cannot be carried out as continuous deposition of nanofibers in the electrospinning process because the airflow channels which have formed in the structure of the membrane will be partly clogged, leading to an increase in the pressure drop. Besides, the pore size distribution of the membranes that were fabricated from the electrospinning of one polymer is usually narrow, which negatively impacts the filtration efficiency in the case of targeting particles of various sizes. Therefore, a multilayer structure is fabricated from the layers with the same composition and porosity, arranged alongside each other to improve filtration efficiency and simultaneously alleviate the enhancement of pressure drop (Fig. 9).

Zhang et al. designed a multilayer filter made of three layers of membranes from PSU fibers with a diameter of about 1 μm, PAN nanofibers with a size of about 200 nm, and the finest layer with the polyamide-6(PA-6) fibers with a size of about 20 nm. This integrated filter demonstrated a low-pressure drop of 118 Pa and a high filtration efficiency with capability of filtration of numerous particles with different sizes which made possible by removing particles larger than 2 μm with PSU layer, capturing particles bigger than 0.5 μm within PAN nanonet, and finally, sieving 0.3 μm sized particles and more by PA-6 membrane [258].

Cellulose derivatives have been generally used for producing comfortable inner layers in commercial face masks comprising multilayers of non-woven fabrics. Furthermore, they can also be deposited on the surface of the outer layer in fiber/particle form or could be added to air filtration equipment as a separate layer before or after the filter layer. For instance, Asper et al. designed a filter paper made entirely from pure cellulose nanofibers with a diameter of 20–30 nm produced by Cladophora sp. Algae and employed it for viral removal. The results of retention tests demonstrated that the nanocellulose filter is capable of removing xenotropic murine leukemia virus and Swine Influenza A virus with high removal capacity [259].

Currently, most the air filtration respirators are designed based on the multilayer structure and comprise an electret filter that is composed of polymeric fibers such as PP, PTFE, poly-butylene terephthalate, and polycarbonate, forming a nonwoven mat which possesses electrostatic charge and placed in the central position of the layered structure [260].

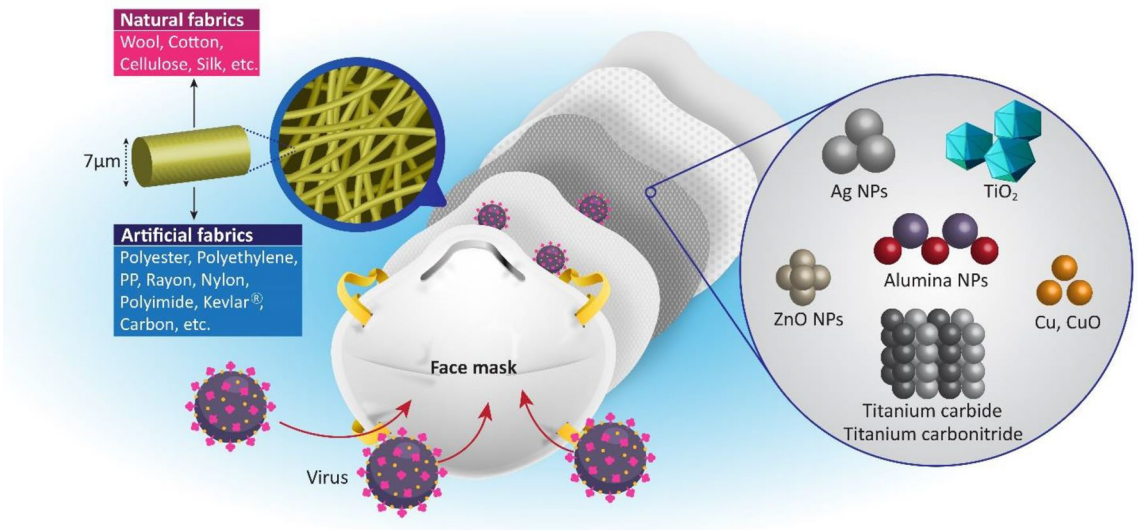


**Fig. 9** The schematic structure of multilayered anti-virus face masks incorporated with metallic nanoparticles

The mechanism of particle trapping in the electret membranes was not limited to the porous structure and they have the ability to capture the particles in an active manner with more attraction distance. Besides, there is no need to provide a high density of small pores and thick filters, and as a result, the appropriate removal efficiency can be achieved in the condition of continuous airflow with a low pressure drop. Through the process of formation of the nanofibrous membranes, electrospinning favorably provides in-situ electrostatic charge by introducing charge storage enhancers to electrospinning polymeric solutions [32].

### Lamination

The nanofibrous web of chitosan possesses unique properties such as biocompatibility, being non-toxic, biodegradability, and special physical and chemical characteristics that enable chitosan to capture and neutralize toxic materials in the liquids or air and destroy the structure of bacteria or viruses. Considering the shortcomings of the fibrous web of chitosan in the filtration process like poor mechanical stability, Mohammadian et al. investigated a method of remediation to strengthen this structure. They laminated the chitosan nanofibrous web into a multilayer system employing cotton fabric and an adhesive via the hot-melt method. In the process of electrospinning, an aluminum-covered collector was covered by polypropylene spun bond nonwoven (PPSN), which is a web form hot-melt adhesive, and the 10 wt.% solutions of chitosan and multiwalled nanotubes (MWNTs) used for the production of the nanofibers, and after removing them from the collector, another layer of PPSN attached on it and after that, the whole three layers placed in the middle of two cotton weft-warp fabrics and then, hot-melt laminating carried out by a flat iron at various temperatures to study the impact of laminating temperature on the multilayer structures. The authors found that the images of optical microscope (and not the cross-sectional SEM) were more applicable for observation of the structural changings, they also used an air permeability tester below 125 Pa air pressure for measurement of the air transport properties. The results showed that as long as the laminating temperature was under the melting point of PPSN, the nanofibrous web remained approximately unchained, but with increasing the temperature, the adhesive force among the layers was improved and gradually, PPSN was flattened between layers, and transformed to film-like structure, and by reaching to the temperatures above the PPSN melting point, the nanofiber web began to damage. On the other hand, increasing the laminating temperature contributed to the reduction of air permeability because of impeding the convective airflow by the adhesive layer. In the temperatures above the melting point, the reduction of airflow was a result of adhesive penetration to other layers (because of the more surface junction with nanofibers, PPSN has more penetration into the nanofibrous web than the fabric) that led to blockage of the nanofibrous porosity and prevention of passing the air during the experiment [261].

Lee et al. developed a membrane filter media using electrospun polybenzimidazole (PBI) nanofibers for application in dust-proof face masks to capture the particulate matters (PMs). The nanofiber layer was formed on a polyester mesh and for improving the mechanical stability against bending or other stresses, was laminated with another polyester mesh at the temperature of 140 °C and PBI fibers were immobilized between the two layers of polyester. PBI nanofibers are capable of making intermolecular electrostatic interactions that are the result of the high electric dipole moment of PBI polymer and made them an appropriate platform for the production of the efficient filter membrane. Based on the observations, the PBI filter kept its inherent function after cleaning and provided the filtering efficiency of about 98.5% at a very lower pressure drop (130 Pa) than commercial masks (386 Pa) with the similar filtering efficiencies, as well as a threefold higher quality factor (~0.032) compared to the commercial ones (~0.011) [262].

Hung et al. mentioned that although the higher weight of the filter membranes can lead to an increase in the filtration efficiency, the quality factor of the filters does not improve because of the unwanted enhancement in the pressure drop [263].

### Increasing the Surface Area

Another method for increasing the specific surface area and improving the efficiency of particle capture is manipulating some features of the electrospun fibers considering two opposite design concepts of "addition" and "subtraction" [264]. The addition of nano-protrusions on the electrospun fibers by incorporation of nanoparticles such as PAN/$SiO_2$ [265], PAN/ $TiO_2$ [266], PSU/$TiO_2$ [267], and so on, leads to increasing the specific surface area and as a result, the chance of capturing the particles enhances. Besides, the presence of these regions on the structure of fibers that possess low air resistance enhances the friction force between fibers and particles and reduces the probability of slipping and moving the captured particles by the shear flow of air [265].

Another way of achieving a higher specific surface area and filtration performance is by constructing porous fibers. Pan et al. generated densely distributed nano-pores on PLA electrospun fibers by regulating RH during the process of electrospinning and obtained the highest quality factor of 0.0276 on RH of 45% [268].

## Face Masks for Viral Filtration

Ren et al. provided information about employing nanoparticles in a formula that contained a compound of metallic nanoparticles along with non-metallic or anionic groups in a fibrous structure with the aim of preventing transmission of the viruses, especially by inhalation of infected droplets. The preferred diameter of the fiber filaments could be around 7 μm and the different forms are nanoparticles such as dry powders, liquids, sol–gels, or nanotubes with a preferred average size up to 100 nm that can be incorporated into protective clothing made of natural (such as wool, cotton, cellulose, silk, etc.) or artificial fabrics (polyester, polyethylene, PP, rayon, nylon, polyimide, Kevlar R, carbon, etc.). The antiviral activity of the formula was evaluated by Hemagglutination assay and reported based on the percentage of viral titer reduction. In the first group of trials, nanoparticles with the concentration of 0.1 to 1 wt.% were tested for inhibitory effects against different strains of flu viruses such as B/GDAL444 and VC1/256 on turkey red blood cells (TRBC's), and based on the obtained results, the authors marked nano-Ag and $TiO_2$ as "poor", ZnO and Alumina as "good", and compounds related to Al (Al-phosphates), $Ca^{2+}$ (Ca phosphates, Ca-silicates and Ca-carbonates), Si ($SiO_2$ and SiC), Cu and Cu oxides, P (Al-phosphates) and active carbons marked as "highly virucidal" by demonstrating over 90% virucidal rates. In another trial, the antiviral activity of different nanoparticles with diameters of 5 nm to 100 nm toward avian H5N1 Influenza NIBRG-14 was evaluated in MDCK cells. The results after 30 min of incubation demonstrated that Tungsten carbide (WC) exhibited the highest viral reduction percentage of 99.992% in the second place, titanium carbide (TiC) and titanium carbonitride ($TiC_{0.5}N_{0.5}$) were the most efficient nanoparticle with the viral reduction of 99.223% and the least reduction belonged to silicon (IV) nitride ($Si_3N_4$) with the reduction rate of 83.400% [269].

Another sample of antiviral fibers for air filtration applications can be produced by loading monovalent copper compounds such as CuCl, $CuOOCCH_3$, CuBr, and CuI particles with the least amount of 0.2% by mass concerning the weight of the fiber. The results of the cellular evaluation of the antiviral properties of the fibers against two model enveloped (influenza A / Kitakyushu / 159/93 (H3N2)) and non-enveloped (FCV (F9 strain)) viruses exhibited that copper (I) iodide and copper (I) chloride powder were the most potent antiviral compounds with the capability of inactivating viruses in a short time of 1 min in MDCK and CrFK cells, respectively [270].

Stewart et al. evaluated the inhibitory influence of four types of multilayer fabrics on Influenza B (B/Lee/40) virus in vitro. The findings showed that adding 2% copper acetate and 2% zinc acetate to the structure of spun-bond nonwoven or melt-blown PP fabric containing 2% citric acid, 2% PVA, and 0.5% polyoxyethylene (20) sorbitan boosted the antiviral activity of the fabric resulting in an appropriate material for making a facial mask to decrease the transmission of human pathogens [271].

Smith et al. designed a face mask that was intended to have antiviral and antibacterial activity and a lower pressure differential as well as offering superior comfort. The face mask comprised of an activated carbon cloth impregnated with silver which had a protective PP membrane on it and they both were placed in the middle of two inner and outer layers. The combination of the abovementioned layers is designed to draw the viruses from a static and mobile environment and capture them into the cloth assembly to be held and destroyed there.

Although activated carbon cloth is intrinsically antibacterial, it is supposed that it's not capable to capture very small particulates of viruses. But impregnation of activated carbon cloth with antiviral metals, such as silver, equipped the cloth with antiviral and virucidal properties. In this process which is called carbonization and activation, the metal salt is sequentially converted to metal oxide and metal and then located in the structure of cloth in any fashion: placed between the fibers, attached to the fibers, or embedded into them, leading to the formation of a microporous structure that has the ability to attract and capture molecules. In this project, the amount of impregnated silver was 0.3% by weight, the thickness of the silver-impregnated activated carbon cloth was 0.2 to 2 mm, and employing an MS-2 coliphage that in comparison with an FFP3 (filtering facepieces with at least 99% particle filtration efficiency at 0.3 microns) facemask, the filtration ability and pressure drop, as well as the virus capture, retention, and elimination efficiency of the cloth were tested.

The results exerted that surprisingly, the activated carbon cloth had virucidal properties, both with and without silver, but the presence of AgNPs in the cloth structure significantly increased the virucidal activity, and had no adverse effect on the efficiency of virus capture, which increased with the enhancement of the weight of the membrane layer, for example, it was 98.26% in case of using a 22 $g.m^{-2}$ membrane and reaches to 99.88% viral capture employing a 60 $g.m^{-2}$ one. However, there is an optimum point for increasing the weight of the membrane because, after that, the permeability will be limited, so here, the membrane weighed 60 $g.m^{-2}$, and the weight of the outer and inner layers were 50 $g.m^{-2}$ and 30 $g.m^{-2}$, respectively. The retention capability of the cloth, which is the number of remaining viruses in the cloth after capture, was 99.9998%. This composite represented a facemask with a lower pressure differential and reasonable cost [272].

A major problem of applicating face masks for viral protection is the accumulation of viral particles on the surface of the filtration membranes or within the membrane fibers, remaining alive and infectious for a relatively long period [273]. To defeat this shortcoming, Davison designed a four-layered filter composed of a central melt-blown PP filtration layer surrounded by an inner spun-bond PP and two layers with antiviral characteristics: the first layer composed of copper and zinc ions incorporated into cellulose/polyester and the second one (outer layer) is another spun-bond PP coated with a hydrophilic plastic coating that acidified with citric acid. Therefore, the infectious droplets and viral particles are absorbed in the outer layer and denatured by the citric acid then the damaged viruses are eliminated by divalent metal cations in the second layer [274].

Even though N95 class face masks demonstrated a greater level of protection compared with surgical/medical masks during the pandemic crisis, such as SARS in 2003 [275], their application has some serious flaws including low breathability, overall discomfort, excessive heat and humidity, malodorousness, facial pressure, skin irritation and, diminished visual, vocal, or auditory acuity, which reduce the favorability of the mask in general applications and more importantly, interfere with occupational duties of the health care employees [276]. Therefore, combining the advantages of each type, low air resistance of surgical/medical face masks, and high protection of N95 respirators leads to manufacturing the most desirable face mask. Besides, the protection level of a mask is dependent on two criteria, possessing the ability to filtration of hazardous particles in a wide diameter range from nanometers to micrometers and perfect sealing to avoid any leakage.

Tong et al. presented a novel face mask with expected antibacterial properties and potent filtration efficiency (more than 95%) with high breathability and also great face seal, including three to four nonwoven layers in the main body, comprising nanofibers with a diameter of 10–99 nm interweaved with partially gelled submicron fibers in the size range of 100–1000 nm. The layers can be attached by ultrasonic welding and the fibers were made of selected polymers such as PU or PHBV and CuO employed as a biocide agent in the concentration of 2% -50% (w /w), which can be incorporated into the structure of submicron and nanosized electrospun fibers by encapsulation into the fibers, or attaching onto the fiber surface, or can be physically trapped in the fiber structure or crosslinked to the fibers.

In the first trial, an electrospun microfibrous PU mat containing 2% (w/w) of CuO with a surface density of 0 0.12 $g.m^{-2}$ and thickness of 230 μm was tested for evaluation of particulate filter penetration using sodium chloride (NaCl) aerosols. In another trial, the same evaluation was performed on electrospun CuO -incorporated PHBV fibers with submicron diameter. Both masks conformed to The National Institute for Occupational Safety and Health (NIOSH) N95 criteria in breathability and filtration efficiency. At an airflow rate of around 85 $L.min^{-1}$, 95–99.999% of NaCl aerosols with a diameter of about 260 nm were successfully filtered. The protective masks exhibited more than 99% reduction of gram-negative bacteria, *Pseudomonas aeruginosa*, within 5 min because of the oligodynamic effect of CuO [277].

## Discussion

There have been some comparative studies with the aim of designating the most promising metallic particle for antiviral applications. For instance, Mallikarjun tested the antiviral properties of Cu (II), Ni (II), and Zn (II) complexed with four groups of ligands: 3-(phenyl)-1-(2'-hydroxynaphthyl)—2—propen—1—one (PHPO), 3—(4-chlorophenyl)—1-(2'-hydroxynaphthyl)–2–propen—1—one (CPHPO), 3—(4 -methoxyphenyl) -1-(2'-hydroxynaphthyl)-2-propen-1-one(MPHPO) and, 3—(3,4-dimethoxyphenyl)–1-(2'-hydroxynaphthyl) —2—propen—1—one (DMPHPO) and declared the effectivity of them in order against tobacco ringspot virus(TRSV). All of them were examined in amounts of 250 ppm to 1500 ppm. The results demonstrated that the antiviral activities of the tested complexes were as follows: $Cu(DMPHO)_2 > Zn(DMPHO)_2 > Ni(DMPHO)_2 > Cu(PHPO)_2 > Zn(PHPO)_2 > Ni(PHPO)_2 > Cu(MPHPO)_2 > Zn(MPHPO)_2 > Ni(MPHPO)_2 > Cu(CPHPO)_2 > Zn(CPHPO)_2 > Ni(CPHPO)_2$. The author mentioned that the most toxic complexes toward the virus have greater solution stability and higher lipid solubility and the toxicity might be due to the interference of metal ions in regular cell proliferation [278]. In another study, Mastro et al. showed that treatment of peripheral blood mononuclear cells with Cu, Ag and, Ag+ Cu resulted in HIV-1 inhibitory degree of 43.82%, 37.15% and, 51.97%, respectively, which demonstrates the ascendancy of copper in viral inhibition [279]. Furthermore, Sagripanti et al. reported that the required amount of Cu (II) ions for achieving a 70% reduction in the titer of cell-free HIV-1 in a solution, is much less than Fe (III): 1.6 mM Cu (II) to 18 mM Fe (III). The required number of copper atoms for the inactivation of HIV-1 is approximately $10^{11}$ per infectious virus particle [280]. Minoshima et al. also reported that solid-state $Cu_2O$ possesses the superior inhibitory ability against both enveloped and nonenveloped viruses (influenza A and bacteriophage Q) in comparison with silver compounds, due to its unique viral inactivation mechanism via direct contact of $Cu_2O$ with viral cells, which disrupts recognition of host by destroying the structure of viral surface proteins and as a result, inactivates the viruses regardless of the viral envelope [281]. Nakano et al. employed highly photocatalytic $WO_3$

microparticles with 0.5 mass % of CuO powder to design an antiviral composite material. The in vitro antiviral evaluation was performed by inoculating two low and high pathogenic viruses, influenza virus (H9N2) and avian influenza virus (H5N1) into the MDCK cells exposed to the irradiation of visible light by the wavelength of 380 nm and illuminance of 6000 Lx for 24 h. Inactivation effect R is a parameter that is used for evaluation of the inhibitory effect of the target particles, which is formulated as [$R = \log C - \log A$], where C denotes the virus concentration of the particle-free visible irradiated sample after 24 h that A denotes the virus concentration of the particle-containing sample that received the same irradiation treatment. The $WO_3$ particles exhibited relatively low antiviral performance; however, making a composition of $WO_3$ with CuO resulted in an increase in the inactivation effect value after 24 h of irradiation in the same condition. Compared to $WO_3$ alone, the Inactivation effect ® was significantly increased from 1.9 to 4.7 [282].

In addition to the fact that the existence of various and feasible methods to synthesize CuNPs has made them a very practical option for widespread application [225], another advantage of employing them as antiviral agent is their synergistic effect in viral inactivation when used along with other metallic particles. Broglie et al. designed a core–shell structure placing Au in the core and Copper (II) Sulfide (CuS) in the shell of the NPs with a diameter of 2–5 nm and evaluated their antiviral properties against norovirus GI.1. The results of the in vitro antiviral test demonstrated that Au/CuS NPs can inactivate 50% of the viruses in the minimum concentration of 0.083 μM by damaging the structure of capsid proteins, which can reach complete viral inhibition by increasing the NPs concentration to 0.83 μM. In another survey, a hybrid coating impregnated with copper, zinc, and silver cations was produced by radical polymerization through a sol–gel process and in vitro evaluations demonstrated the ability of this coating for viral titer reduction: 98–100% after 120 min exposure to HIV-1 and slower virucidal kinetics for other enveloped viruses in the exposure time of 240 min: 97% for DENV, 100% for HSV-1, 77% for influenza and only marginal reduction in viral titer for the non-enveloped coxsackie B3 virus [283]. Kanovsky tested the anti-HIV-1 properties of active polymeric fibers containing varying amounts and ratios of $Cu_2O$ and tetrasilver tetroxide ($Ag_4O_4$). The antiviral test was performed on MT-2 cells and the measurement of the concentration of p24 (HIV-1 capsid protein) was the basis of virus proliferation determination. No cytotoxicity was observed for the combination of $Ag_4O_4$ and $Cu_2O$ and the results of antiviral tests showed that using the amount of 1% wt. of $Ag_4O_4$ alone, results in 76% inhibition while the presence of $Cu_2O$ in the composite led to achieving the ability to inactivate 96% of the viral titer [284].

Shimabuku et al. reported that granular activated carbon in the water filtration device was not capable of inactivating T4 bacteriophage after incorporation of minimum concentration (0.5 and 1.0 w/w (%)) of Ag into the structure, but the synergistic effect of CuO NPs in viral inactivation with the particle size of 22 to 37 nm and the concentration of 1.0 w/w (%) along with 0.5 w/w (%) of 25 to 40 nm-sized Ag NPs, caused 5.53 log reduction in T4 bacteriophage titer [285].

The application of nanofibers as a substitute for conventional material for producing filtration devices can reduce mask airflow resistance significantly and direct more airflow through the mask, which leads to enhancement of the filtration efficiency. The improvement of the fit, is the only way of increasing the filtration efficiency and reduction of receiver exposure in existing commercial face masks, while this solution also results in increasing the airflow resistance in the face mask, because of forcing a greater part of the airstream to passage the mask. But in the case of employing nanofibers, the intrinsic decrease in mask airflow resistance minimizes leaking around the mask and provides a better chance for passing particles through the filter and capturing them without the requirement of a perfect seal, and ultimately reduces the receiver exposure levels in comparison with conventional face masks. With the incorporation of nanoparticles in the structure of nanofibers, the electrospun mat will benefit from increasing the surface area and at the same time, will be equipped with potent antiviral agents [286].

In the end, having a brief glimpse of three commercial face masks can feasibly declare the potent effectivity and applicability of using copper compounds in the structure of face masks with the aim of viral inhibition of respiratory viruses. Three face masks made by BioFriend™ BioMask™, Cufitec® Surgical Mask, and Innonix Anti-Influenza Child's Mask possess the ability to inactivate 99.99% of various types of influenza viruses and their active ingredients are: citric acid 2% wt. (in the outer layer) and copper 1.6% wt. and zinc 1.6% wt. (in the 2$^{nd}$ layer) for BioFriend™ BioMask™ and Innonix Anti-Influenza Child's Mask, CuI in the amount of 0.5% wt. (in the outer and inner layers) for Cufitec® Surgical Mask.

Copper compounds are low-cost and feasibly applicable as promising antiviral agents and can also be combined with other biocidal metallic particles to intensify the overall antiviral effect, especially when placed in the structure of face masks with the aim of protecting the wearers against lethal pathogens such as COVID-19.

## Conclusion

Wearing protective masks is still the most powerful strategy for preventing viral transmission and managing the outbreak of COVID-19. Designing the innovative face masks, equipped with antiviral agents, can be a great step forward

to enhance the security level of the mask wearers. The metal and metal oxide NPs as potent candidates possessing antiviral activity have been studied for years. The majority of the essays on the antiviral properties of these NPs are limited to in vitro and cellular studies on human cell lines, and the number of in vivo experiments is considerably fewer. Based on these reports, a number of metal and metal oxide NPs have shown propitious antiviral activity, especially against respiratory viruses and a bright future is visible for their application in the structure of anti-virus masks.

The nanofibrous layers, on the other hand, were reviewed as the most promising material for developing face masks with great filtration qualities. The non-hazardous nature and intrinsic antiviral properties of the polymers, as well as the most practicable methods for improving the structural and filtration characteristics of the nanofibrous mats with the aim of using them in face masks fabrication, have been introduced and examples of patents and products which have been developed based on the abovementioned criteria were mentioned. In the end, this field of study has been shown to possess a vast potential for making innovations at both experimental and industrial levels with the aim of fulfilling the need for safe antiviral respiratory protecting materials.

The most challenging issue in the application of metal nanoparticles is their cytotoxicity on human cells (especially through inhalation), which makes the necessity to determine the accurate effective and safe dose of metal NPs for loading into nanofibrous layers more prominent. On the other hand, according to the potentials of this field, the upcoming researches in the field of proving the antiviral properties of metal NPs should change direction from in vitro and cellular studies to in vivo and clinical ones. The ease of use and accessibility of metal NPs-loaded face masks should be studied clinically as well. The combination of this field of nanotechnology with superior technologies based on artificial intelligence in the context of interdisciplinary collaborations will provide the possibility of making a wide variety of innovations in the fabrication of multi-layer face masks to finally approach the most suitable face mask in terms of reaching the maximum protection, applicability and, the possibility of monitoring the face mask's functionality from biological and technical aspects, which will upgrade the application of face masks from a protection-only device to an ever-growing biosensing tool.

**Acknowledgements** E.M. would like to acknowledge the support from the National Institute of Biomedical Imaging and Bioengineering (5T32EB009035).

**Data Availability** Data sharing not applicable to this review article as no datasets were generated or analysed during the current study.

## Declarations

**Conflict of interest** The authors declare that no competing interest exists.

## References

1. Yin Y, Wunderink RG. MERS, SARS and other coronaviruses as causes of pneumonia. *Respirology*. **2018**;*23*:130.
2. Sekimukai H, Iwata-Yoshikawa N, Fukushi S, Tani H, Kataoka M, Suzuki T, Hasegawa H, Niikura K, Arai K, Nagata N. Gold nanoparticle-adjuvanted S protein induces a strong antigen-specific IgG response against severe acute respiratory syndrome-related coronavirus infection, but fails to induce protective antibodies and limit eosinophilic infiltration in lungs. *Microbiol Immunol*. **2020**;*64*:33.
3. Johnson NP, Mueller J. Updating the accounts: global mortality of the 1918–1920" Spanish" influenza pandemic. *Bulletin of the History of Medicine*. **2002**, 105.
4. Viboud C, Simonsen L, Fuentes R, Flores J, Miller MA, Chowell G. Global mortality impact of the 1957–1959 influenza pandemic. *J Infect Dis*. **2016**;*213*:738.
5. Simonsen L, Clarke MJ, Schonberger LB, Arden NH, Cox NJ, Fukuda K. Pandemic versus epidemic influenza mortality: a pattern of changing age distribution. *J Infect Dis*. **1998**;*178*:53.
6. Kain T, Fowler R. Preparing intensive care for the next pandemic influenza. *Crit Care*. **2019**;*23*:1.
7. Raj VS, Mou H, Smits SL, Dekkers DH, Müller MA, Dijkman R, Muth D, Demmers JA, Zaki A, Fouchier RA. Dipeptidyl peptidase 4 is a functional receptor for the emerging human coronavirus-EMC. *Nature*. **2013**;*495*:251.
8. Joseph J, Baby HM, Zhao S, Li XL, Cheung KC, Swain K, Agus E, Ranganathan S, Gao J, Luo JN, editors. Role of bioaerosol in virus transmission and material-based countermeasures. Exploration; 2022: Wiley Online Library.
9. Kaushik A, Mostafavi E. To manage long COVID by selective SARS-CoV-2 infection biosensing. *Innovation*. **2022**;*3*: 100303.
10. Mostafavi E, Dubey AK, Teodori L, Ramakrishna S, Kaushik A. SARS-CoV-2 Omicron variant: a next phase of the COVID-19 pandemic and a call to arms for system sciences and precision medicine. *MedComm*. **2022**;*3*: e119.
11. Tebyetekerwa M, Xu Z, Yang S, Ramakrishna S. Electrospun nanofibers-based face masks. *Adv Fiber Mat*. **2020**;2:161.
12. Jefferson T, Foxlee R, Del Mar C, Dooley L, Ferroni E, Hewak B, Prabhala A, Nair S, Rivetti A. Physical interventions to interrupt or reduce the spread of respiratory viruses: systematic review. *BMJ*. **2008**;*336*:77.
13. Cho D, Naydich A, Frey MW, Joo YL. Further improvement of air filtration efficiency of cellulose filters coated with nanofibers via inclusion of electrostatically active nanoparticles. *Polymer*. **2013**;*54*:2364.
14. Skaria SD, Smaldone GC. Respiratory source control using surgical masks with nanofiber media. *Ann Occup Hyg*. **2014**;*58*:771.
15. Larrondo L, John MR. Electrostatic fiber spinning from polymer melts. II. Examination of the flow field in an electrically driven jet. *J Polymer Sci*. **1981**;*19*:921.
16. Cui H, Li Y, Zhao X, Yin X, Yu J, Ding B. Multilevel porous structured polyvinylidene fluoride/polyurethane fibrous membranes for ultrahigh waterproof and breathable application. *Compos Commun*. **2017**;*6*:63.
17. Chaudhary V, Gautam A, Silotia P, Malik S, de Oliveira HR, Khalid M, Khosla A, Kaushik A, Mishra YK.

Internet-of-nano-things (IoNT) driven intelligent face masks to combat airborne health hazard. *Mater Today*. **2022**;*2*:2.
18. Lv D, Zhu M, Jiang Z, Jiang S, Zhang Q, Xiong R, Huang C. Green electrospun nanofibers and their application in air filtration. *Macromol Mater Eng*. **2018**;*303*:1800336.
19. Kaushik AK, Dhau JS. Photoelectrochemical oxidation assisted air purifiers; perspective as potential tools to control indoor SARS-CoV-2 Exposure. *Appl Surf Sci Adv*. **2022**;*9*: 100236.
20. Saghati S, Akbarzadeh A, Del Bakhshayesh A, Sheervalilou R, Mostafavi E. Electrospinning and 3D printing: prospects for market opportunity. *Electrospinning*. **2018**;*2*:136.
21. Hosseini S, Tafreshi HV. On the importance of fibers' cross-sectional shape for air filters operating in the slip flow regime. *Powder Technol*. **2011**;*212*:425.
22. Brown TD, Dalton PD, Hutmacher DW. Melt electrospinning today: An opportune time for an emerging polymer process. *Prog Polym Sci*. **2016**;*56*:116.
23. Yun KM, Hogan CJ Jr, Matsubayashi Y, Kawabe M, Iskandar F, Okuyama K. Nanoparticle filtration by electrospun polymer fibers. *Chem Eng Sci*. **2007**;*62*:4751.
24. Komur B, Bayrak F, Ekren N, Eroglu M, Oktar FN, Sinirlioglu Z, Yucel S, Guler O, Gunduz O. Starch/PCL composite nanofibers by co-axial electrospinning technique for biomedical applications. *Biomed Eng Online*. **2017**;*16*:1.
25. Lu P, Ding B. Applications of electrospun fibers. *Recent Pat Nanotechnol*. **2008**;*2*:169.
26. Qin XH, Wang SY. Electrospun nanofibers from crosslinked poly (vinyl alcohol) and its filtration efficiency. *J Appl Polym Sci*. **2008**;*109*:951.
27. Wang N, Wang X, Ding B, Yu J, Sun G. Tunable fabrication of three-dimensional polyamide-66 nano-fiber/nets for high efficiency fine particulate filtration. *J Mater Chem*. **2012**;*22*:1445.
28. Kim GT, Ahn YC, Lee JK. Characteristics of Nylon 6 nanofilter for removing ultra fine particles. *Korean J Chem Eng*. **2008**;*25*:368.
29. Matulevicius J, Kliucininkas L, Martuzevicius D, Krugly E, Tichonovas M, Baltrusaitis J. Design and characterization of electrospun polyamide nanofiber media for air filtration applications. *J Nanomater*. **2014**;*20*:14.
30. Ni Q-Q, Xia H, Jin X, Liu F. Application of electrospun nanofibers in electromagnetic interference shielding. Electrospun nanofibers for energy and environmental applications. Berlin: Springer; 2014. p. 497.
31. Gopal R, Kaur S, Feng CY, Chan C, Ramakrishna S, Tabe S, Matsuura T. Electrospun nanofibrous polysulfone membranes as pre-filters: Particulate removal. *J Membr Sci*. **2007**;*289*:210.
32. Tsai PP, Schreuder-Gibson H, Gibson P. Different electrostatic methods for making electret filters. *J Electrostat*. **2002**;*54*:333.
33. Chattopadhyay S, Hatton TA, Rutledge GC. Aerosol filtration using electrospun cellulose acetate fibers. *J Mater Sci*. **2016**;*51*:204.
34. Desai K, Kit K, Li J, Davidson PM, Zivanovic S, Meyer H. Nanofibrous chitosan non-wovens for filtration applications. *Polymer*. **2009**;*50*:3661.
35. Yu M, Guo Y, Wang X, Zhu H, Li W, Zhou J. Lignin-based electrospinning nanofibers for reversible iodine capture and potential applications. *Int J Biol Macromol*. **2022**;*208*:782.
36. Zhou J, Hu Z, Zabihi F, Chen Z, Zhu M. Progress and perspective of antiviral protective material. *Adv Fiber Mater*. **2020**;*2*:123.
37. Rai M, Deshmukh SD, Ingle AP, Gupta IR, Galdiero M, Galdiero S. Metal nanoparticles: the protective nanoshield against virus infection. *Crit Rev Microbiol*. **2016**;*42*:46.
38. Aderibigbe BA. Metal-based nanoparticles for the treatment of infectious diseases. *Molecules*. **2017**;*22*:1370.
39. Gupta AK, Gupta M. Synthesis and surface engineering of iron oxide nanoparticles for biomedical applications. *Biomaterials*. **2005**;*26*:3995.
40. Ahamed M, Akhtar MJ, Alhadlaq HA, Alrokayan SA. Assessment of the lung toxicity of copper oxide nanoparticles: current status. *Nanomedicine*. **2015**;*10*:2365.
41. Park S, Lee YK, Jung M, Kim KH, Chung N, Ahn E-K, Lim Y, Lee K-H. Cellular toxicity of various inhalable metal nanoparticles on human alveolar epithelial cells. *Inhalation Toxicol*. **2007**;*19*:59.
42. Abe S, Iwadera N, Esaki M, Kida I, Mutoh M, Akasaka T, Uo M, Yawaka Y, Morita M, Haneda K, editors. Internal distribution of micro-/nano-sized inorganic particles and their cytocompatibility. IOP Conference Series: Materials Science and Engineering; 2011: IOP Publishing.
43. Yang Z, Liu Z, Allaker R, Reip P, Oxford J, Ahmad Z, Ren G. A review of nanoparticle functionality and toxicity on the central nervous system. *J R Soc Interface*. **2010**;*7*:S411.
44. Lysenko V, Lozovski V, Spivak M. Nanophysics and antiviral therapy. *Ukr J Phys*. **2013**;*58*:77.
45. Crozier K, Sundaramurthy A, Kino G, Quate C. Optical antennas: resonators for local field enhancement. *J Appl Phys*. **2003**;*94*:4632.
46. Lozovski V, Lysenko V, Piatnytsia V, Scherbakov O, Zholobak N, Spivak M. Physical point of view for antiviral effect caused by the interaction between the viruses and nanoparticles. *J Bionanosci*. **2012**;*6*:109.
47. Marsh M, Helenius A. Virus entry: open sesame. *Cell*. **2006**;*124*:729.
48. Skehel JJ, Wiley DC. Receptor binding and membrane fusion in virus entry: the influenza hemagglutinin. *Annu Rev Biochem*. **2000**;*69*:531.
49. Sullivan N, Sun Y, Sattentau Q, Thali M, Wu D, Denisova G, Gershoni J, Robinson J, Moore J, Sodroski J. CD4-induced conformational changes in the human immunodeficiency virus type 1 gp120 glycoprotein: consequences for virus entry and neutralization. *J Virol*. **1998**;*72*:4694.
50. Bewley MC, Springer K, Zhang Y-B, Freimuth P, Flanagan JM. Structural analysis of the mechanism of adenovirus binding to its human cellular receptor. *CAR Sci*. **1999**;*286*:1579.
51. Sturman LS, Ricard C, Holmes K. Conformational change of the coronavirus peplomer glycoprotein at pH 8.0 and 37 degrees C correlates with virus aggregation and virus-induced cell fusion. *J Virol*. **1990**;*64*:3042.
52. Longmire M, Choyke PL, Kobayashi H. Clearance properties of nano-sized particles and molecules as imaging agents: considerations and caveats. **2008**.
53. Liu J, Yu M, Zhou C, Zheng J. Renal clearable inorganic nanoparticles: a new frontier of bionanotechnology. *Mater Today*. **2013**;*16*:477.
54. Novello F, Stirpe F. The effects of copper and other ions on the ribonucleic acid polymerase activity of isolated rat liver nuclei. *Biochem J*. **1969**;*111*:115.
55. Fahmy B, Cormier SA. Copper oxide nanoparticles induce oxidative stress and cytotoxicity in airway epithelial cells. *Toxicol In Vitro*. **2009**;*23*:1365.
56. Fujimori Y, Sato T, Hayata T, Nagao T, Nakayama M, Nakayama T, Sugamata R, Suzuki K. Novel antiviral characteristics of nanosized copper (I) iodide particles showing inactivation activity against 2009 pandemic H1N1 influenza virus. *Appl Environ Microbiol*. **2012**;*78*:951.
57. Oikawa S, Kawanishi S. Distinct mechanisms of site-specific DNA damage induced by endogenous reductants in the presence of iron (III) and copper (II). *Biochim Biophys Acta Gene Struct Exp*. **1998**;*1399*:19.

58. Rifkind JM, Shin YA, Heim JM, Eichhorn GL. Cooperative disordering of single-stranded polynucleotides through copper crosslinking. *Biopolym Original Res Biomol*. **1879**;*1976*:15.
59. Burkitt MJ. A critical overview of the chemistry of copper-dependent low density lipoprotein oxidation: roles of lipid hydroperoxides, α-tocopherol, thiols, and ceruloplasmin. *Arch Biochem Biophys*. **2001**;*394*:117.
60. Segelmark M, Persson B, Hellmark T, Wieslander J. Binding and inhibition of myeloperoxidase (MPO): a major function of ceruloplasmin? *Clin Exp Immunol*. **1997**;*108*:167.
61. Kenneth N, Hucks G, Kocab A, McCollom A, Duckett C. Copper is a potent inhibitor of both the canonical and non-canonical NFκB pathways. *Cell Cycle*. **2014**;*13*:1006.
62. Zischka H, Kroemer G. Copper—a novel stimulator of autophagy. *Cell stress*. **2020**;*4*:92.
63. Jin S. The cross-regulation between autophagy and type I interferon signaling in host defense. *Autophagy Regul Innate Immunity*. **2019**;*125*:2.
64. Lysenko V, Lozovski V, Lokshyn M, Gomeniuk YV, Dorovskih A, Rusinchuk N, Pankivska Y, Povnitsa O, Zagorodnya S, Tertykh V. Nanoparticles as antiviral agents against adenoviruses. *Adv Nat Sci Nanosci Nanotechnol*. **2018**;*9*: 025021.
65. Das S, Debnath N, Mitra S, Datta A, Goswami A. Comparative analysis of stability and toxicity profile of three differently capped gold nanoparticles for biomedical usage. *Biometals*. **2012**;*25*:1009.
66. Wang C, Zhu W, Luo Y, Wang B-Z. Gold nanoparticles conjugating recombinant influenza hemagglutinin trimers and flagellin enhanced mucosal cellular immunity. *Nanomed Nanotechnol Biol Med*. **2018**;*14*:1349.
67. Te Velthuis AJ, van den Worm SH, Sims AC, Baric RS, Snijder EJ, van Hemert MJ. Zn2+ inhibits coronavirus and arterivirus RNA polymerase activity in vitro and zinc ionophores block the replication of these viruses in cell culture. *PLoS Pathog*. **2010**;*6*: e1001176.
68. Jiang J, Pi J, Cai J. The advancing of zinc oxide nanoparticles for biomedical applications. *Bioinorgan Chem Appl*. **2018**;*20*:18.
69. Prasad AS, Bao B, Beck FW, Sarkar FH. Zinc-suppressed inflammatory cytokines by induction of A20-mediated inhibition of nuclear factor-κB. *Nutrition*. **2011**;*27*:816.
70. Friedman RL, Manly SP, McMahon M, Kerr IM, Stark GR. Transcriptional and posttranscriptional regulation of interferon-induced gene expression in human cells. *Cell*. **1984**;*38*:745.
71. Overbeck S, Rink L, Haase H. Modulating the immune response by oral zinc supplementation: a single approach for multiple diseases. *Arch Immunol Ther Exp*. **2008**;*56*:15.
72. Lv X, Wang P, Bai R, Cong Y, Suo S, Ren X, Chen C. Inhibitory effect of silver nanomaterials on transmissible virus-induced host cell infections. *Biomaterials*. **2014**;*35*:4195.
73. Hu S, Yi T, Huang Z, Liu B, Wang J, Yi X, Liu J. Etching silver nanoparticles using DNA. *Mater Horiz*. **2019**;*6*:155.
74. Rahman K. Studies on free radicals, antioxidants, and co-factors. *Clin Interv Aging*. **2007**;*2*:219.
75. Stambe C, Atkins RC, Tesch GH, Masaki T, Schreiner GF, Nikolic-Paterson DJ. The role of p38α mitogen-activated protein kinase activation in renal fibrosis. *J Am Soc Nephrol*. **2004**;*15*:370.
76. Chaudhary V, Mostafavi E, Kaushik A. De-coding Ag as an efficient antimicrobial nano-system for controlling cellular/biological functions. *Matter*. **1995**;*2022*:5.
77. Du T, Liang J, Dong N, Lu J, Fu Y, Fang L, Xiao S, Han H. Glutathione-capped Ag2S nanoclusters inhibit coronavirus proliferation through blockage of viral RNA synthesis and budding. *ACS Appl Mater Interfaces*. **2018**;*10*:4369.
78. Villeret B, Dieu A, Straube M, Solhonne B, Miklavc P, Hamadi S, Le Borgne R, Mailleux A, Norel X, Aerts J. Silver nanoparticles impair retinoic acid-inducible gene I-mediated mitochondrial antiviral immunity by blocking the autophagic flux in lung epithelial cells. *ACS Nano*. **2018**;*12*:1188.
79. Li Y, Lin Z, Xu T, Wang C, Zhao M, Xiao M, Wang H, Deng N, Zhu B. Delivery of VP1 siRNA to inhibit the EV71 virus using functionalized silver nanoparticles through ROS-mediated signaling pathways. *RSC Adv*. **2017**;*7*:1453.
80. Gerrity D, Ryu H, Crittenden J, Abbaszadegan M. Photocatalytic inactivation of viruses using titanium dioxide nanoparticles and low-pressure UV light. *J Environ Sci Health, Part A*. **2008**;*43*:1261.
81. Levina AS, Repkova MN, Zarytova VF, Mazurkova NA, editors. TiO2~ DNA nanocomposites as efficient site-specific antiviral agents against influenza A virus in cell culture. 2015 IEEE 15th International Conference on Nanotechnology (IEEE-NANO); 2015: IEEE.
82. Eom H-J, Choi J. Oxidative stress of CeO2 nanoparticles via p38-Nrf-2 signaling pathway in human bronchial epithelial cell, Beas-2B. *Toxicol Lett*. **2009**;*187*:77.
83. Jebali A, Hekmatimoghaddam S, Kazemi B, Allaveisie A, Masoudi A, Daliri K, Sedighi N, Ranjbari J. Lectin coated MgO nanoparticle: its toxicity, antileishmanial activity, and macrophage activation. *Drug Chem Toxicol*. **2014**;*37*:400.
84. Li Y, Lin Z, Gong G, Guo M, Xu T, Wang C, Zhao M, Xia Y, Tang Y, Zhong J. Inhibition of H1N1 influenza virus-induced apoptosis by selenium nanoparticles functionalized with arbidol through ROS-mediated signaling pathways. *J Mater Chem B*. **2019**;*7*:4252.
85. Wang C, Chen H, Chen D, Zhao M, Lin Z, Guo M, Xu T, Chen Y, Hua L, Lin T. The inhibition of H1N1 influenza virus-induced apoptosis by surface decoration of selenium nanoparticles with β-thujaplicin through reactive oxygen species-mediated AKT and p53 signaling pathways. *ACS Omega*. **2020**;*5*:30633.
86. Olakanmi O, Britigan BE, Schlesinger LS. Gallium disrupts iron metabolism of mycobacteria residing within human macrophages. *Infect Immun*. **2000**;*68*:5619.
87. Zhang L, Chen Y, Wu L, Liu Y, Wang J. Effects of iron nanoparticles on immune response of two immunocytes like virus. *Nanosci Nanotechnol Lett*. **1934**;*2017*:9.
88. Tiwari PM, Vig K, Dennis VA, Singh SR. Functionalized gold nanoparticles and their biomedical applications. *Nanomaterials*. **2011**;*1*:31.
89. Mostafavi E, Zarepour A, Barabadi H, Zarrabi A, Truong LB, Medina-Cruz D. Antineoplastic activity of biogenic silver and gold nanoparticles to combat leukemia: beginning a new era in cancer theragnostic. *Biotechnol Rep*. **2022**;*34*: e00714.
90. Huaizhi Z, Yuantao N. China's ancient gold drugs. *Gold Bull*. **2001**;*34*:24.
91. Sutton BM. Gold compounds for rheumatoid arthritis. *Gold Bull*. **1986**;*19*:15.
92. Berners-Price SJ, Filipovska A. Gold compounds as therapeutic agents for human diseases. *Metallomics*. **2011**;*3*:863.
93. Fricker SP. Medicinal chemistry and pharmacology of gold compounds. *Transition Met Chem*. **1996**;*21*:377.
94. Li F, Li W, Farzan M, Harrison SC. Structure of SARS coronavirus spike receptor-binding domain complexed with receptor. *Science*. **1864**;*2005*:309.
95. Peña-González CE, García-Broncano P, Ottaviani MF, Cangiotti M, Fattori A, Hierro-Oliva M, González-Martín ML, Pérez-Serrano J, Gómez R, Muñoz-Fernández MÁ. Dendronized anionic gold nanoparticles: synthesis, characterization, and antiviral activity. *Chem A Eur J*. **2016**;*22*:2987.
96. Di Gianvincenzo P, Marradi M, Martínez-Ávila OM, Bedoya LM, Alcamí J, Penadés S. Gold nanoparticles capped with sulfate-ended ligands as anti-HIV agents. *Bioorg Med Chem Lett*. **2010**;*20*:2718.

97. Bowman M-C, Ballard TE, Ackerson CJ, Feldheim DL, Margolis DM, Melander C. Inhibition of HIV fusion with multivalent gold nanoparticles. *J Am Chem Soc*. **2008**;*130*:6896.
98. Baram-Pinto D, Shukla S, Gedanken A, Sarid R. Inhibition of HSV-1 attachment, entry, and cell-to-cell spread by functionalized multivalent gold nanoparticles. *Small*. **2010**;*6*:1044.
99. Cagno V, Andreozzi P, D'Alicarnasso M, Jacob Silva P, Mueller M, Galloux M, Le Goffic R, Jones ST, Vallino M, Hodek J. Broad-spectrum non-toxic antiviral nanoparticles with a virucidal inhibition mechanism. *Nat Mater*. **2018**;*17*:195.
100. Carja G, Grosu EF, Petrarean C, Nichita N. Self-assemblies of plasmonic gold/layered double hydroxides with highly efficient antiviral effect against the hepatitis B virus. *Nano Res*. **2015**;*8*:3512.
101. Mukherjee P, Bhattacharya R, Wang P, Wang L, Basu S, Nagy JA, Atala A, Mukhopadhyay D, Soker S. Antiangiogenic properties of gold nanoparticles. *Clin Cancer Res*. **2005**;*11*:3530.
102. Papp I, Sieben C, Ludwig K, Roskamp M, Böttcher C, Schlecht S, Herrmann A, Haag R. Inhibition of influenza virus infection by multivalent sialic-acid-functionalized gold nanoparticles. *Small*. **2010**;*6*:2900.
103. Tazaki T, Tabata K, Ainai A, Ohara Y, Kobayashi S, Ninomiya T, Orba Y, Mitomo H, Nakano T, Hasegawa H. Shape-dependent adjuvanticity of nanoparticle-conjugated RNA adjuvants for intranasal inactivated influenza vaccines. *RSC Adv*. **2018**;*8*:16527.
104. Mishra YK, Adelung R, Röhl C, Shukla D, Spors F, Tiwari V. Virostatic potential of micro–nano filopodia-like ZnO structures against herpes simplex virus-1. *Antiviral Res*. **2011**;*92*:305.
105. Ghaffari H, Tavakoli A, Moradi A, Tabarraei A, Bokharaei-Salim F, Zahmatkeshan M, Farahmand M, Javanmard D, Kiani SJ, Esghaei M. Inhibition of H1N1 influenza virus infection by zinc oxide nanoparticles: another emerging application of nanomedicine. *J Biomed Sci*. **2019**;*26*:1.
106. Tavakoli A, Ataei-Pirkooh A, Mm Sadeghi G, Bokharaei-Salim F, Sahrapour P, Kiani SJ, Moghoofei M, Farahmand M, Javanmard D, Monavari SH. Polyethylene glycol-coated zinc oxide nanoparticle: an efficient nanoweapon to fight against herpes simplex virus type 1. *Nanomedicine*. **2018**;*13*:2675.
107. Farouk F, Shebl R. Comparing surface chemical modifications of zinc oxide nanoparticles for modulating their antiviral activity against herpes simplex virus type-1. *Int J Nanopart Nanotechnol*. **2018**;*4*:21.
108. Antoine TE, Mishra YK, Trigilio J, Tiwari V, Adelung R, Shukla D. Prophylactic, therapeutic and neutralizing effects of zinc oxide tetrapod structures against herpes simplex virus type-2 infection. *Antiviral Res*. **2012**;*96*:363.
109. Talank N, Morad H, Barabadi H, Mojab F, Amidi S, Kobarfard F, Mahjoub MA, Jounaki K, Mohammadi N, Salehi G. Bioengineering of green-synthesized silver nanoparticles: In vitro physicochemical, antibacterial, biofilm inhibitory, anticoagulant, and antioxidant performance. *Talanta*. **2022**;*243*: 123374.
110. Gaikwad S, Ingle A, Gade A, Rai M, Falanga A, Incoronato N, Russo L, Galdiero S, Galdiero M. Antiviral activity of mycosynthesized silver nanoparticles against herpes simplex virus and human parainfluenza virus type 3. *Int J Nanomed*. **2013**;*8*:4303.
111. Lu L, Sun RW-Y, Chen R, Hui C-K, Ho C-M, Luk JM, Lau GK, Che C-M. Silver nanoparticles inhibit hepatitis B virus replication. *Antivir Ther*. **2008**;*13*:253.
112. Speshock JL, Murdock RC, Braydich-Stolle LK, Schrand AM, Hussain SM. Interaction of silver nanoparticles with Tacaribe virus. *J Nanobiotechnol*. **2010**;*8*:1.
113. Dos Santos CA, Seckler MM, Ingle AP, Gupta I, Galdiero S, Galdiero M, Gade A, Rai M. Silver nanoparticles: therapeutical uses, toxicity, and safety issues. *J Pharm Sci*. **1931**;*2014*:103.
114. Trefry JC, Wooley DP. Silver nanoparticles inhibit vaccinia virus infection by preventing viral entry through a macropinocytosis-dependent mechanism. *J Biomed Nanotechnol*. **2013**;*9*:1624.
115. Lara HH, Ixtepan-Turrent L, Garza-Treviño EN, Rodriguez-Padilla C. PVP-coated silver nanoparticles block the transmission of cell-free and cell-associated HIV-1 in human cervical culture. *J Nanobiotechnol*. **2010**;*8*:1.
116. Castro-Mayorga JL, Randazzo W, Fabra MJ, Lagaron J, Aznar R, Sánchez G. Antiviral properties of silver nanoparticles against norovirus surrogates and their efficacy in coated polyhydroxyalkanoates systems. *LWT-Food Sci Technol*. **2017**;*79*:503.
117. Xiang D-x, Chen Q, Pang L, Zheng C-l. Inhibitory effects of silver nanoparticles on H1N1 influenza A virus in vitro. *J Virol Methods*. **2011**;*178*:137.
118. Mehrbod P, Motamed N, Tabatabaeian M, Soleimani ER, Amini E, Shahidi M, Kheyri M. In Vitro Antiviral Effect Of " Nanosilver " on Influenza Virus. **2009**.
119. Zheng Y, Cloutier P, Hunting DJ, Sanche L. Radiosensitization by gold nanoparticles: comparison of DNA damage induced by low and high-energy electrons. *J Biomed Nanotechnol*. **2008**;*4*:469.
120. Lara HH, Ayala-Nuñez NV, Ixtepan-Turrent L, Rodriguez-Padilla C. Mode of antiviral action of silver nanoparticles against HIV-1. *J Nanobiotechnol*. **2010**;*8*:1.
121. Elechiguerra JL, Burt JL, Morones JR, Camacho-Bragado A, Gao X, Lara HH, Yacaman MJ. Interaction of silver nanoparticles with HIV-1. *J Nanobiotechnol*. **2005**;*3*:1.
122. Mori Y, Ono T, Miyahira Y, Nguyen VQ, Matsui T, Ishihara M. Antiviral activity of silver nanoparticle/chitosan composites against H1N1 influenza A virus. *Nanoscale Res Lett*. **2013**;*8*:1.
123. Sreekanth T, Nagajyothi P, Muthuraman P, Enkhtaivan G, Vattikuti S, Tettey C, Kim DH, Shim J, Yoo K. Ultra-sonication-assisted silver nanoparticles using Panax ginseng root extract and their anti-cancer and antiviral activities. *J Photochem Photobiol, B*. **2018**;*188*:6.
124. Huy TQ, Thanh NTH, Thuy NT, Van Chung P, Hung PN, Le A-T, Hanh NTH. Cytotoxicity and antiviral activity of electrochemical–synthesized silver nanoparticles against poliovirus. *J Virol Methods*. **2017**;*241*:52.
125. Baram-Pinto D, Shukla S, Perkas N, Gedanken A, Sarid R. Inhibition of herpes simplex virus type 1 infection by silver nanoparticles capped with mercaptoethane sulfonate. *Bioconjug Chem*. **2009**;*20*:1497.
126. Chen N, Zheng Y, Yin J, Li X, Zheng C. Inhibitory effects of silver nanoparticles against adenovirus type 3 in vitro. *J Virol Methods*. **2013**;*193*:470.
127. Rogers JV, Parkinson CV, Choi YW, Speshock JL, Hussain SM. A preliminary assessment of silver nanoparticle inhibition of monkeypox virus plaque formation. *Nanoscale Res Lett*. **2008**;*3*:129.
128. Xiang D, Zheng Y, Duan W, Li X, Yin J, Shigdar S, O'Connor ML, Marappan M, Zhao X, Miao Y. Inhibition of A/Human/Hubei/3/2005 (H3N2) influenza virus infection by silver nanoparticles in vitro and in vivo. *Int J Nanomed*. **2013**;*8*:4103.
129. Navarro E, Piccapietra F, Wagner B, Marconi F, Kaegi R, Odzak N, Sigg L, Behra R. Toxicity of silver nanoparticles to Chlamydomonas reinhardtii. *Environ Sci Technol*. **2008**;*42*:8959.
130. Hatchett DW, White HS. Electrochemistry of sulfur adlayers on the low-index faces of silver. *J Phys Chem*. **1996**;*100*:9854.
131. Munger MA, Radwanski P, Hadlock GC, Stoddard G, Shaaban A, Falconer J, Grainger DW, Deering-Rice CE. In vivo human time-exposure study of orally dosed commercial silver nanoparticles. *Nanomed Nanotechnol Biol Med*. **2014**;*10*:1.
132. Akhtar S, Shahzad K, Mushtaq S, Ali I, Rafe MH, Fazal-ul-Karim SM. Antibacterial and antiviral potential of colloidal

Titanium dioxide (TiO2) nanoparticles suitable for biological applications. *Mater Res Exp*. **2019**;*6*: 105409.
133. Mazurkova N, Spitsyna YE, Shikina N, Ismagilov Z, Zagrebel'Nyi S, Ryabchikova E. Interaction of titanium dioxide nanoparticles with influenza virus. *Nanotechnol Russ*. **2010**;*5*:417.
134. Lokshyn M, Lozovski V, Lysenko V, Piatnytsia V, Spivak M, Sterligov V, editors. Nanoparticles in antivirus therapy. Advanced Materials Research; 2014: Trans Tech Publ.
135. Motoike K, Hirano S, Yamana H, Onda T, Maeda T, Ito T, Hayakawa M. Antiviral activities of heated dolomite powder. *Biocontrol Sci*. **2008**;*13*:131.
136. Koper OB, Klabunde JS, Marchin GL, Klabunde KJ, Stoimenov P, Bohra L. Nanoscale powders and formulations with biocidal activity toward spores and vegetative cells of bacillus species, viruses, and toxins. *Curr Microbiol*. **2002**;*44*:49.
137. Rafiei S, Rezatofighi SE, Ardakani MR, Madadgar O. In vitro anti-foot-and-mouth disease virus activity of magnesium oxide nanoparticles. *IET Nanobiotechnol*. **2015**;*9*:247.
138. Li Y, Lin Z, Guo M, Xia Y, Zhao M, Wang C, Xu T, Chen T, Zhu B. Inhibitory activity of selenium nanoparticles functionalized with oseltamivir on H1N1 influenza virus. *Int J Nanomed*. **2017**;*12*:5733.
139. Lin Z, Li Y, Guo M, Xiao M, Wang C, Zhao M, Xu T, Xia Y, Zhu B. Inhibition of H1N1 influenza virus by selenium nanoparticles loaded with zanamivir through p38 and JNK signaling pathways. *RSC Adv*. **2017**;*7*:35290.
140. Ramya S, Shanmugasundaram T, Balagurunathan R. Biomedical potential of actinobacterially synthesized selenium nanoparticles with special reference to anti-biofilm, anti-oxidant, wound healing, cytotoxic and anti-viral activities. *J Trace Elem Med Biol*. **2015**;*32*:30.
141. Liu X, Chen D, Su J, Zheng R, Ning Z, Zhao M, Zhu B, Li Y. Selenium nanoparticles inhibited H1N1 influenza virus-induced apoptosis by ROS-mediated signaling pathways. *RSC Adv*. **2022**;*12*:3862.
142. Singh A, Singh P, Kumar R, Kaushik A. Exploring nanoselenium to tackle mutated SARS-CoV-2 for efficient COVID-19 management. *Front Nanotechnol*. **2022**;*4*:1004729.
143. Choi S-r, Britigan BE, Narayanasamy P. Ga (III) nanoparticles inhibit growth of both Mycobacterium tuberculosis and HIV and release of interleukin-6 (IL-6) and IL-8 in coinfected macrophages. *Antimicrob Agents Chemother*. **2017**;*61*: e02505.
144. Narayanasamy P, Switzer BL, Britigan BE. Prolonged-acting, multi-targeting gallium nanoparticles potently inhibit growth of both HIV and mycobacteria in co-infected human macrophages. *Sci Rep*. **2015**;*5*:1.
145. Kumar R, Nayak M, Sahoo GC, Pandey K, Sarkar MC, Ansari Y, Das V, Topno R, Madhukar M, Das P. Iron oxide nanoparticles based antiviral activity of H1N1 influenza A virus. *J Infect Chemother*. **2019**;*25*:325.
146. Savarino A, Pescarmona GP, Boelaert JR. Iron metabolism and HIV infection: reciprocal interactions with potentially harmful consequences? *Cell Biochem Funct*. **1999**;*17*:279.
147. Masarwa M, Cohen H, Meyerstein D, Hickman DL, Bakac A, Espenson JH. Reactions of low-valent transition-metal complexes with hydrogen peroxide. Are they" Fenton-like" or not? 1. The case of Cu+ aq and Cr2+ aq. *J Am Chem Soc*. **1988**;*110*:4293.
148. Noyce J, Michels H, Keevil C. Inactivation of influenza A virus on copper versus stainless steel surfaces. *Appl Environ Microbiol*. **2007**;*73*:2748.
149. Shionoiri N, Sato T, Fujimori Y, Nakayama T, Nemoto M, Matsunaga T, Tanaka T. Investigation of the antiviral properties of copper iodide nanoparticles against feline calicivirus. *J Biosci Bioeng*. **2012**;*113*:580.
150. Gledhill M, Devez A, Highfield A, Singleton C, Achterberg EP, Schroeder D. Effect of metals on the lytic cycle of the coccolithovirus, EhV86. *Front Microbiol*. **2012**;*3*:155.
151. Weaver L, Noyce J, Michels H, Keevil C. Potential action of copper surfaces on meticillin-resistant Staphylococcus aureus. *J Appl Microbiol*. **2010**;*109*:2200.
152. Yamamoto K, Miyoshi-Koshio T, Utsuki Y, Mizuno S, Suzuki K. Virucidal activity and viral protein modification by myeloperoxidase: a candidate for defense factor of human polymorphonuclear leukocytes against influenza virus infection. *J Infect Dis*. **1991**;*164*:8.
153. Sucipto TH, Churrotin S, Setyawati H, Kotaki T, Martak F, Soegijanto S. Antiviral activity of copper(II) chlorid dihydrate against Dengue virus type-2 in vero cell.
154. Borkow G, Sidwell RW, Smee DF, Barnard DL, Morrey JD, Lara-Villegas HH, Shemer-Avni Y, Gabbay J. Neutralizing viruses in suspensions by copper oxide-based filters. *Antimicrob Agents Chemother*. **2007**;*51*:2605.
155. Borkow G, Lara HH, Covington CY, Nyamathi A, Gabbay J. Deactivation of human immunodeficiency virus type 1 in medium by copper oxide-containing filters. *Antimicrob Agents Chemother*. **2008**;*52*:518.
156. Borkow G, Zhou SS, Page T, Gabbay J. A novel anti-influenza copper oxide containing respiratory face mask. *PLoS ONE*. **2010**;*5*: e11295.
157. Hang X, Peng H, Song H, Qi Z, Miao X, Xu W. Antiviral activity of cuprous oxide nanoparticles against Hepatitis C Virus in vitro. *J Virol Methods*. **2015**;*222*:150.
158. Yugandhar P, Vasavi T, Jayavardhana Rao Y, Uma Maheswari Devi P, Narasimha G, Savithramma N. Cost effective, green synthesis of copper oxide nanoparticles using fruit extract of Syzygium alternifolium (Wt) Walp, characterization and evaluation of antiviral activity. *J Clust Sci*. **2018**;*29*:743.
159. Tavakoli A, Hashemzadeh MS. Inhibition of herpes simplex virus type 1 by copper oxide nanoparticles. *J Virol Methods*. **2020**;*275*: 113688.
160. Chen Z, Meng H, Xing G, Chen C, Zhao Y, Jia G, Wang T, Yuan H, Ye C, Zhao F. Acute toxicological effects of copper nanoparticles in vivo. *Toxicol Lett*. **2006**;*163*:109.
161. Prabhu BM, Ali SF, Murdock RC, Hussain SM, Srivatsan M. Copper nanoparticles exert size and concentration dependent toxicity on somatosensory neurons of rat. *Nanotoxicology*. **2010**;*4*:150.
162. Sun T, Yan Y, Zhao Y, Guo F, Jiang C. Copper oxide nanoparticles induce autophagic cell death in A549 cells. **2012**.
163. Karlsson HL, Gustafsson J, Cronholm P, Möller L. Size-dependent toxicity of metal oxide particles—a comparison between nano-and micrometer size. *Toxicol Lett*. **2009**;*188*:112.
164. Ahamed M, Siddiqui MA, Akhtar MJ, Ahmad I, Pant AB, Alhadlaq HA. Genotoxic potential of copper oxide nanoparticles in human lung epithelial cells. *Biochem Biophys Res Commun*. **2010**;*396*:578.
165. Akhtar MJ, Kumar S, Alhadlaq HA, Alrokayan SA, Abu-Salah KM, Ahamed M. Dose-dependent genotoxicity of copper oxide nanoparticles stimulated by reactive oxygen species in human lung epithelial cells. *Toxicol Ind Health*. **2016**;*32*:809.
166. Karlsson HL, Cronholm P, Gustafsson J, Moller L. Copper oxide nanoparticles are highly toxic: a comparison between metal oxide nanoparticles and carbon nanotubes. *Chem Res Toxicol*. **2008**;*21*:1726.
167. Wang Z, Li N, Zhao J, White JC, Qu P, Xing B. CuO nanoparticle interaction with human epithelial cells: cellular uptake, location, export, and genotoxicity. *Chem Res Toxicol*. **2012**;*25*:1512.
168. Hanagata N, Zhuang F, Connolly S, Li J, Ogawa N, Xu M. Molecular responses of human lung epithelial cells to the toxicity

of copper oxide nanoparticles inferred from whole genome expression analysis. *ACS Nano*. **2011**;*5*:9326.
169. Cronholm P, Karlsson HL, Hedberg J, Lowe TA, Winnberg L, Elihn K, Wallinder IO, Möller L. Intracellular uptake and toxicity of Ag and CuO nanoparticles: a comparison between nanoparticles and their corresponding metal ions. *Small*. **2013**;*9*:970.
170. Midander K, Cronholm P, Karlsson HL, Elihn K, Möller L, Leygraf C, Wallinder IO. Surface characteristics, copper release, and toxicity of nano-and micrometer-sized copper and copper (II) oxide particles: a cross-disciplinary study. *Small*. **2009**;*5*:389.
171. Moschini E, Gualtieri M, Colombo M, Fascio U, Camatini M, Mantecca P. The modality of cell–particle interactions drives the toxicity of nanosized CuO and TiO2 in human alveolar epithelial cells. *Toxicol Lett*. **2013**;*222*:102.
172. Zhang H, Ji Z, Xia T, Meng H, Low-Kam C, Liu R, Pokhrel S, Lin S, Wang X, Liao Y-P. Use of metal oxide nanoparticle band gap to develop a predictive paradigm for oxidative stress and acute pulmonary inflammation. *ACS Nano*. **2012**;*6*:4349.
173. Cho W-S, Duffin R, Poland CA, Howie SE, MacNee W, Bradley M, Megson IL, Donaldson K. Metal oxide nanoparticles induce unique inflammatory footprints in the lung: important implications for nanoparticle testing. *Environ Health Perspect*. **2010**;*118*:1699.
174. Yokohira M, Hashimoto N, Yamakawa K, Suzuki S, Saoo K, Kuno T, Imaida K. Lung carcinogenic bioassay of CuO and TiO2 nanoparticles with intratracheal instillation using F344 male rats. *J Toxicol Pathol*. **2009**;*22*:71.
175. Yokohira M, Kuno T, Yamakawa K, Hosokawa K, Matsuda Y, Hashimoto N, Suzuki S, Saoo K, Imaida K. Lung toxicity of 16 fine particles on intratracheal instillation in a bioassay model using f344 male rats. *Toxicol Pathol*. **2008**;*36*:620.
176. Sagripanti J-L, Routson LB, Bonifacino AC, Lytle CD. Mechanism of copper-mediated inactivation of herpes simplex virus. *Antimicrob Agents Chemother*. **1997**;*41*:812.
177. Miyamoto D, Kusagaya Y, Endo N, Sometani A, Takeo S, Suzuki T, Arima Y, Nakajima K, Suzuki Y. Thujaplicin–copper chelates inhibit replication of human influenza viruses. *Antiviral Res*. **1998**;*39*:89.
178. Borkow G, Gabbay J. Putting copper into action: copper-impregnated products with potent biocidal activities. *FASEB J*. **2004**;*18*:1728.
179. Imai K, Ogawa H, Bui VN, Inoue H, Fukuda J, Ohba M, Yamamoto Y, Nakamura K. Inactivation of high and low pathogenic avian influenza virus H5 subtypes by copper ions incorporated in zeolite-textile materials. *Antiviral Res*. **2012**;*93*:225.
180. Bleichert P, Espírito Santo C, Hanczaruk M, Meyer H, Grass G. Inactivation of bacterial and viral biothreat agents on metallic copper surfaces. *Biometals*. **2014**;*27*:1179.
181. Warnes SL, Keevil CW. Inactivation of norovirus on dry copper alloy surfaces. *PLoS ONE*. **2013**;*8*: e75017.
182. Sundberg K, Champagne V, McNally B, Helfritch D, Sisson R. Effectiveness of nanomaterial copper cold spray surfaces on inactivation of influenza A virus. *J Biotechnol Biomater*. **2015**;*5*:205.
183. Gordon NA, McGuire KL, Wallentine SK, Mohl GA, Lynch JD, Harrison RG, Busath DD. Divalent copper complexes as influenza A M2 inhibitors. *Antiviral Res*. **2017**;*147*:100.
184. Sunada K, Minoshima M, Hashimoto K. Highly efficient antiviral and antibacterial activities of solid-state cuprous compounds. *J Hazard Mater*. **2012**;*235*:265.
185. Vijayakumar S, Ganesan S. Gold nanoparticles as an HIV entry inhibitor. *Curr HIV Res*. **2012**;*10*:643.
186. Sun L, Singh AK, Vig K, Pillai SR, Singh SR. Silver nanoparticles inhibit replication of respiratory syncytial virus. *J Biomed Nanotechnol*. **2008**;*4*:149.
187. Sano Y. Antiviral activity of alginate against infection by tobacco mosaic virus. *Carbohyd Polym*. **1999**;*38*:183.
188. Morad H, Jahanshahi M, Akbari J, Saeedi M, Gill P, Enayatifard R. Novel topical and transdermal delivery of colchicine with chitosan based biocomposite nanofibrous system; formulation, optimization, characterization, ex vivo skin deposition/permeation, and anti-melanoma evaluation. *Mater Chem Phys*. **2021**;*263*: 124381.
189. Asgarirad H, Ebrahimnejad P, Mahjoub MA, Jalalian M, Morad H, Ataee R, Hosseini SS, Farmoudeh A. A promising technology for wound healing; in-vitro and in-vivo evaluation of chitosan nano-biocomposite films containing gentamicin. *J Microencapsul*. **2021**;*38*:100.
190. Chirkov S. The antiviral activity of chitosan. *Appl Biochem Microbiol*. **2002**;*38*:1.
191. Synowiecki J, Al-Khateeb NA. Production, properties, and some new applications of chitin and its derivatives. **2003**.
192. Bacon A, Makin J, Sizer P, Jabbal-Gill I, Hinchcliffe M, Illum L, Chatfield S, Roberts M. Carbohydrate biopolymers enhance antibody responses to mucosally delivered vaccine antigens. *Infect Immun*. **2000**;*68*:5764.
193. Sosa MAG, Fazely F, Koch JA, Vercellotti SV, Ruprecht RM. *N*-Carboxymethylchitosan-N, O-sulfate as an anti-HIV-1 agent. *Biochem Biophys Res Commun*. **1991**;*174*:489.
194. Ahn M-J, Yoon K-D, Min S-Y, Lee JS, Kim JH, Kim TG, Kim SH, Kim N-G, Huh H, Kim J. Inhibition of HIV-1 reverse transcriptase and protease by phlorotannins from the brown alga Ecklonia cava. *Biol Pharm Bull*. **2004**;*27*:544.
195. Witvrouw M, De Clercq E. Sulfated polysaccharides extracted from sea algae as potential antiviral drugs. *Gen Pharmacol Vasc Syst*. **1997**;*29*:497.
196. Bourgougnon N, Lahaye M, Quemener B, Chermann J, Rimbert M, Cormaci M, Furnari G, Kornprobst J. Annual variation in composition and in vitro anti-HIV-1 activity of the sulfated glucuronogalactan from Schizymenia dubyi (Rhodophyta, Gigartinales). *J Appl Phycol*. **1996**;*8*:155.
197. Sato T, Hori K. Cloning, expression, and characterization of a novel anti-HIV lectin from the cultured cyanobacterium Oscillatoria agardhii. *Fish Sci*. **2009**;*75*:743.
198. Vo T-S, Kim S-K. Potential anti-HIV agents from marine resources: an overview. *Mar Drugs*. **2010**;*8*:2871.
199. Noordeen F, Scougall CA, Grosse A, Qiao Q, Ajilian BB, Reaiche-Miller G, Finnie J, Werner M, Broering R, Schlaak JF. Therapeutic antiviral effect of the nucleic acid polymer REP 2055 against persistent duck hepatitis B virus infection. *PLoS ONE*. **2015**;*10*: e0140909.
200. Al-Mahtab M, Bazinet M, Vaillant A. Safety and efficacy of nucleic acid polymers in monotherapy and combined with immunotherapy in treatment-naive Bangladeshi patients with HBeAg+ chronic hepatitis B infection. *PLoS ONE*. **2016**;*11*: e0156667.
201. Neyts J, Reymen D, Letourneur D, Jozefonvicz J, Schols D, Este J, Andrei G, McKenna P, Witvrouw M, Ikeda S. Differential antiviral activity of derivatized dextrans. *Biochem Pharmacol*. **1995**;*50*:743.
202. Neyts J, Snoeck R, Schols D, Balzarini J, Esko JD, Van Schepdael A, De Clercq E. Sulfated polymers inhibit the interaction of human cytomegalovirus with cell surface heparan sulfate. *Virology*. **1992**;*189*:48.
203. Yamamoto I, Takayama K, Honma K, Gonda T, Matsuzaki K, Hatanaka K, Uryu T, Yoshida O, Nakashima H, Yamamoto N. Synthesis, structure and antiviral activity of sulfates of cellulose and its branched derivatives. *Carbohyd Polym*. **1990**;*14*:53.
204. Neurath AR, Strick N, Li Y-Y, Lin K, Jiang S. Design of a "microbicide" for prevention of sexually transmitted diseases using "inactive" pharmaceutical excipients. *Biologicals*. **1999**;*27*:11.
205. Gyotoku T, Aurelian L, Neurath A. Cellulose acetate phthalate (CAP): an 'inactive" pharmaceutical excipient with antiviral

activity in the mouse model of genital herpesvirus infection. *Antiviral Chem Chemother*. **1999**;*10*:327.
206. Neurath AR, Strick N, Li Y-Y, Debnath AK. Cellulose acetate phthalate, a common pharmaceutical excipient, inactivates HIV-1 and blocks the coreceptor binding site on the virus envelope glycoprotein gp120. *BMC Infect Dis*. **2001**;*1*:1.
207. Tempesta MS. Proanthocyanidin polymers having antiviral activity and methods of obtaining same. Google Patents; **1993**.
208. Hsu BB, Yinn Wong S, Hammond PT, Chen J, Klibanov AM. Mechanism of inactivation of influenza viruses by immobilized hydrophobic polycations. *Proc Natl Acad Sci*. **2011**;*108*:61.
209. Park D, Larson AM, Klibanov AM, Wang Y. Antiviral and antibacterial polyurethanes of various modalities. *Appl Biochem Biotechnol*. **2013**;*169*:1134.
210. Wang Y, Canady TD, Zhou Z, Tang Y, Price DN, Bear DG, Chi EY, Schanze KS, Whitten DG. Cationic phenylene ethynylene polymers and oligomers exhibit efficient antiviral activity. *ACS Appl Mater Interfaces*. **2011**;*3*:2209.
211. Chai Y, Feng Y, Zhang K, Li J. Preparation of fluorescent carbon dots composites and their potential applications in biomedicine and drug delivery—a review. *Pharmaceutics*. **2022**;*14*:2482.
212. Belza J, Opletalová A, Poláková K. Carbon dots for virus detection and therapy. *Microchim Acta*. **2021**;*188*:1.
213. Dong X, Moyer MM, Yang F, Sun Y-P, Yang L. Carbon dots' antiviral functions against noroviruses. *Sci Rep*. **2017**;*7*:1.
214. Ting D, Dong N, Fang L, Lu J, Bi J, Xiao S, Han H. Multisite inhibitors for enteric coronavirus: antiviral cationic carbon dots based on curcumin. *ACS Appl Nano Mater*. **2018**;*1*:5451.
215. Hu Z, Song B, Xu L, Zhong Y, Peng F, Ji X, Zhu F, Yang C, Zhou J, Su Y. Aqueous synthesized quantum dots interfere with the NF-κB pathway and confer anti-tumor, anti-viral and anti-inflammatory effects. *Biomaterials*. **2016**;*108*:187.
216. Amankwaah C. Incorporation of selected plant extracts into edible chitosan films and the effect on the antiviral, antibacterial and mechanical properties of the material. Ohio: The Ohio State University; 2013.
217. Fabra MJ, Castro-Mayorga JL, Randazzo W, Lagarón J, López-Rubio A, Aznar R, Sánchez G. Efficacy of cinnamaldehyde against enteric viruses and its activity after incorporation into biodegradable multilayer systems of interest in food packaging. *Food Environ Virol*. **2016**;*8*:125.
218. Martínez-Abad A, Ocio M, Lagarón J, Sánchez G. Evaluation of silver-infused polylactide films for inactivation of Salmonella and feline calicivirus in vitro and on fresh-cut vegetables. *Int J Food Microbiol*. **2013**;*162*:89.
219. Ueda T, Yamashina D, Kinugawa K. Copper complex titanium oxide dispersion liquid, coating agent composition, and antibacterial/antiviral member. Google Patents; **2017**.
220. Aniagyei SE, Sims LB, Malik DA, Tyo KM, Curry KC, Kim W, Hodge DA, Duan J, Steinbach-Rankins JM. Evaluation of poly (lactic-co-glycolic acid) and poly (dl-lactide-co-ε-caprolactone) electrospun fibers for the treatment of HSV-2 infection. *Mater Sci Eng, C*. **2017**;*72*:238.
221. Cordero HCP, ABARCA RQ, Vargas KD, Troncoso IP. Polymeric materials with antifouling, biocidal, antiviral and antimicrobial properties; Elaboration method and its uses. Google Patents; **2016**.
222. Roner MR, Shahi KR, Barot G, Battin A, Carraher CE. Preliminary results for the inhibition of pancreatic cancer cells by organotin polymers. *J Inorg Organomet Polym Mater*. **2009**;*19*:410.
223. Roner MR, Carraher CE Jr, Shahi K, Barot G. Antiviral activity of metal-containing polymers—Organotin and cisplatin-like polymers. *Materials*. **2011**;*4*:991.
224. Barot G, Roner MR, Naoshima Y, Nagao K, Shahi K, Carraher CE. Synthesis, structural characterization, and preliminary biological characterization of organotin polyethers derived from hydroquinone and substituted hydroquinones. *J Inorg Organomet Polym Mater*. **2009**;*19*:12.
225. Hadinejad F, Jahanshahi M, Morad H. Microwave-assisted and ultrasonic phyto-synthesis of copper nanoparticles: a comparison study. *Nano Biomed Eng*. **2021**;*13*:6.
226. Zhang S, Tang Y, Vlahovic B. A review on preparation and applications of silver-containing nanofibers. *Nanoscale Res Lett*. **2016**;*11*:1.
227. Takayama S, Nagato Y, Okubo T, Ogasawara Y. Medical mask with a functional material. Google Patents; **2013**.
228. Gabbay J. Antimicrobial and antiviral polymeric materials. Google Patents; **2007**.
229. Gabbay J. Antimicrobial, antifungal and antiviral rayon fibers. Google Patents; **2014**.
230. Yang W, Marr LC. Dynamics of airborne influenza A viruses indoors and dependence on humidity. *PLoS ONE*. **2011**;*6*: e21481.
231. Yang W, Elankumaran S, Marr LC. Concentrations and size distributions of airborne influenza A viruses measured indoors at a health centre, a day-care centre and on aeroplanes. *J R Soc Interface*. **2011**;*8*:1176.
232. Jefferson T, Foxlee R, Del Mar C, Dooley L, Ferroni E, Hewak B, Prabhala A, Nair S, Rivetti A. Interventions for the interruption or reduction of the spread of respiratory viruses. *Cochrane Database Syst Rev*. **2007**;*2*:2.
233. Conlon M. A facemask having one or more nanofiber layers. Google Patents; **2016**.
234. Grafe T, Graham K. Polymeric nanofibers and nanofiber webs: a new class of nonwovens. *Int Nonwovens J*. **2003**;*15*: 589250.
235. Faccini M, Vaquero C, Amantia D. Development of protective clothing against nanoparticle based on electrospun nanofibers. *J Nanomater*. **2012**;*20*:12.
236. Liu Y, Park M, Ding B, Kim J, El-Newehy M, Al-Deyab SS, Kim H-Y. Facile electrospun polyacrylonitrile/poly (acrylic acid) nanofibrous membranes for high efficiency particulate air filtration. *Fibers Polymers*. **2015**;*16*:629.
237. Reyes CG, Frey MW. Morphological traits essential to electrospun and grafted Nylon-6 nanofiber membranes for capturing submicron simulated exhaled breath aerosols. *J Appl Polym Sci*. **2017**;*134*:2.
238. Humphrey AE, Gaden EL. Air sterilization by fibrous media. *Ind Eng Chem*. **1955**;*47*:924.
239. Decker H, Geile F, Moorman H, Glick C. Removal of bacteria and baeterio-phage from the air by electrostatic preoipitators and spun glass filter pads. *Heat Piping Air Cond*. **1951**;*23*:125.
240. Allen HF. Air hygiene for hospitals: II. Efficiency of fibrous filters against staphylococcic droplet nuclei and bacteria-bearing dust. *J Am Med Assoc*. **1959**;*170*:261.
241. Solanki K, Grover N, Downs P, Paskaleva EE, Mehta KK, Lee L, Schadler LS, Kane RS, Dordick JS. Enzyme-based listericidal nanocomposites. *Sci Rep*. **2013**;*3*:1.
242. Gogotsi Y. Metal or metal oxide deposited fibrous materials. Google Patents; **2011**.
243. Leung WW. Nanofiber filter facemasks and cabin filters. Google Patents; **2012**.
244. Li X, Gong Y. Design of polymeric nanofiber gauze mask to prevent inhaling PM2.5 particles from haze pollution. *J Chem*. **2015**;*20*:15.
245. Gao H, Yang Y, Akampumuza O, Hou J, Zhang H, Qin X. A low filtration resistance three-dimensional composite membrane fabricated via free surface electrospinning for effective PM 2.5 capture. *Environ Sci Nano*. **2017**;*4*:864.
246. Li P, Wang C, Zhang Y, Wei F. Air filtration in the free molecular flow regime: a review of high-efficiency particulate air filters based on carbon nanotubes. *Small*. **2014**;*10*:4543.

247. Choi DY, Heo KJ, Kang J, An EJ, Jung S-H, Lee BU, Lee HM, Jung JH. Washable antimicrobial polyester/aluminum air filter with a high capture efficiency and low pressure drop. *J Hazard Mater*. **2018**;*351*:29.
248. Kharaghani D, Khan MQ, Shahzad A, Inoue Y, Yamamoto T, Rozet S, Tamada Y, Kim IS. Preparation and in-vitro assessment of hierarchal organized antibacterial breath mask based on polyacrylonitrile/silver (PAN/AgNPs) nanofiber. *Nanomaterials*. **2018**;*8*:461.
249. Hashmi M, Ullah S, Kim IS. Copper oxide (CuO) loaded polyacrylonitrile (PAN) nanofiber membranes for antimicrobial breath mask applications. *Curr Res Biotechnol*. **2019**;*1*:1.
250. Seo IY, Jeong UY. Mask having adsorption membrane provided therein. Google Patents; **2021**.
251. Zhang J, Wang X-X, Zhang B, Ramakrishna S, Yu M, Ma J-W, Long Y-Z. In situ assembly of well-dispersed Ag nanoparticles throughout electrospun alginate nanofibers for monitoring human breath—Smart fabrics. *ACS Appl Mater Interfaces*. **2018**;*10*:19863.
252. Yang A, Cai L, Zhang R, Wang J, Hsu P-C, Wang H, Zhou G, Xu J, Cui Y. Thermal management in nanofiber-based face mask. *Nano Lett*. **2017**;*17*:3506.
253. Li X, Wang N, Fan G, Yu J, Gao J, Sun G, Ding B. Electreted polyetherimide–silica fibrous membranes for enhanced filtration of fine particles. *J Colloid Interface Sci*. **2015**;*439*:12.
254. Nasiri F, Ajeli S, Semnani D, Jahanshahi M, Morad H. Fuzzy VIKOR optimization for designing high performance hydroxyapatite/polycaprolactone scaffolds for hard tissue engineering. *J Text Polymers*. **2020**;*8*:17.
255. Morad H, Jahanshahi M, Akbari J, Saeedi M, Gill P, Enayatifard R. Formulation, optimization and evaluation of nanofiber based fast dissolving drug delivery system of colchicine for pediatrics. *Int J Pediatr*. **2021**;*9*:13213.
256. Shou D, Ye L, Fan J. Gas transport properties of electrospun polymer nanofibers. *Polymer*. **2014**;*55*:3149.
257. Zhang S, Liu H, Zuo F, Yin X, Yu J, Ding B. A controlled design of ripple-like polyamide-6 nanofiber/nets membrane for high-efficiency air filter. *Small*. **2017**;*13*:1603151.
258. Zhang S, Tang N, Cao L, Yin X, Yu J, Ding B. Highly integrated polysulfone/polyacrylonitrile/polyamide-6 air filter for multilevel physical sieving airborne particles. *ACS Appl Mater Interfaces*. **2016**;*8*:29062.
259. Asper M, Hanrieder T, Quellmalz A, Mihranyan A. Removal of xenotropic murine leukemia virus by nanocellulose based filter paper. *Biologicals*. **2015**;*43*:452.
260. Thakur R, Das D, Das A. Electret air filters. *Sep Purif Rev*. **2013**;*42*:87.
261. Mohammadian M, Haghi A. Some aspects of multilayer chitosan electrospun nanofibers web. *Bulg Chem Commun*. **2013**;*45*:336.
262. Lee S, Cho AR, Park D, Kim JK, Han KS, Yoon I-J, Lee MH, Nah J. Reusable polybenzimidazole nanofiber membrane filter for highly breathable PM2.5 dust proof mask. *ACS Appl Mater Interfaces*. **2019**;*11*:2750.
263. Hung C-H, Leung WW-F. Filtration of nano-aerosol using nanofiber filter under low Peclet number and transitional flow regime. *Sep Purif Technol*. **2011**;*79*:34.
264. Sambaer W, Zatloukal M, Kimmer D. 3D air filtration modeling for nanofiber based filters in the ultrafine particle size range. *Chem Eng Sci*. **2012**;*82*:299.
265. Wang N, Si Y, Wang N, Sun G, El-Newehy M, Al-Deyab SS, Ding B. Multilevel structured polyacrylonitrile/silica nanofibrous membranes for high-performance air filtration. *Sep Purif Technol*. **2014**;*126*:44.
266. Su J, Yang G, Cheng C, Huang C, Xu H, Ke Q. Hierarchically structured TiO2/PAN nanofibrous membranes for high-efficiency air filtration and toluene degradation. *J Colloid Interface Sci*. **2017**;*507*:386.
267. Wan H, Wang N, Yang J, Si Y, Chen K, Ding B, Sun G, El-Newehy M, Al-Deyab SS, Yu J. Hierarchically structured polysulfone/titania fibrous membranes with enhanced air filtration performance. *J Colloid Interface Sci*. **2014**;*417*:18.
268. Wang Z, Pan Z. Preparation of hierarchical structured nano-sized/porous poly (lactic acid) composite fibrous membranes for air filtration. *Appl Surf Sci*. **2015**;*356*:1168.
269. Ren G. Anti-viral formulations nanomaterials and nanoparticles. Google Patents; **2013**.
270. Fujimori Y. Anti-viral agent. Google Patent; **2002**.
271. Stewart NG, Lau FCN, Kung TW, Lo LY, Ryan DJ, Von Borstel RW. Composition for use in decreasing the transmission of human pathogens. Google Patents; **2018**.
272. Smith A, Taylor J. Antiviral metal impregnated activated carbon cloth components. Google Patents; **2011**.
273. Coulliette A, Perry K, Edwards J, Noble-Wang J. Persistence of the 2009 pandemic influenza A (H1N1) virus on N95 respirators. *Appl Environ Microbiol*. **2013**;*79*:2148.
274. Davison AM. Pathogen inactivation and filtration efficacy of a new anti-microbial and anti-viral surgical facemask and N95 against dentistry-associated microorganisms. *Int Dentist Aust Ed*. **2012**;*7*:2.
275. Lau JT, Fung KS, Wong TW, Kim JH, Wong E, Chung S, Ho D, Chan LY, Lui S, Cheng A. SARS transmission among hospital workers in Hong Kong. *Emerg Infect Dis*. **2004**;*10*:280.
276. Radonovich LJ, Cheng J, Shenal BV, Hodgson M, Bender BS. Respirator tolerance in health care workers. *JAMA*. **2009**;*301*:36.
277. Tong HW, Kwok SKC, Kwok HC. Protective masks with coating comprising different electrospun fibers interweaved with each other, formulations forming the same, and method of producing thereof. Google Patents; **2019**.
278. Mallikarjun K. Antiviral activity of substituted chalcones and their respective Cu (ii), Ni (ii) and Zn (ii) complexes. *E-J Chem*. **2005**;*2*:58.
279. Mastro MA, Hardy AW, Boasso A, Shearer GM, Eddy CR, Kub FJ. Non-toxic inhibition of HIV-1 replication with silver–copper nanoparticles. *Med Chem Res*. **2010**;*19*:1074.
280. Sagripanti J-LL, Marilyn M. Cupric and ferric ions inactivate HIV. *AIDS Res Hum Retroviruses*. **1996**;*12*:333.
281. Minoshima M, Lu Y, Kimura T, Nakano R, Ishiguro H, Kubota Y, Hashimoto K, Sunada K. Comparison of the antiviral effect of solid-state copper and silver compounds. *J Hazard Mater*. **2016**;*312*:1.
282. Nakano K, Sato A, Kusaka T, Kasamatsu S, Sasaki A, Fukushi D. Antiviral material, antiviral film, antiviral fiber, and antiviral product. Google Patents; **2014**.
283. Broglie JJ, Alston B, Yang C, Ma L, Adcock AF, Chen W, Yang L. Antiviral activity of gold/copper sulfide core/shell nanoparticles against human norovirus virus-like particles. *PLoS ONE*. **2015**;*10*: e0141050.
284. Kanovsky M. Antimicrobial material comprising synergistic combinations of metal oxides. Google Patents; **2020**.
285. Shimabuku QL, Arakawa FS, Fernandes Silva M, FerriColdebella P, Ueda-Nakamura T, Fagundes-Klen MR, Bergamasco R. Water treatment with exceptional virus inactivation using activated carbon modified with silver (Ag) and copper oxide (CuO) nanoparticles. *Environ Technol*. **2017**;*38*:2058.
286. Li Y, Yin X, Yu J, Ding B. Electrospun nanofibers for high-performance air filtration. *Compos Commun*. **2019**;*15*:6.

**Farinaz Hadinejad** is a master's graduate of Chemical Engineering majoring in biotechnology from Babol Noushirvani University of Technology and an active researcher at the Nano Technology Research Institute in the same faculty. Her research focuses on synthesizing and functionalizing nanofibers to customize them for biomedical applications.

**Hamed Morad** Hamed Morad (Pharm.D and PhD in Pharmaceutical Nanotechnology) is an assistant professor at the school of pharmacy, IUMS, Tehran, Iran. His research is focused on nanostructured drug delivery systems, especially nanofibers, Polymeric nanoparticles, and metal nanoparticles for wound healing, topical diseases, and chemotherapy. Hamed Has numerous publications and patents. He is the Vice-president of "STMA" Invention and innovation company and the Managing director of "Noavaran Teb Tabarestan". He was selected as the top researcher of Mazandaran twice, in 2014 and 2023. Hamed was responsible for university and industry relations. He was the product and R&D manager at FCP-Pharma company.

**Mohsen Jahanshahi** graduated from Shiraz University, Iran, in 1995 with a B.Sc. degree in the field of Chemical Engineering and also received his M.Sc. degree from Tarbiat Modares University in 1997. He completed his PhD in 2002 at the University of Birmingham, UK. He is currently a professor of Chemical Engineering at Babol Noshirvani University of Technology. Mohsen has more than 500 publications with an h-index and i10-index of 49 and 222, respectively. Mohsen is the Head of Nanotechnology Research Institute and Editor in Chief of the Journal of Water and Environmental Nanotechnology. His research interests are nanobiotechnology, drug delivery, bioseparation,biorecovery, water, and wastewater treatment.

**Ali Zarrabi** is an Associate Professor and Principal Investigator in the Faculty of Engineering & Natural Sciences, Istinye University, Turkey. He holds a bachelor's degree of Chemical Engineering from Isfahan University of Technology, a master's degree of Chemical Engineering from Sharif University of Technology, and a PhD of nanobiotechnology from Sharif University of Technology. His group works at the interface of supramolecular chemistry, bioengineering, and medicine to develop approaches for simultaneous diagnosis and treatment of diseases. He has been an active faculty member for more than 10 years. His current research interests include nanomaterials, nanotheranostics, novel wound dressing and skin patches, and translational nanomedicine. Developing wearable biosensors and diagnostic patches has recently been considered in Zarrabi Lab.

**Hamidreza Pazoki-Toroudi** is an associate professor at the Iran University of Medical Sciences. His research focuses on ischemia-reperfusion injury, regenerative medicine, clinical trials, and bio-nanomaterials. He is listed in the world's top 2% scientists ranking in 2023. He has been regularly working as a GBD collaborator since 2018.

**Ebrahim Mostafavi** has so far received training at Stanford Cardiovascular Institute, Stanford University School of Medicine (Post-Doc), Northeastern University (Ph.D.), Harvard Medical School (Researcher), and University of Tehran (M.Sc. and B.Sc.). His research interests revolve around the engineering and development of (nano) biomaterials, nanocarriers, and 3D in vitro models (hydrogels, 3D bioprinted constructs, nanofibrous scaffolds, organoids, vascular grafts, and microfluidic systems) to create biologically complex systems for a range of applications such as tissue engineering and regenerative medicine, translational medicine, cancer therapy (with focus on women's cancer), biosensing, and infectious diseases. Dr. Mostafavi serves as an Associate Editor-in-Chief of several prestigious and high-impact journals within Elsevier, Springer, Cell Press, Dove Medical Press, Taylor & Francis, Frontiers, etc. He is also serving as an Editorial Board Member of 30+ impactful and prestigious biomedical, medicine, and materials science journals. His scholarly work comprises > 150 publications with an H-index of 32 (i10-index = 85), including papers published in The Lancet family (i.e., Oncology, Infectious Diseases, Public Health, Global Health, etc.) and JAMA Network (Oncology, Cardiology) journals. So far, he has edited several books such as "Pharmaceutical Nanobiotechnology for Targeted Therapy" and "Emerging Nanomaterials and Nano-Based Drug Delivery Approaches to Combat Antimicrobial Resistance". He has also contributed to leading more than 50 introductory book chapters in a very multidisciplinary field of bio/medical engineering, biotechnology, nanotechnology, materials science, and regenerative/translational medicine.